EXPLOSIVE SELECTION AND FALLOUT SIMULATION EXPERIMENTS NUCLEAR CRATERING DEVICE SIMULATION (PROJECT DIAMOND ORE)

J. M. O'Connor, et al

Army Engineer Waterways Experiment Station
Vicksburg, Mississippi

October 1973

Destroy this report when no longer needed.
Do not return it to the originator.

The findings in this report are not to be construed as an official Department of the Army position unless so designated by other authorized documents.

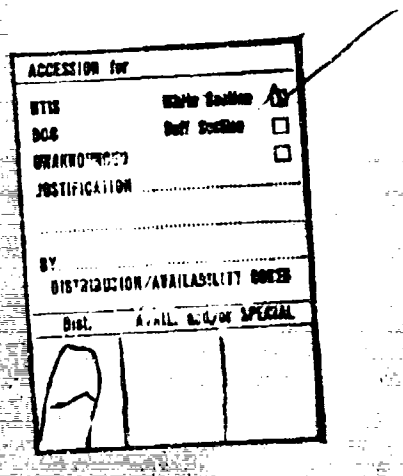

Printed in USA. Available from Defense Documentation Center,
Cameron Station, Alexandria, Virginia 22314 or
National Technical Information Service,
U. S. Department of Commerce
Springfield, Virginia 22151

UNCLASSIFIED
SECURITY CLASSIFICATION OF THIS PAGE (When Data Entered)

REPORT DOCUMENTATION PAGE		READ INSTRUCTIONS BEFORE COMPLETING FORM
1. REPORT NUMBER TR-E-73-6	2. GOVT ACCESSION NO.	3. RECIPIENT'S CATALOG NUMBER AD 776 361
4. TITLE (and Subtitle) EXPLOSIVE SELECTION AND FALLOUT SIMULATION EXPERIMENTS: NUCLEAR CRATERING DEVICE SIMULATION (PROJECT DIAMOND ORE)		5. TYPE OF REPORT & PERIOD COVERED Final 6. PERFORMING ORG. REPORT NUMBER
7. AUTHOR(s) J. M. O'Connor (author) T. J. Donlan, D. E. Burton (contributing authors)		8. CONTRACT OR GRANT NUMBER(s)
9. PERFORMING ORGANIZATION NAME AND ADDRESS U. S. Army Engineer Waterways Experiment Station Explosive Excavation Research Laboratory Livermore, California 94550		10. PROGRAM ELEMENT, PROJECT, TASK AREA & WORK UNIT NUMBERS See reverse
11. CONTROLLING OFFICE NAME AND ADDRESS Defense Nuclear Agency ATTN: SPSS Washington, D. C. 20305		12. REPORT DATE October 1973 13. NUMBER OF PAGES 145
14. MONITORING AGENCY NAME & ADDRESS(if different from Controlling Office)		15. SECURITY CLASS. (of this report) UNCLASSIFIED 15a. DECLASSIFICATION/DOWNGRADING SCHEDULE

16. DISTRIBUTION STATEMENT (of this Report)

Approved for public release; distribution unlimited.

17. DISTRIBUTION STATEMENT (of the abstract entered in Block 20, if different from Report)

18. SUPPLEMENTARY NOTES

19. KEY WORDS (Continue on reverse side if necessary and identify by block number)

Project Diamond Ore	Gelled nitromethane explosive
Nuclear cratering simulation	Slurry explosive equation of state
Fallout simulation	Unstemmed detonation

20. ABSTRACT (Continue on reverse side if necessary and identify by block number)

Project Diamond Ore was initiated in FY 1971 to determine the effects of different types of stemming, depths of burial, and geologic conditions on the crater size and collateral effects produced by the subsurface detonation of a nuclear cratering device.

This determination is being made by using a combination of hydrodynamic code calculations and large-scale chemical explosive charges to model the nuclear explosive energy source. The research program also includes development of a nuclear fallout simulant. This report presents a detailed summary of the

DD FORM 1 JAN 73 1473 EDITION OF 1 NOV 65 IS OBSOLETE

UNCLASSIFIED
SECURITY CLASSIFICATION OF THIS PAGE (When Data Entered)

20. Abstract (Continued)
explosive selection and testing process and the development and testing of the fallout simulant.

To model the nuclear explosive, the program required a high-energy chemical explosive that had reproducible detonation properties, could retain the fallout simulant material in suspension, and had a definable equation of state. A specially formulated water-gelled aluminized ammonium nitrate slurry was selected and tested in both laboratory and large-scale field tests. While standard explosive tests performed by explosives manufacturers indicated a satisfactory energy, laboratory and field measurements of explosive detonation parameters in the micro-time frame required for equation of state programs indicated that the slurry explosive did not possess reproducible detonation parameters. Changes in explosive composition to improve the reproducibility of the detonation parameters desensitized the explosive. Nitromethane was then studied. This is an explosive liquid avoided initially because of difficulties encountered in containing the liquid and supporting the fallout simulant. A gelling system was developed to overcome the containment and fallout simulant support problems. Techniques were successfully developed for simulating radioactive fallout using inert tracer particles. These particles are mixed uniformly with the explosive and are identifiable in the collected fallout debris using neutron activation and gamma-ray-spectrometry techniques. The resulting tracer mass deposition curves are easily related to the radioactivity dose rate curves obtained on previous nuclear cratering detonations at the Nevada Test Site.

Instrumentation and effects data from three large-scale detonations conducted at Fort Peck, Montana, are presented although much of the data is suspect due to the nonreproducibility of the slurry explosive employed and loss of much of the data due to gage failures.

10.

Program Element	Project	Task Area	Work Unit Numbers
L19	BAXSX301	01	01
L19	BAXSX302	01	01
L19	BAXSX303	01	01
L19	BAXYX921	01	01
L19	BAXYX970	01	01
L19	BAXYX971	01	01
L19	CAXSX301	01	01
L19	CAXSX303	01	01
L19	CAXYX971	01	01
L19	CAXYX972	01	01
L19	CAXYX978	01	01
6.21.18A	4A062118A880	06	003

TECHNICAL REPORT E-73-6
EXPLOSIVE SELECTION AND FALLOUT SIMULATION EXPERIMENTS: NUCLEAR CRATERING DEVICE SIMULATION (PROJECT DIAMOND ORE)

Author, John M. O'Connor

Contributing Authors, Terrence J. Donlan
Donald E. Burton

Sponsored by
DEFENSE NUCLEAR AGENCY

Subtask	Work Unit	Work Unit Title
L19BAXSX301	01	Crater Parameters
L19BAXSX302	01	Unstemmed Cratering
L19BAXSX303	01	Ejecta and Tracer
L19BAXYX921	01	Technical Photography
L19BAXYX970	01	Event Support
L19BAXYX971	01	Site Preparation
L19CAXSX301	01	Crater Parameters
L19CAXSX303	01	Ejecta Measurements and Evaluation
L19CAXYX971	01	Site Preparation
L19CAXYX972	01	Geologic Investigations
L19CAXYX978	01	Technical Director Activities

and
OFFICE OF THE CHIEF OF ENGINEERS

Appropriation	Project	Title
21X2040	4A062118A880	Nuclear Weapons Effects Research Test
2122040	4A062118A880	Nuclear Weapons Effects

Conducted by

U.S. ARMY ENGINEER WATERWAYS EXPERIMENT STATION
EXPLOSIVE EXCAVATION RESEARCH LABORATORY
Livermore, California

MS. date: May 1973

Preface

The U.S. Army Engineer Waterways Experiment Station (USAEWES) Explosive Excavation Research Laboratory (EERL) was the USAEWES Explosive Excavation Research Office (EERO) prior to 21 April 1972. Prior to 1 August 1971 the organization was known as the USAE Nuclear Cratering Group.

This portion of the Diamond Ore Project, a series of cratering experiments, was jointly sponsored by the Defense Nuclear Agency and Office, Chief of Engineers.

The Director of the Waterways Experiment Station during this research effort was COL Ernest D. Peixotto.

The Directors of the Explosive Excavation Research Laboratory (EERL) were LTC Robert L. LaFrenz and LTC Robert R. Mills, Jr

Abstract

Project Diamond Ore was initiated in FY 1971 to determine the effects of different types of stemming, depths of burial, and geologic conditions on the crater size and collateral effects produced by the subsurface detonation of a nuclear cratering device.

This determination is being made by using a combination of hydrodynamic code calculations and large-scale chemical explosive charges to model the nuclear explosive energy source. The research program also includes development of a nuclear fallout simulant. This report presents a detailed summary of the explosive selection and testing process and the development and testing of the fallout simulant.

To model the nuclear explosive, the program required a high-energy chemical explosive that had reproducible detonation properties, could retain the fallout simulant material in suspension, and had a definable equation of state. A specially formulated water-gelled aluminized ammonium nitrate slurry was selected and tested in both laboratory and large-scale field tests. While standard explosive tests performed by explosives manufacturers indicated a satisfactory energy, laboratory and field measurements of explosive detonation parameters in the micro-time frame required for equation of state programs indicated that the slurry explosive did not possess reproducible detonation parameters. Changes in explosive composition to improve the reproducibility of the detonation parameters desensitized the explosive. Nitromethane was then studied. This is an explosive liquid avoided initially because of difficulties encountered in containing the liquid and supporting the fallout simulant. A gelling system was developed to overcome the containment and fallout simulant support problems. Techniques were successfully developed for simulating radioactive fallout using inert tracer particles. These particles are mixed uniformly with the explosive and are identifiable in the collected fallout debris using neutron activation and gamma-ray-spectrometry techniques. The resulting tracer mass deposition curves are easily related to the radioactivity dose rate curves obtained on previous nuclear cratering detonations at the Nevada Test Site.

Instrumentation and effects data from three large-scale detonations conducted at Fort Peck, Montana are presented although much of the data is suspect due to the nonreproducibility of the slurry explosive employed and loss of much of the data due to gage failures.

Acknowledgments

This study is being conducted under the joint sponsorship of the Defense Nuclear Agency (DNA) and the Office, Chief of Engineers (OCE). The experimental programs reported in this, the first, summary report of the Diamond Ore investigations, represent the efforts of an interdisciplinary team from many agencies within the Nuclear Weapons Effects community.

The DNA Project Officers during this phase of the Diamond Ore investigations were LTC Louis J. Circeo and LTC Richard Pierce. The OCE Project Officers were LTC Gerald W. Chase and LTC Douglas A. Hughes.

The guidance and encouragement of LTC Robert L. LaFrenz and LTC Robert R. Mills, Jr., Directors of the Explosive Excavation Research Laboratory (EERL), and MAJ Richard H. Gates, Deputy Director at EERL for Military Funded Programs, during this research effort are greatly appreciated.

The authors wish to acknowledge and to express sincere appreciation to the following individuals and agencies for their efforts in support of these investigations: Dr. Thomas Blake and Dr. Robert Allen of Systems, Science, and Software, Inc.; Dr. Alfred Holzer, Mrs. Barbara K. Crowley, Dr. Jon B. Bryan, Mr. Clyde J. Sisemore and Mr. Marvin D. Denny of K Division, LLL; Mr. Milton Finger, Dr. Edward L. Lee, Mr. Ronald M. Boat, Mr. Franklin H. Helm, and Dr. Henry Cheung, of the Chemistry Department, LLL; Mr. William B. Lane of the Stanford Research Institute; Mr. James Rupley of Sandia Laboratories, Albuquerque; Mr. David L. Wooster of the Mechanical Engineering Department, LLL, Mr. Charles Grant and Mr. Jerome Landerville, Dow Chemical Company; Mr. Donald Beckman and Mr. John Kuncheff, Fort Peck Area Officer, U.S. Army Corps of Engineers, Omaha Engineer District, and, finally, Mr. Edward J. Leahy, Mr. Richard L. Fraser, MAJ Donald J. Fitchett, MAJ George M. Miller, CPT Robert J. Bourque, Mr. Charles Snell, Mr. Jerome E. Lattery, Mr. Thomas M. Tami, CPT Howard H. Reed, CPT Wade Wnuk, and Mr. John F. Dishon of EERL.

Contents

FIGURES

FIGURES (continued)

FIGURES (continued)

TABLES

TABLES (continued)

Conversion Factors

Metric units of measurement used in this report can be converted to English units as follows:

Multiply	By	To obtain
centimeters (cm)	0.3937	inches (in.)
meters (m)	3.2808	feet (ft)
cubic meters (m^3)	35.311	cubic feet (ft^3)
cubic meters (m^3)	1.30795	cubic yards (yd^3)
kilograms (kg)	2.204622	pounds (lb)
kilograms per square meter (kg/m^2)	1.422×10^{-3}	pounds per square inch (psi)
pounds per cubic foot (lb/ft^3)	0.062422	kilograms per cubic meter (kg/m^3)
Fahrenheit degrees (F)	—[a]	Celsius or Kelvin degrees (C, K)
ton (nuclear equivalent of TNT)[b]	4.2×10^9	joules (J)

[a]To obtain Celsius (C) temperature readings from Fahrenheit (F) readings, use the following formula: C = (5/9) (F - 32). To obtain Kelvin (K) readings, use: K = (5/9) (F - 32) + 273.15.

[b]All references to yield are in terms of energy; therefore, joules will be the primary value in accordance with the International System of Units (SI) and the alternate will be tons (nuclear equivalent of TNT).

EXPLOSIVE SELECTION AND FALLOUT SIMULATION EXPERIMENTS: NUCLEAR CRATERING DEVICE SIMULATION (PROJECT DIAMOND ORE)

Chapter 1

Introduction

DESCRIPTION AND PURPOSE

The overall objective of Project Diamond Ore is to determine what effects different types of stemming, depth of burial, and geologic media will have on the crater dimensions and collateral effects resulting from the subsurface detonation of a nuclear device. The determination of these effects is to be accomplished with chemical explosive cratering detonations designed to model the nuclear detonations. An additional objective is to develop a means of simulating the radioactive fallout intensity levels and the fraction of radioactivity vented that would accompany the subsurface detonations. Comparative effects studies are to include airblast, ground motion, crater size and shape, continuous ejecta limits and composition, missile limits and densities, and radioactive vent fraction and fallout distribution.

SCOPE OF REPORT

This report describes the research efforts conducted in FY 71 and FY 72 leading to the selection of the explosive fallout simulation system to be used in the nuclear modeling detonations of Project Diamond Ore. Specifically, these experiments are directed at the selection of a chemical explosive, the defining of its detonation parameters, the selection of a fallout tracing method, and the development and testing of the tracer techniques required for use in large-scale field experiments. These objectives of the Diamond Ore program are the only ones addressed in this report. The Diamond Ore program is jointly funded by the Defense Nuclear Agency (DNA) and the Office of the Chief of Engineers (OCE) with program management and principal participation provided by the U.S. Army Engineer Waterways Experiment Station Explosive Excavation Research Laboratory (EERL).

PARTICIPATING AGENCIES

These experiments were conducted by EERL [initially as the U.S. Army Engineer Nuclear Cratering Group (NCG)] with participation from the Chemistry Department, Lawrence Livermore Laboratory (LLL); K Division, LLL; Systems, Science, and Software, Inc.; and the Operations Evaluation Department, Stanford

Research Institute (SRI). The Chemistry Department, LLL, was responsible for explosive testing and for determining the detonation characteristics of the explosives considered. K Division, LLL, Systems, Science, and Software, Inc., and EERL were responsible for the calculation efforts. EERL and the Operations Evaluation Department of SRI were responsible for development and testing of the fallout simulation program.

PROJECT BACKGROUND

Atomic Demolition Munitions (ADM) are tactical nuclear weapons capable of being employed in a variety of modes. Emplacement doctrine for the ADM is contained in Ref. 1. This document and all other doctrine for the employment of low-yield nuclear devices in a cratering mode are based primarily on data from cratering tests conducted at the Nevada Test Site (NTS). All of these tests were conducted as fully stemmed detonations. Thus, information is lacking on the effects of geologic medium, stemming variations, and depth of burial (DOB) on crater parameters.

The subsurface employment of nuclear devices, particularly optimum DOB rather than surface employment, can result in a significant reduction in yield requirements. Subsurface employment can also result in significant reductions in collateral effects. The collateral effects, prompt nuclear radiation, thermal radiation, and airblast, decrease as the DOB increases. Other collateral effects, such as fallout and missiles, increase initially, then decrease as DOB increases. Current data also indicate that the fraction of radioactivity produced by a cratering detonation and deposited in the local area fallout is about 50% for a surface burst and 10 to 35% for a fully stemmed detonation at optimum DOB. Thus, a reduction is also obtained in the radioactivity found in the ground surface area surrounding the detonation.

Fully stemmed employment of low-yield nuclear devices in tactical situations is not desirable. The requirement to fully stem the emplacement hole limits the flexibility and rapidity of deployment by increasing emplacement time. Additional problems and time expenditure would be involved in device recovery if a mission is aborted. Subsurface employment utilizing simplified stemming, such as water or possibly no stemming, would resolve the problems of loss of flexibility and rapidity of emplacement and recovery. Data on the effects of simplified stemming on crater dimensions and collateral effects are thus required to permit development of employment doctrine.

Due to restrictions of the 1963 Limited Nuclear Test Ban Treaty on fallout levels that may cross national boundaries, the use of actual nuclear cratering experiments to determine stemming and media effects on crater size and collateral effects is considered infeasible. Also, the existing nuclear test sites do not provide tactically significant geologic media. These restrictions require the use of a chemical explosive energy source to model the nuclear explosive devices. These chemical explosive charge designs are to be developed through a sequence of numerical modeling calculations followed by field experiments designed to provide empirical input data for the next

calculations. Once developed, and determined to model adequately a nuclear detonation through field experiments, these high explosive and numerical models will be employed in tactically significant media and terrain to obtain the data required to evaluate the effects of water and air stemming.

The scope of Project Diamond Ore has been expanded from its initial objective to determine the effects of simplified stemming. Beginning in late FY 73 the chemical charge design developed in Project Diamond Ore will be used to obtain effects data for obstacles, barriers, and targeting studies against specific targets, such as airfields, bridges, or railroad marshaling yards. This expanded program is titled ESSEX (Effects of Subsurface Explosions)

Chapter 2

Initial Studies

GENERAL

The planning for the Diamond Ore program was initiated in the spring of 1971 by the Nuclear Cratering Group (now EERL) under Defense Atomic Support Agency (now DNA) sponsorship. The study was directed at subkiloton yields. The 84×10^9 J (20-ton) yield was selected for the initial high-explosive experiments.* This is the lowest yield that would allow for confident scaling up to 1 kt and was the highest yield that would not impose severe restrictions on test site selection. In addition, this yield would allow for direct use of considerable data from previous 18,140-kg (20-ton) chemical explosive detonations.

The initial planning called for two 18,140-kg (20-ton) chemical detonations at NTS. These detonations were to be conducted in areas adjacent to the Danny Boy (0.42 kt) and the Teapot ESS (1.2 kt) nuclear craters. The explosive model development was to be based on comparisons of the resulting craters with the nuclear craters using empirical scaling relationships. The modeling of these craters was also to permit the nuclear fallout and fallout simulant to be compared. If these tests proved successful, additional testing was to be accomplished in a more tactically significant medium.

EXPLOSIVE SELECTION

In order to make the broadest use of the explosive testing planned for the Diamond Ore program, the initial explosive selection studies were directed at the possible use of composite explosives, specifically the use of the water-gelled aluminized ammonium nitrate slurry type of explosive. Although this type of explosive was in use in commercial applications, its detonation characteristics had not been studied in the detail planned in

*All references to yield are in terms of energy; therefore, joules will be the primary value in accordance with the International System of Units (SI) and the alternate will be tons (nuclear equivalent of TNT).

the Diamond Ore program. This type of explosive was being studied for possible military engineering and civil works excavation purposes at EERL and was also being considered for use in research programs being conducted at LLL and at other laboratories. The detonation characteristics of this type of explosive can be altered to meet specific requirements through changes in the compositions. This ability to tailor the explosive's detonation characteristics was ideally suited to the explosive needs of the Diamond Ore program.

Previous studies in modeling nuclear explosions with chemical explosives had generally assumed a one-to-one energy equivalence. More recent cratering experience has shown that chemical explosives, employed at cratering depths, are more efficient from an energy-use standpoint than were nuclear explosives. In the nuclear detonation, energy is consumed in vaporizing the surrounding media. This energy is lost in the sense that it does not do useful work in the formation of the crater. This vaporization phenomenon is not found in the detonation of chemical explosives because much lower temperatures and pressures are produced. Therefore, the simulation of an 84×10^9 J (20-ton) nuclear cratering detonation would require less than 84×10^9 J (20 tons) of equivalent chemical explosive energy. Because it is impossible to model this vaporization phenomenon with chemical explosives, it would be necessary to initiate the chemical explosive detonation in a cavity equal in size to the vaporized nuclear cavity. For cratering purposes, the chemical explosive would also have to produce the same amount of energy as the nuclear detonation would contain at the end of cavity vaporization.

Based on this concept of modeling, the following criteria were established for the selection of a chemical explosive for the Diamond Ore program:

1. The total energy release of the chemical explosive must equal that of the nuclear device minus that energy expended by the latter to vaporize the medium.

2. The size and geometry of the chemical explosive charge must equal that of the gas cavity formed by the nuclear detonation. Consideration must be given to the type of medium and stemming.

3. The pressure-volume history of the chemical explosive products must coincide as closely as possible with that of the vaporized gas produced by the nuclear detonation at the time vaporization is completed. A corollary, but less exacting requirement, is that the integrals of the pressure-volume adiabats within the limits from the initial cavity radius to a radius at atmospheric pressure must be equal.

4. The chemical explosive must be solid or semisolid in order to hold fallout tracer particles in suspension and must be capable of detonation with up to 20% by weight contamination by these simulant particles.

Calculations were performed to determine the energy density requirements for the chemical explosive based on Butkovich.[2] The energy consumed in vaporization of the medium and thus lost in the crater formation processes was found to

be about 20% or 16.8×10^9 J (4 tons) (at optimum DOB). The remaining 67.2×10^9 J (16 tons) was assumed to be the equivalent cratering energy. The radius of the vaporized cavity was calculated at about 60 cm (23.6 in.) (Ref. 2). The energy density of the ideal explosive to meet requirement No. 1 was on the order of 36,960 J/cm^3. This high an energy density was not available from chemical explosives that could be considered feasible for use in this project, leading to the abandonment of the concept of initiating the chemical explosive detonations at the point at which the nuclear explosion completed cavity vaporization.

While planning for the empirical approach to the Diamond Ore program was continuing, K Division, LLL, and Systems, Science and Software, Inc. were funded by DNA to perform calculations related to 84×10^9 J (20-ton) subsurface nuclear detonations. A series of meetings was held to coordinate the two calculational efforts and the experimental program to be conducted by EERL. Because the calculational programs were to develop actual chemical explosive charge designs to model the nuclear detonations, the explosive selection criteria were respecified as follows:

1. A high-energy density on the order of 12,600 J/cm^3.

2. Reproducible and definable detonation parameters (an equation-of state would be required for code calculations) in both the pure form and with up to 20% contamination of simulant particles.

3. Capability of maintaining up to 20% by weight of simulant material (sand) in uniform suspension.

4. Commercial availability in large quantities.

In May 1971, a solicitation for bids was released for development, supply, and testing of the "Diamond Ore Explosive." Appendix A contains the slurry explosives contract specifications. Award of this contract was to be based on a demonstrated proficiency in the explosives field and the lowest unit price for the explosive. The contract was awarded to Dow Chemical Company as the only firm that was fully responsive to this solicitation.

FALLOUT SIMULATION

Previous attempts at simulating fallout from nuclear cratering detonations involved the use of radioactive materials placed in the chemical explosive charge in some type of capsule or container. Other methods included the use of fluorescent materials. None of these methods was applicable to the Diamond Ore program because testing was contemplated at various locations outside nuclear test sites where the use of radioactive materials would be prohibited and because none of these systems had proved successful in providing the accuracy desired for the Diamond Ore program. Studies were conducted with the assistance of the Stanford Research Institute (SRI) to select a trace element that could be mixed uniformly with the explosive, would survive the detonation, would simulate radioactive fallout transportation in the cloud, and could be detected in postshot fallout samples through neutron activation and gamma ray spectrometry.

The following criteria were established for selection of the tracer material:

1. Reasonable cost.
2. Distinct gamma ray spectrum for ease in identification.
3. High neutron cross section to minimize irradiation time.
4. High isotopic abundance to minimize the mass of tracer material required and to increase sensitivity.
5. Radioactive half-life longer than 25 hr to allow for the handling time of large numbers of samples but not so long as to require excessive irradiation time.
6. A high boiling point to insure stability in the explosive environment.

Examination of the work done by Day and Paul[3] in element abundance in natural soils led to the selection of 12 candidate elements. Soil samples from prospective test sites were obtained and activated to determine the soil gamma ray spectrum. Samples of candidate trace elements were also irradiated. The gamma ray spectrum of each element was superimposed on each soil spectrum to determine its detectability over the soil background. The iridium-192 nuclide was found to be the most desirable. At 20 days after irradiation, 10^{-7} g of iridium was readily detected in the presence of 1 g of each of the soils tested (counting time of 1 min, irradiation for 1 hr at a flux of 5×10^{12} $cm^2 \cdot sec$).[4]

Studies of fallout particle sizes and fall rates at various downwind ranges were examined to determine the particle size on which the tracer material should be placed within the explosive. Particle sizes of 125 to 175 μm were selected as being representative of the radioactive fallout particles found downwind at the ranges of interest: 300 to 2,600 m (330 to 2,850 yd). Wedron sand was selected as the carrier for the tracer material. These sand particles are pure quartz and ideally suited for this purpose. Quartz has a 1,600°C melting point and a low thermal conductivity that enhance particle survival in the explosive environment. Quartz also has no induced radionuclides that would interfere with the detection of the iridium-192 nuclide. Since the particle density is 2.6 g/cm^3, which is about that of radioactive particles from a land detonation, the particles will travel in much the same way as like particles from a nuclear detonation.[4]

Techniques were developed at SRI for the adsorption of iridium on the sand particles. The tagged particles were then overcoated with sodium silicate to reduce the possibility of iridium migration in the explosives environment.

Discussions were held with explosives manufacturers to confirm that the traced particulate matter was chemically compatible with explosives of the type being considered for the Diamond Ore program.

CALCULATION AND TESTING PROGRAM DEVELOPMENT

As previously discussed, the original concept for the development of the chemical explosive charge model was to rely on empirical scaling techniques developed in previous nuclear and chemical explosive testing. Chemical explosive experiments were to be conducted adjacent to nuclear craters at NTS. The resulting crater dimensions could then be scaled to the nuclear craters (Danny Boy and Teapot ESS) and refinements in the yields of the chemical charge could be made.

Fallout patterns could also be compared and relationships developed between the simulated and actual fallout.

This concept was altered significantly when calculational support from K Division, LLL, and Systems, Science, and Software, Inc., was phased into the program. A series of meetings was held to develop a program of calculations and experiments that would lead to the development of the high explosive models. Calculational support was divided between Systems, Science, and Software, Inc. and LLL based on the DOB's of interest. LLL was to provide calculations in support for experiments at the 12.5-m (41-ft) DOB [~optimum DOB for 84×10^9 J (20 tons)] with Systems, Science, and Software, Inc. providing calculational support for the 6-m (19.7-ft) DOB program (~1/2 of optimum DOB). Systems, Science and Software, Inc. calculational work was to be based on the use of the HELP Code. This code had been developed and used previously at Systems, Science, and Software, Inc. to conduct cratering calculations under DNA sponsorship. The HELP Code is suitable for calculating both stemmed and unstemmed detonations. LLL support was to be based on the use of the TENSOR code for stemmed detonations and the development and use of a combination of the TENSOR and PUFL codes for the unstemmed/water-stemmed detonations.

The use of these numerical modeling codes requires the input of equations-of-state (EOS) for both the medium in which the detonations are to be conducted and the explosive (chemical or nuclear) to be used. The responsibility for determining the EOS for the slurry explosive to be used in field-testing was given to the Chemistry Department at LLL. The need for an EOS for the geologic medium dictated a change of test sites from NTS to Fort Peck, Montana for the first series of large-scale experiments. The Bearpaw clay shale found at Fort Peck had been extensively investigated during the Pre-Gondola cratering tests and extensive EOS data were already available. Compilation of the data into a usable EOS was accomplished by K Division, LLL, and EERL.[5]

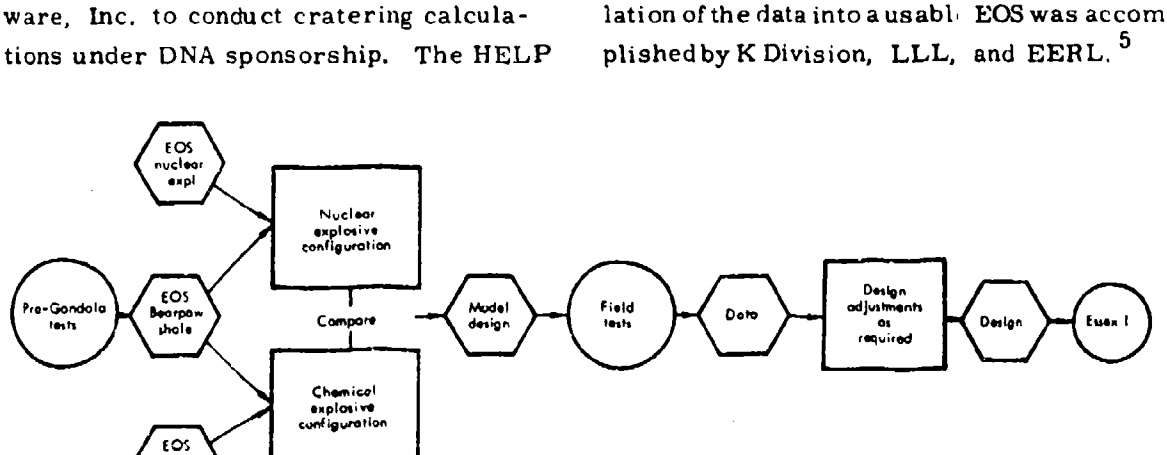

Fig. 2.1. Diamond Ore program planning logic (generalized).

The program for calculations and testing was to be conducted under the title of Phase II, Project Diamond Ore. The general plan was for calculations to be performed for the nuclear cases of interest. In addition to final crater dimensions, these calculations predict velocity, density, and pressure data within the crater at various times during the detonation. Chemical explosive calculations would then be conducted. Changes in chemical explosive yield and charge shape would be made in an attempt to match the predicted nuclear velocity, energy, pressure, and density levels. The resulting charge configurations would then be tested at Fort Peck. These detonations would be instrumented to record the actual stress and velocity levels experienced by the medium during crater formation. The field data would then be used to verify the code predictions and/or direct corrections in the codes or designs. The results of these corrections would be the model designs. Figure 2.1 is a generalized flow chart for the logic of these calculational and experimental programs.

Chapter 3

Small-Scale and 1-Ton Slurry Testing

GENERAL

As stated in Chapter 2, Dow Chemical Company was selected to supply a slurry explosive for use in the Diamond Ore program. Included in this contract was a series of safety and performance tests to be conducted by the manufacturer. The initial supply of explosives to EERL was for the conduct of cratering tests with both the pure and the traced, sand-contaminated explosive. The percentage of sand contamination was to be specified after initial testing of the sensitivity of the fallout simulation program. Testing of the fallout simulation program was also to be conducted at the 907-kg (1-ton) level in conjunction with the Middle Course II cratering experiments conducted by EERL at Trinidad, Colorado.

CONTRACTOR TESTING

Under the provisions of the contract awarded to Dow (see Appendix A for specifications), performance tests were to be conducted on the explosive in a pure form, and with sand contamination levels of 5, 10, 15, and 20% by weight. These performance tests were required to determine the effect of the sand contamination on the energy produced by the explosive. The results of these tests are shown in Table 3.1. Initial results of the fallout simulation program indicated that a 10% (by weight) level of sand contamination would provide sufficient sensitivity, and Dow was directed to conduct the required safety tests with this level of contamination. These safety tests were to be conducted on 15.2-cm (6-in.) diameter polyvinyl chloride spherical containers filled with explosive. These spheres

Table 3.1. Dow underwater energy test results (booster energy subtracted out).

% contaminate		Shock energy (J/g)	Shock energy (cal/g)[a]	Bubble energy (J/g)	Bubble energy (cal/g)	Total energy (J/g)	Total energy (cal/g)	Average total energy (J/g)	Average total energy (cal/g)
Pure (0)	(a)	2,961	705	4,192	998	7,153	1,703		
	(b)	3,158	752	4,137	985	7,295	1,737	7,115	1,694
	(c)	2,801	667	4,099	976	6,901	1,643		
2	(a)	2,348	559	3,847	916	6,195	1,475		
	(b)	2,512	598	4,032	960	6,544	1,558	6,258	1,490
	(c)	2,251	536	3,881	924	6,132	1,460		
5	(a)	2,764	658	3,893	927	6,657	1,585		
	(b)	2,159	514	3,864	920	6,023	1,434	6,363	1,515
	(c)	2,419	576	3,990	950	6,409	1,526		
10	(a)	2,075	494	3,654	870	5,729	1,364		
	(b)	2,310	550	3,654	870	5,964	1,420	5,926	1,411
	(c)	2,310	550	3,780	900	6,090	1,450		
15	(a)	2,050	488	3,574	851	5,624	1,339		
	(b)	2,066	492	3,318	790	5,384	1,282	5,355	1,275
	(c)	1,743	415	3,318	790	5,061	1,205		
20	(a)	2,071	493	3,310	788	5,380	1,281		
	(b)	2,020	481	3,276	780	5,296	1,261	5,296	1,261
	(c)	1,936	461	3,276	780	5,212	1,241		

[a] 1 cal = 4.2 joules.

were the same charges to be used by EERL in the conduct of a series of small-scale cratering tests. When cap sensitivity tests were conducted with both No. 6 and No. 8 blasting caps, the explosive failed to detonate or to react to these tests. In order to determine minimum booster requirements, tests were conducted with three sizes of 50/50 pentolite boosters and No. 8 electric blasting caps. Testing resulted in a partial detonation with a 5-g booster, and high-order detonations with 15- and 37.5-g boosters. These test results met the contract specifications (Appendix A).

SMALL-SCALE CRATERING TESTS

In order to determine the cratering characteristic of both the pure slurry explosive and the 10% sand-contaminated explosive, EERL conducted a series of cratering experiments at the LLL Site 300 test facility. The charges detonated in this series were 15.2-cm (6-in.) diameter spheres containing about

2.7-kg (6-lb) of slurry explosive. Standard SE-1 detonators were used with a C-4 explosive booster. Figure 3.1 shows a typical charge. The sand medium test pit used for these detonations had been used in many previous small-scale tests. The sand specifications and the operating procedures are described in Appendix B.

The first series of cratering detonations to be conducted was 15 detonations with the pure explosive. Three detonations were conducted at each of five DOB's: 0.46 m (1.5 ft), 0.69 m (2.25 ft), 0.91 m (3.00 ft), 1.14 m (3.75 ft), and 1.37 m (4.5 ft). Standard surveying techniques were used to measure the crater dimensions. These data were processed using EERL's CRATER DATA code[6] to produce cratering curves. The apparent crater volume, the apparent crater radius, and the apparent crater depth are shown in Figs. 3.2, 3.3, and 3.4. Individual shot points are also plotted on these curves. Scatter in the data is considered typical of the test medium used.

The second series of 2.7-kg (6-lb) tests was conducted with the 10% sand-contaminated explosive. The sand was first coated with the iridium trace element at SRI and then mixed with the explosive during manufacturing. In addition to obtaining cratering data, fallout samples were collected as a test of the tracer program's compatability with the Dow slurry explosive. The series was originally planned for the 15 detonations in the pure explosive program. Delays in the series were encountered due to the necessity of waiting for winds that would carry the detonation clouds over the array of fallout collection trays. The original 15 detonations were therefore reduced to five with one detonation at each DOB. The results of these cratering detonations were again processed using EERL's CRATER DATA code.[6] The resulting cratering curves are shown in Figs. 3.5, 3.6, and 3.7 with the individual data points. For comparison, cratering curves for the pure explosive have been added to the figures. Previous experience at the sand test pit shows that differences between the pure and contaminated explosive curves are not significant

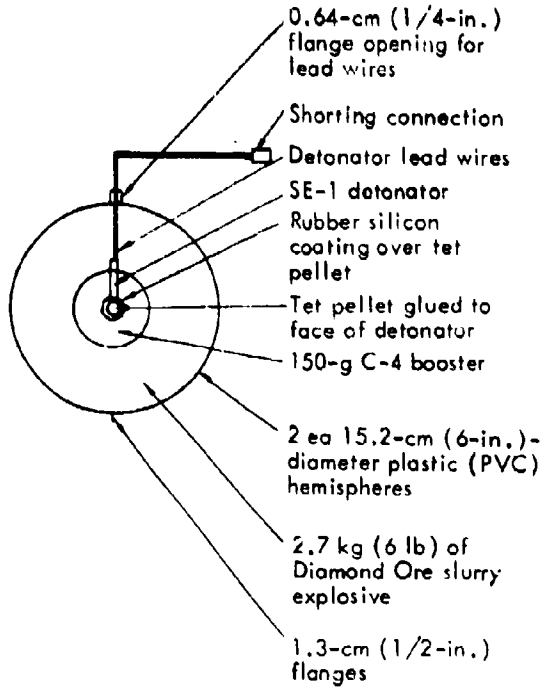

Notes: 1. The plastic hemispheres come filled with explosive and covered with thin plastic sheet.

2. Preparation—A small portion of the slurry explosive is removed from each hemisphere to allow placement of the detonator and booster. The two hemispheres are mated and the flanges are glued together with a rubber silicon adhesive and then stapled to insure assembly.

Fig. 3.1. Diamond Ore 2.7-kg (6-lb) spherical charge (typical).

due to the scatter of the data. Therefore, the addition of the sand does not cause any apparent loss of cratering efficiency.

As a test of the sensitivity of the fallout tracing system and to provide an insight (within the limits of the test pit) into the effects that simplified stemming would have on both the fallout and the cratering mechanisms, three additional traced detonations were conducted. The first two were detonated at DOB's of 0.69 m (2.25 ft) and 0.91 m (3.00 ft with the 15.24-cm (6-in.) radius emplacement hole left open (air-stemmed). The third detonation was conducted at a DOB of 0.91 m (3.00 ft) with the 15.2-cm (6-in.) radius emplacement hole filled with water (water stemmed). The resulting crater dimensions are plotted in Figs. 3.8, 3.9, and 3.10. The curves

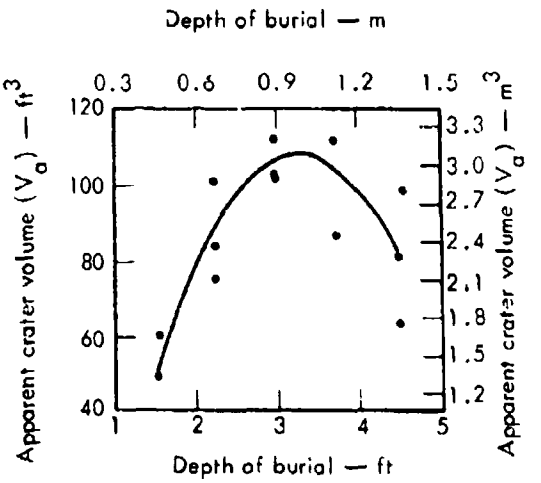

Fig. 3.2. Site 300 stemmed cratering curve (V_a) for the 2.7-kg (6-lb) pure explosive detonations.

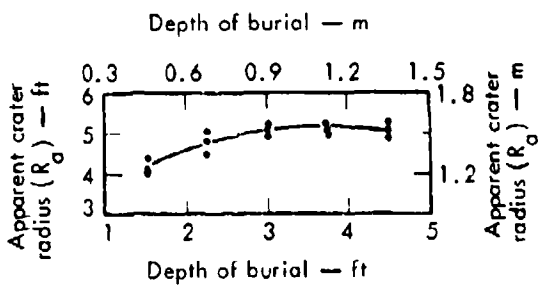

Fig. 3.3. Site 300 stemmed cratering curve (R_a) for 2.7-kg (6-lb) pure explosive detonations.

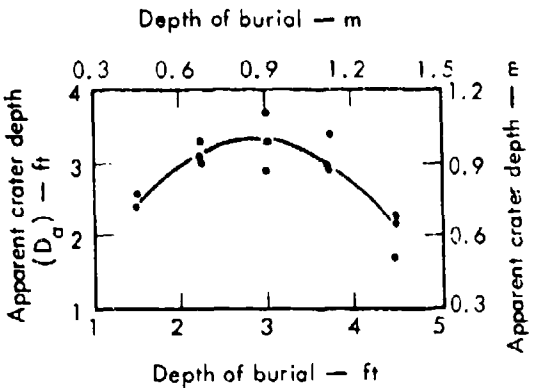

Fig. 3.4. Site 300 stemmed cratering curve (D_a) for 2.7-kg (6-lb) pure explosive detonations.

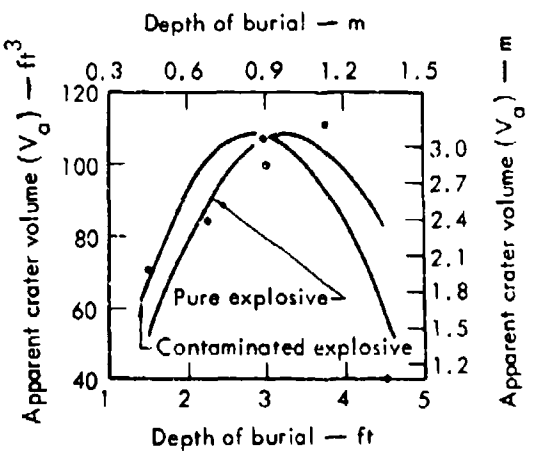

Fig. 3.5. Site 300 stemmed cratering curves (V_a) for 2.7-kg (6-lb) pure and contaminated explosive detonations.

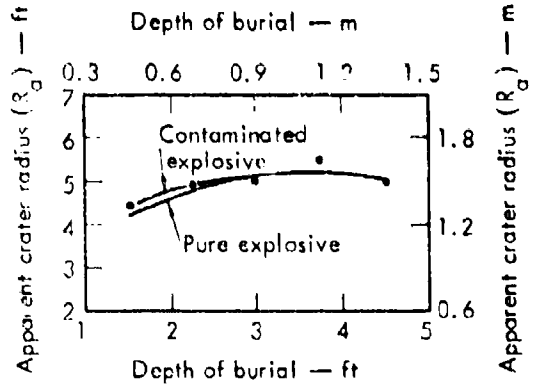

Fig. 3.6. Site 300 stemmed cratering curves (R_a) for 2.7-kg (6-lb) pure and contaminated explosive detonations.

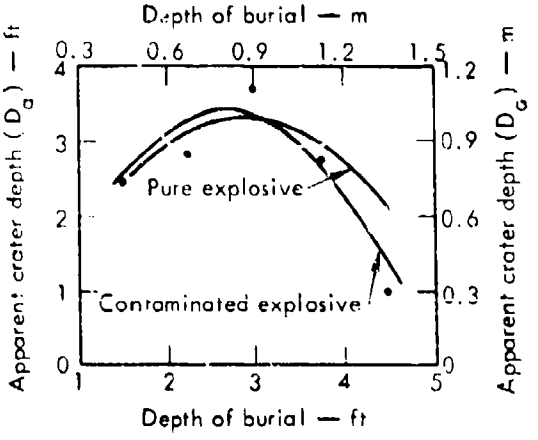

Fig. 3.7. Site 300 stemmed cratering curves (D_a) for 2.7-kg (6-lb) pure and contaminated explosive detonations.

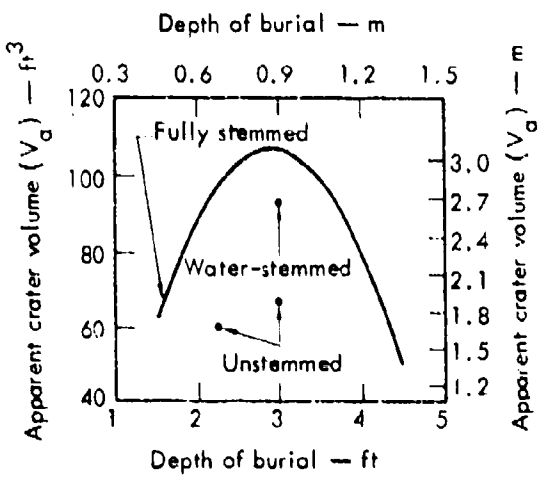

Fig. 3.8. Site 300 cratering data (V_a) for 2.7-kg (6-lb) sand-contaminated explosive detonations and various stemming conditions.

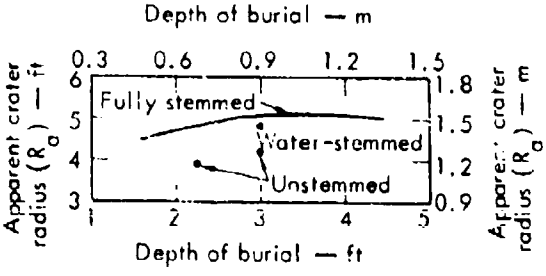

Fig. 3.9. Site 300 cratering data (R_a) for 2.7-kg (6-lb) sand-contaminated explosive detonations and various stemming conditions.

for sand-contaminated, stemmed detonations are added for comparison. These points indicate what would be logically assumed: that the lack of stemming may have a significant effect on the crater size and that the result of a water-stemmed detonation would lie somewhere between the stemmed case and the unstemmed case. Table 3.2 is a listing of the crater data for each of the 24 detonations conducted in the series. The results of the fallout simulation program are presented in a subsequent section.

TRACER TESTING

As mentioned in the previous section, nine of the 2.7-kg (6-lb) sand-contaminated

Table 3.2. Site 300 crater data.

Event[a]	Depth of burial (m)	Depth of burial (ft)	Apparent crater radius, R_a (m)	Apparent crater radius, R_a (ft)	Apparent crater depth, D_a (m)	Apparent crater depth, D_a (ft)	Crater volume, V_a (m^3)	Crater volume, V_a (ft^3)
A-1	0.46	1.5	1.34	4.4	0.79	2.6	1.71	60.5
A-2	0.46	1.5	1.28	4.2	0.73	2.4	1.40	49.5
A-3	0.46	1.5	1.25	4.1	0.73	2.4	1.40	49.5
A-4	0.69	2.25	1.49	4.9	1.01	3.3	2.86	101.0
A-5	0.69	2.25	1.40	4.6	0.91	3.0	2.14	75.5
A-6	0.69	2.25	1.49	4.9	0.94	3.1	2.38	84.0
A-7	0.91	3.0	1.62	5.3	1.01	3.3	3.16	111.75
A-8	0.91	3.0	1.52	5.0	1.13	3.7	2.91	102.75
A-9	0.91	3.0	1.58	5.2	0.88	2.9	2.87	101.2
A-10	1.14	3.75	1.55	5.1	1.04	3.4	3.16	111.5
A-11	1.14	3.75	1.62	5.3	0.88	2.9	3.16	111.5
A-12	1.14	3.75	1.52	5.0	0.88	2.9	2.46	86.75
A-13	1.37	4.5	1.62	5.3	0.67	2.2	2.78	98.25
A-14	1.37	4.5	1.52	5.0	0.70	2.3	2.28	80.50
A-15	1.37	4.5	1.52	5.0	0.52	1.7	1.80	63.75
B-1	0.46	1.5	1.37	4.5	0.76	2.5	1.97	69.5
B-2	0.68	2.25	1.49	4.9	0.85	2.8	2.41	85.25
B-3	0.91	3.0	1.49	4.9	1.04	3.4	2.79	98.5
B-3R	0.91	3.0	1.52	5.0	1.13	3.7	3.03	106.9
B-4	1.14	3.75	1.71	5.6	0.79	2.6	3.16	111.5
B-5	1.37	4.5	1.49	4.9	0.30	1.0	1.13	40.0
C-1	0.686	2.25	1.19	3.9	0.85	2.8	1.46	51.44
C-2	0.914	3.0	1.31	4.3	0.91	3.0	1.89	66.67
D-1	—[b]							
D-2	0.914	3.0	1.43	4.7	1.04	3.4	2.66	93.85

[a]"A" series was fully stemmed using the pure explosive; "B" series was fully stemmed using the sand-contaminate explosive; "C" series was air-stemmed using the sand-contaminate explosive; "D" series was water-stemmed using the sand-contaminate explosive.

[b]Misfired due to detonator separation.

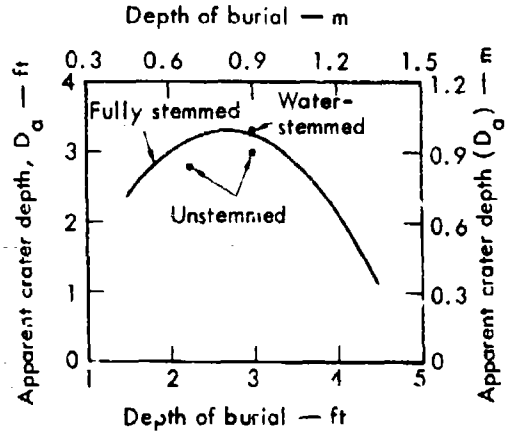

Fig. 3.10. Site 300 cratering data (D_a) for 2.7-kg (6-lb) sand-contaminated explosive detonations and various stemming conditions.

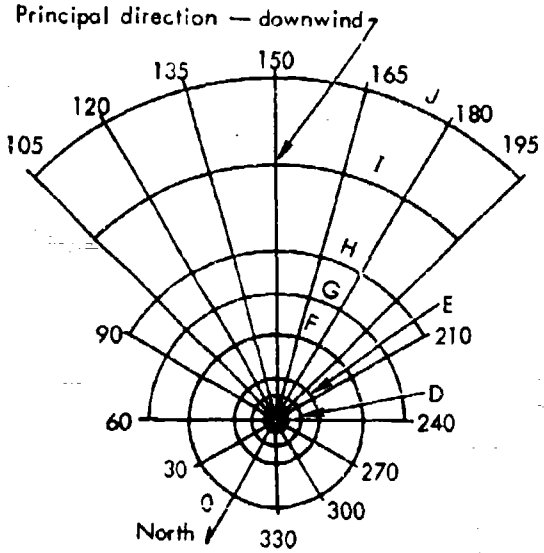

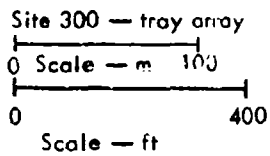

Arc designation	Distance from SGZ (m)	(ft)
A	2	6.5
B	4	14
C	7	21.5
D	13	44
E	23	75
F	46	150
G	69	225
H	91	300
I	137	450
J	183	600

Fig. 3.11. Site 300 fallout collection array.[4]

detonations conducted at the Site 300 test facility included a test of the fallout tracer program. The 270 g (0.6 lb) of sand placed in the explosive in each of these detonations was coated with 0.25 g of the trace element iridium. The steeply rolling terrain at the test site and the location of buildings dictated the placement of the fallout sample collection array. The collection array, in turn, dictated the wind conditions to be met at the time of each detonation. The collection array is shown in Fig. 3.11. A 0.61- × 0.61-m (2- × 2-ft) aluminum tray was placed at the intersection of each arc and radial line. Louvers were installed in each tray to prevent the escape of particles entering the tray. This type of collection tray had been used previously in the collection of radioactive fallout from nuclear cratering detonations at NTS.

Following each detonation, the material collected from each tray was weighed, sieved for the desired particle sizes, and an aliquot of each particle size was activated with neutrons. Following neutron activation and about a 3-week wait to maximize the iridium signal to background noise, the samples were counted in the SRI sodium-iodide gamma ray spectrometer.[4] The number of disintegrations per minute for the iridium-192 gamma ray at 0.506×10^{-13} J (0.316 MeV) was then converted to grams of iridium

for each sample. With the grams of iridium recovered from each tray, isodeposition lines were plotted for each detonation as shown in Figs. 3.12 through 3.15. The integration of the amount of iridium deposited over the fallout area produced the amount of iridium vented by the detonation. The vent fraction, f_v, for each detonation was then determined through the formula[4]:

$$f_{v_{(Ir)}} = \frac{Ir\ (out)}{Ir\ (placed\ in\ charge)}$$

Table 3.3 shows the results of the Site 300 tracer program. A total of

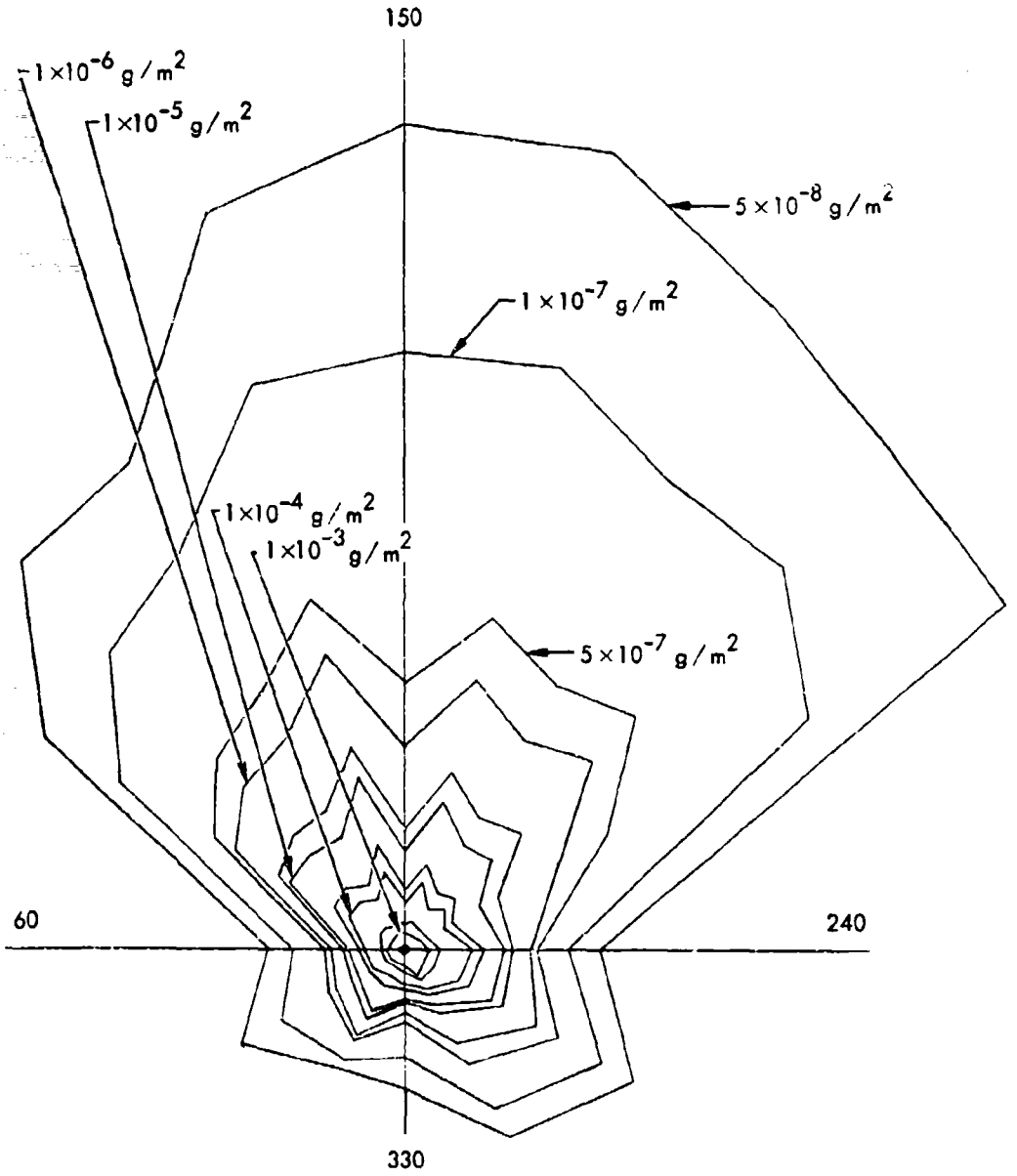

Fig. 3.12. Iridium deposition density contours from 1×10^{-3} to 5×10^{-8} g/m^2 for all particle sizes (Event B-3R).[4]

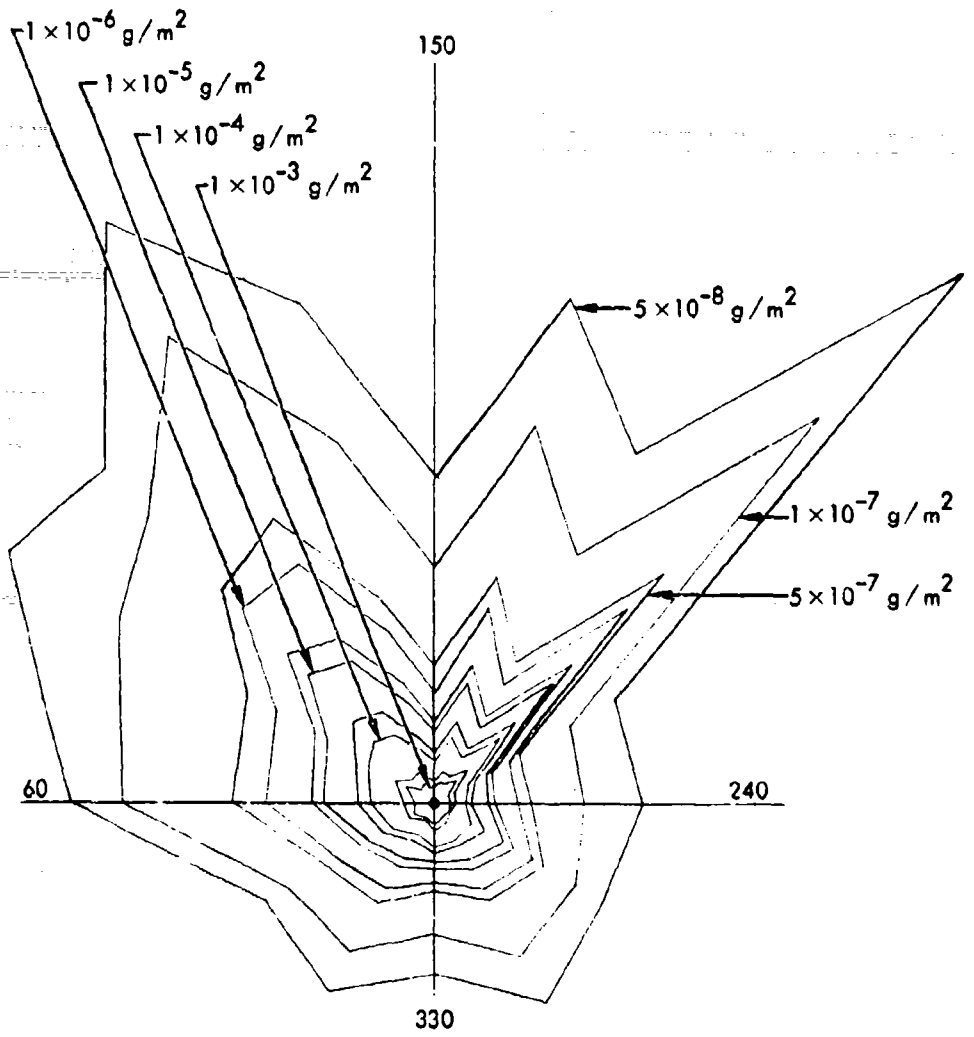

Fig. 3.13. Iridium deposition density contours from 1×10^{-3} to 5×10^{-8} g/m^2 for all particle sizes (Event B-3).[4]

Table 3.3. Site 300 tracer test results.

Event	Date	DOB (m)	DOB (ft)	Stemming	Wind direction	Wind speed (km/hr)	Wind speed (mi/hr)	Vent fraction	Number of samples
B-3	12/29/71	0.9	3.0	sand	150	6.4	4	21.0	300
C-2	3/7/72	0.9	3.0	air	120	12.9	8	36.4	254
D-2	4/19/72	0.9	3.0	water	130-165	11.8	7.3	43.4	298
B-3R	4/4/72	0.9	3.0	sand	195	11.6	7.2	20.8	312

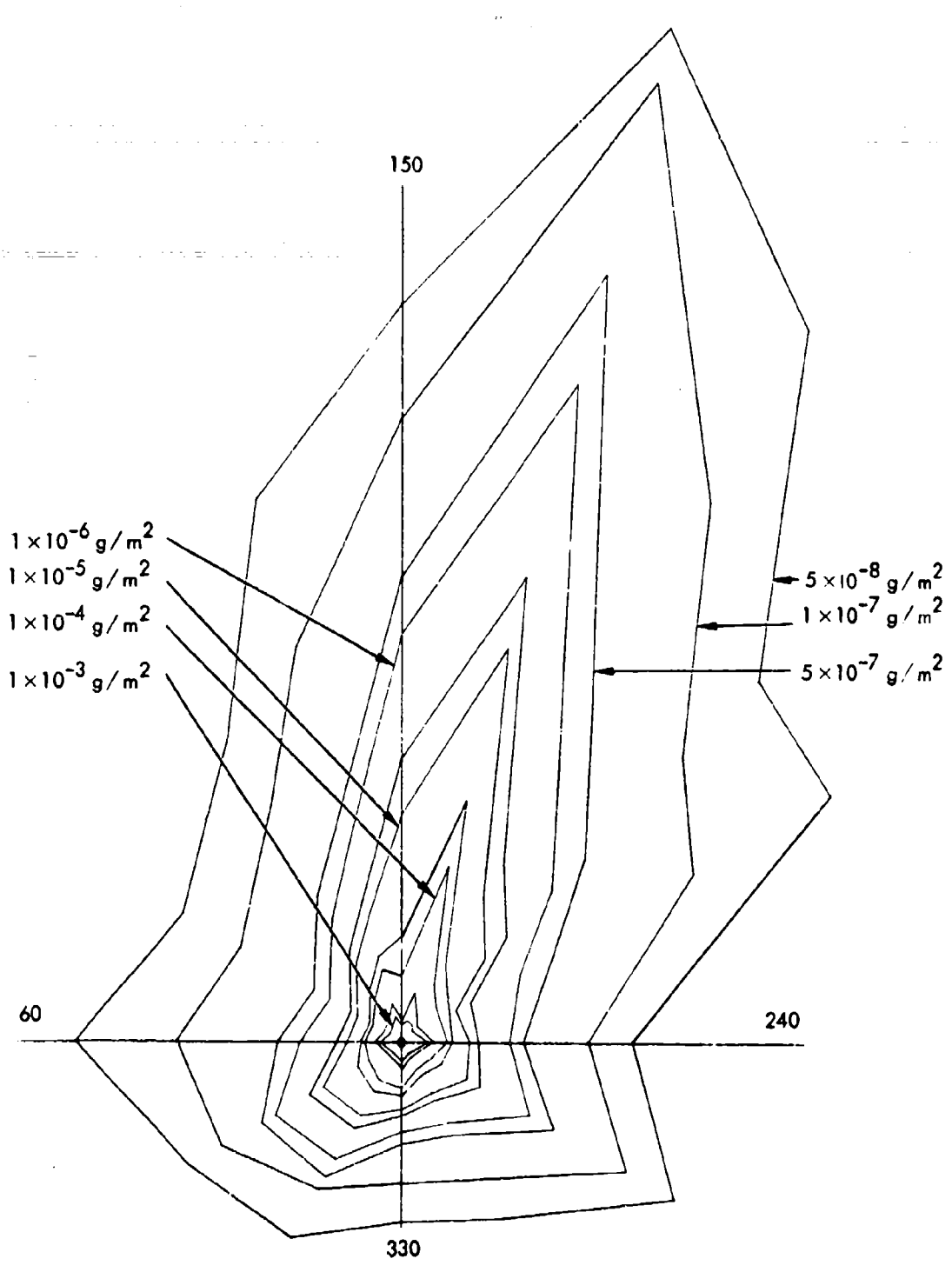

Fig. 3.14. Iridium deposition density contours from 1×10^{-3} to 5×10^{-8} g/m^2 for all particle sizes (Event C-2).[4]

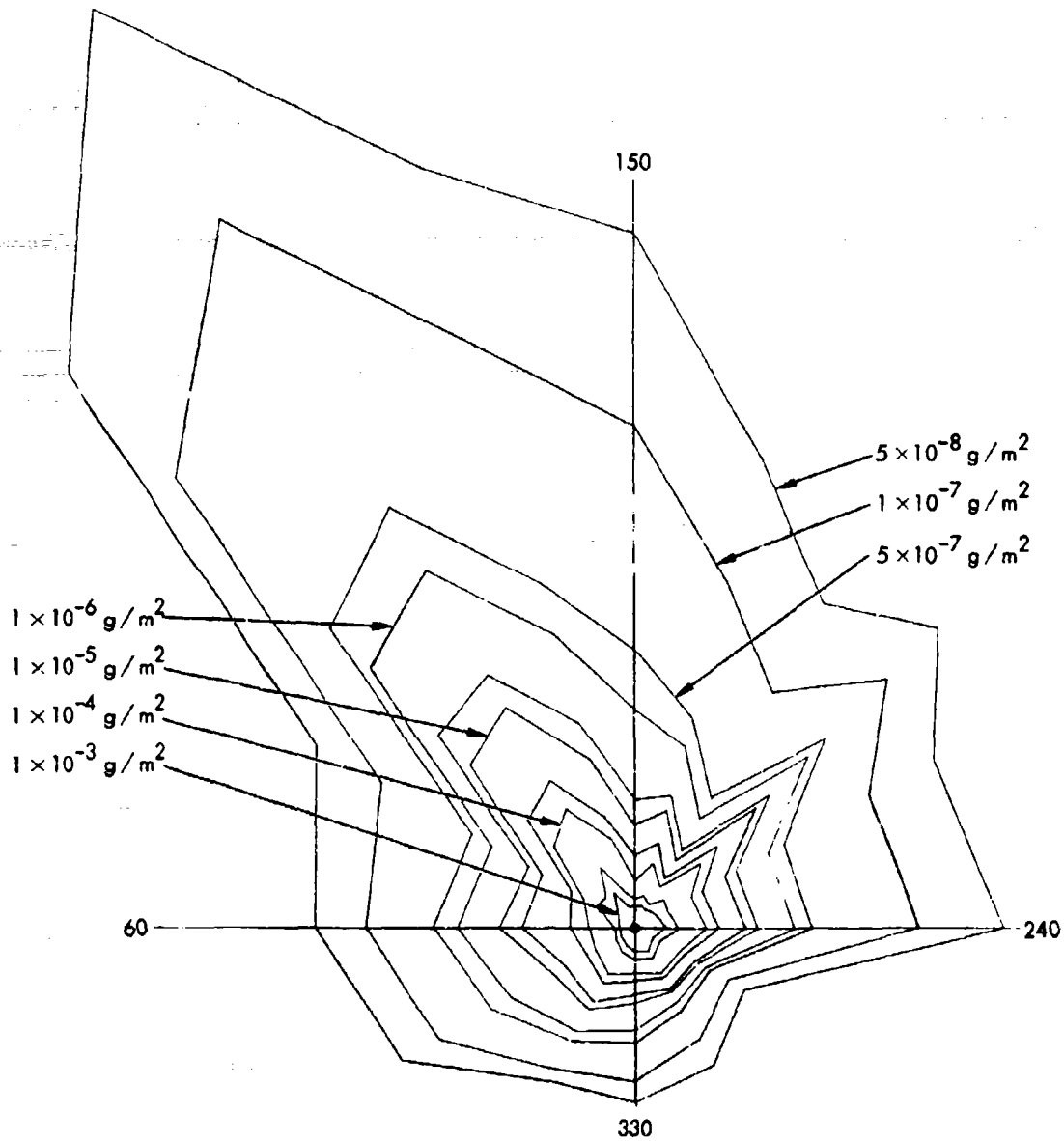

Fig. 3.15. Iridium deposition density contours from 1×10^{-3} to 5×10^{-8} g/m^2 for all particle sizes (Event D-2).[4]

1, 354 samples were processed as described above. The event listed as B-3R is a repeat of the B-3 event. The purpose of this duplication was to verify the reproducibility of the tracer system.

The differences in the vent fractions for the B-3, C-2, and D-2 points demonstrate the sensitivity of the tracer program to the different types of stemming employed. The reproducibility of the vent fractions obtained from this system

is demonstrated in the duplication of the results obtained in the B-3 and B-3R tests. The vent fractions obtained in this series of tests cannot be related directly to nuclear events with like stemming conditions. Not only are the charges very small, but no consideration was given to matching uphole velocities, scaling of emplacement hole size, or other modeling considerations. Comparison within the test results themselves does point out some generalities. The vent fraction for an unstemmed detonation, as would be expected, is higher than the vent fraction for a fully stemmed detonation. However, the water-stemmed detonation which produced a crater very close to that of the fully stemmed detonation yielded a significantly higher vent fraction. The similarity in crater size would indicate a similarity in cratering phenomena, yet the differences in vent fraction indicate a possibly significant difference in cratering phenomena between the two stemming conditions. This paradox has not been resolved to date.

ONE-TON TRACER TESTING

During the same time period that the Site 300 2.7-kg (6-lb) test series was being planned and conducted, EERL was conducting a series of sixteen 907-kg (1-ton) detonations at Trinidad, Colorado. The background, the purpose, and the results of this test series are reported in Ref. 7. Charges were detonated at various depths of burial and with various types of stemming. This opportunity was used to develop the tracer program data collection and analysis techniques in detonations at the 907-kg (1-ton) level prior to the conduct of any large detonations in the 63×10^9 J to 84×10^9 J (15- to 20-ton) yield range.

Four traced detonations were conducted in a massive sandstone formation. The charges were identical except for the type of stemming employed. Table 3.4 lists emplacement characteristics for each of the traced events. Each charge consisted of 907-kg (1 ton) of IRECO slurry blasting agent, TD-2. Table 3.5 shows the characteristics of this aluminized ammonium nitrate slurry explosive.

The cylindrical charge cavities were 0.91 m (3 ft) in diameter and 1.07 m (3.5 ft) in height. Each charge contained 91 kg (200 lb) (10% by weight) of the sand particles tagged with approximately 90 g of iridium. The sand particles were uniformly distributed throughout the explosive. Charges were detonated with a 5.4-kg (12-lb) pentolite booster, which was initiated with primacord. The resulting crater dimensions are shown in Table 3.6. The significantly larger crater produced by the M-16 detonation is attributed to the greater effectiveness of the concrete stemming compared to the other types of stemming. High-speed photography of this event showed that the 10-cm (4-in.) open hole "pinched off" and did not permit complete escape of the explosive gases.[7]

Fallout sample collection was accomplished utilizing the same 0.61-m^2 (2-ft^2) aluminum louvered trays as used in the Site 300 testing. Figures 3.16 and 3.17 show the collection array used for each of these detonations. Debris collected in each tray was weighed, packaged, and returned to SRI for processing. The mass of

Table 3.4. Middle Course II tracer detonations.

Event	DOB (m)	DOB (ft)	Stemming	Emplacement hole size (m)	Emplacement hole size (ft)
M-4	6.1	20	Water	0.91	3
M-9	6.1	20	Air	0.91	3
M-13	6.1	20	Native material	0.91	3
M-16	6.1	20	Partially stemmed[a]	0.91	3

[a]The 0.91-m (3 ft) emplacement hole was partially stemmed with concrete 4.57 m (15 ft) and native material—top 1.5 m (5 ft)—leaving a 10.2-cm (4-in.) unstemmed (open hole). This test was sponsored by the Sandia Laboratories, Albuquerque.

Table 3.5. TD-2 explosive characteristics.[7]

Aluminum content, %	18 to 20
Density, g/cm^3	1.35
Detonation velocity, m/sec	4,450.
Detonation pressure, kbar	75
Heat of detonation, cal/g	1,500 ± 50
TNT equivalence	1.4

iridium in each tray was determined as discussed in the previous section. Iridium isodeposition lines were plotted and the mass of iridium vented was determined by integration of the fallout area. Problems were encountered in determining the local fallout area due to the lack of an accurate definition of the limit of the continuous ejecta. The term vent fraction, f_v, is defined as the percentage of the radioactivity produced by a detonation that is deposited in the local fallout area. The local fallout area is defined as the area from beyond the limits of the continuous ejecta produced by the crater to the limit of significant gravity fallout. The value of the outer limit is not critical in determining the vent fraction because the amount of fallout deposited at large ranges is orders of magnitude less than the amounts found very close to the crater. The value of the limit of the continuous ejecta is, however, very critical in determining the fraction vented. Samples of the debris were collected very

Table 3.6. Middle Course II crater dimensions.[7]

Event	Depth of burial (m)	Depth of burial (ft)	Apparent crater radius, R_a (m)	Apparent crater radius, R_a (ft)	Apparent crater depth, D_a (m)	Apparent crater depth, D_a (ft)	Crater volume, V_a (m^3)	Crater volume, V_a (yd^3)	Lip crest radius, R_{al} (m)	Lip crest radius, R_{al} (ft)
M-4	6.1	20	6.9	22.7	3.4	11.3	187	244	8.2	27
M-9	6.1	20	6.6	21.5	3.0	10	200	261	9.3	36.5
M-13	6.1	20	7.2	23.5	3.8	12.6	232	304	9.6	31.5
M-16	6.1	20	8.2	27.0	4.5	14.8	401	524	10.1	33

Note: For convenience, the Middle Course II collector grid was labeled counterclockwise beginning at an arbitrary zero point.

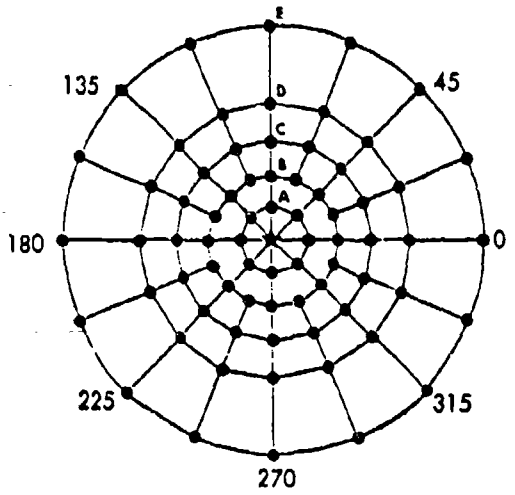

● Debris collector
★ SGZ

Arc designation	Distance from SGZ (m)	(yd)
A	23	25
B	46	50
C	69	75
D	100	110
E	160	170
F	190	210
G	230	250
H	280	310
I	340	370
J	400	440
K	440	480
L	460	500
M	530	580
N	670	730
O	800	880
P	1,010	1,100
Q	1,190	1,300
R	1,460	1,600
S	1,740	1,900
T	1,830	2,000

Fig. 3.16. Close-in fallout collection array for Project Middle Course II.[4]

close to the crater well within the continuous ejecta, but those samples determined to be within the continuous ejecta during postshot data analysis were not included in the summation of the iridium deposition. Table 3.7 shows the vent fraction determined for various limits of continuous ejecta for each of the Middle Course II detonations. Examination of the vent fractions shown in this table demonstrates the sensitivity of these calculations to the value of the limit of continuous ejecta. An approximate limit of continuous ejecta of 36.6 m (40 yd) has been selected based on the observed mass deposition in the fallout collection trays located at ranges of 22.9 and 45.7 m (25 and 50 yd).

In looking at the vent fraction data it must be understood that as in the Site 300 tests, no attempt was made to model nuclear detonation parameters. A general comparison could be made for the stemmed detonation except that it was stemmed with layers of the material removed from the access hole and not the intricately keyed and designed stemming employed in previous nuclear detonations.[7]

The M-9 (unstemmed) detonation shows a consistently lower vent fraction regardless of the radius of continuous ejecta used. These values demonstrate a significant constraint in the use of the fallout simulation system; i.e., the need to have proper wind direction. The wind direction on the other three traced detonations was such that the debris cloud was directed over the collection array. The wind for the M-9 event was not in the proper direction at shot time and carried the fallout across only a portion of the collection array. In comparing the vent fractions obtained at Tr dad and at Site 300 there is consistency in the results in that the vent fraction for the

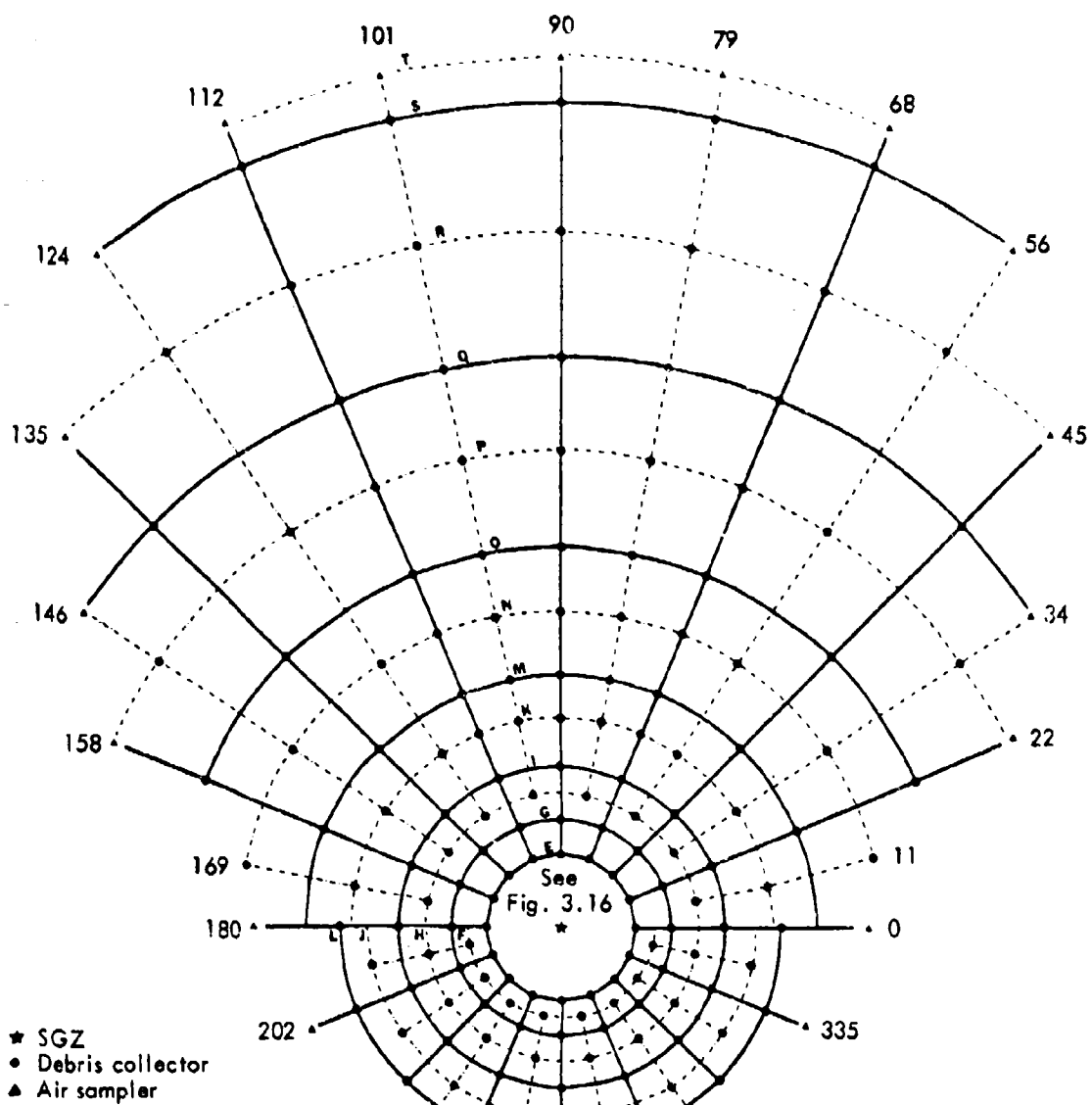

Fig. 3.17. Intermediate range fallout collection array for Project Middle Course II.[4]

water-stemmed detonations is higher than the stemmed detonations in both tests. These data demonstrate the sensitivity of the fallout simulation system to the various stemming conditions to include sensitivity to different sized unstemmed emplacement holes (M-13 vs M-16).

The deposition of iridium in the Middle Course II events has been related to nuclear fallout dose rate contours and is reported in Ref. 4. This was done by scaling the iridium deposition curves to a normalized iridium deposition curve. The normalized iridium deposition curve

Table 3.7. Middle Course II iridium vent fractions[4] for various radii of continuous ejecta.

Event[a]	Assumed radius of continuous ejecta (yd)	Assumed radius of continuous ejecta (m)	Area of continuous ejecta (m^2)	Calculated weight of iridium (g)	Iridium vent fraction; total weight = 83.5 g (%)
M-4	25	22.9	1,640	66.7	79.9
M-9[b]	25	22.9	1,640	28.1	33.6
M-13	25	22.9	1,640	48.6	58.2
M-16	25	22.9	1,640	47.5	56.8
M-4	30	27.4	2,360	59.6	71.5
M-9[b]	30	27.4	2,360	20.2	24.2
M-13	30	27.4	2,360	40.2	48.1
M-16	30	27.4	2,360	43.1	51.6
M-4	35	32.0	3,220	51.2	61.3
M-9[b]	35	32.0	3,220	14.1	16.9
M-13	35	32.0	3,220	34.2	40.9
M-16	35	32.0	3,220	39.7	47.5
M-4	40	36.6	4,200	43.6	52.1
M-9[b]	40	36.6	4,200	10.1	12.0
M-13	40	36.6	4,200	28.9	34.6
M-16	40	36.6	4,200	36.4	43.6
M-4	45	41.1	5,320	37.1	44.4
M-9[b]	45	41.1	5,320	7.7	9.3
M-13	45	41.1	5,320	25.1	30.1
M-16	45	41.1	5,320	34.7	41.6
M-4	50	45.7	6,570	32.3	38.6
M-9[b]	50	45.7	6,570	6.4	7.7
M-13	50	45.7	6,570	21.2	25.4
M-16	50	45.7	6,570	30.4	36.5
M-4	55	50.3	7,950	27.7	33.1
M-9[b]	55	50.3	7,950	5.3	6.4
M-13	55	50.3	7,950	18.3	21.9
M-16	55	50.3	7,950	28.2	33.8

[a]Values for all events are based on measured points from the 45.7-m (50-yd) ejecta range out.

[b]Due to winds at firing time, Event M-9 was not contained within the collection array.

was then related to the normalized nuclear curve by means of a scaling factor of 5×10^4. Both curves were then used to make fallout predictions for an assumed situation. The predictions developed are illustrated in Fig. 3.18. It can be seen that the correlation between the normalized iridium model and the normalized nuclear data is excellent out to a dose rate of approximately 10 Roentgens per hour (R/hr).* However, the far-out regions of the iridium contours (at ranges beyond those equivalent to downwind dose rates of about 10 R/hr) do not match the nuclear contours.

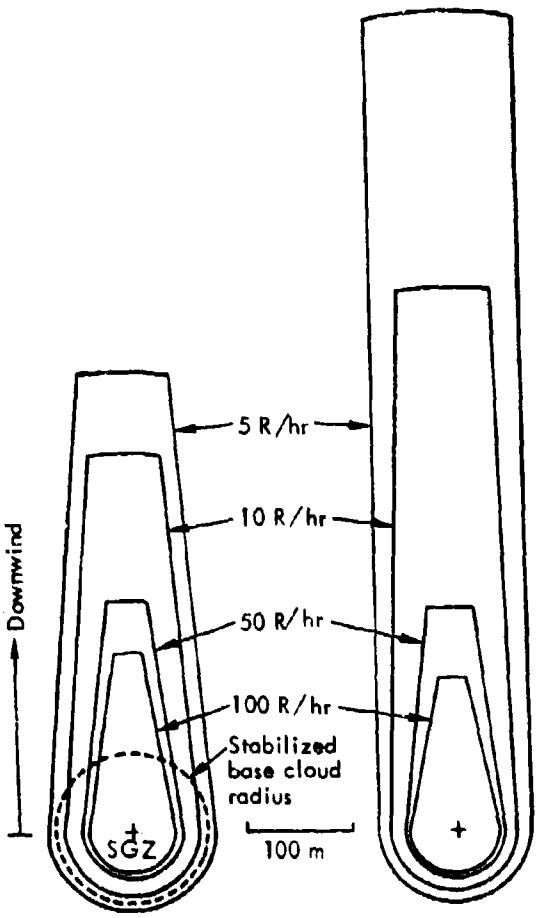

Fig. 3.18. Comparison of dose rate contours for iridium model and equivalent nuclear event at H+1 hr.[4]

*1 Roentgen = 2.579×10^{-4} coulomb/kilogram (c/kg).

Chapter 4

Multiton Slurry Testing

GENERAL

In October 1971, a series of multiton cratering experiments was conducted at Fort Peck, Montana, as Phase IIA of Project Diamond Ore. Three cratering charges, each having a weight of about 9,070 kg (10 tons) of the sand-contaminated slurry explosive, were detonated. Two of these detonations were at a DOB of 12.5 m (41 ft) with one detonation unstemmed, DOIIA-1, and one detonation stemmed, DOIIA-2. The third detonation, DOIIA-3, had a DOB of 6 m (19.7 ft) and was stemmed. The purpose, experimental description, and results of these detonations are described in detail in Appendix C. This chapter is a discussion of the explosives instrumentation program performed on these three detonations.

EXPLOSIVES INSTRUMENTATION PLAN

The slurry charges detonated in Phase IIA were instrumented to obtain data for use in verifying the equation of state (EOS) data to be obtained by the Chemistry Department at LLL from smaller laboratory tests. These laboratory tests had not been initiated at the time the Phase IIA detonations were conducted. Two types of measurements, detonation velocity and detonation pressure, were attempted in each detonation.

"Rate sticks" were used to measure the explosives detonation velocity. These rate sticks were constructed of a series of piezoelectric, coaxial transducer pins (PZ) as shown in Fig. 4.1. Piezoelectric pins are signal self-generating and operate at lower pressures than conventional self-shorting pins. The active element is a $BaTiO_3$ disk that accumulates a charge upon its poled faces when compressed. The output signal shape is related to the input pressure in a complex

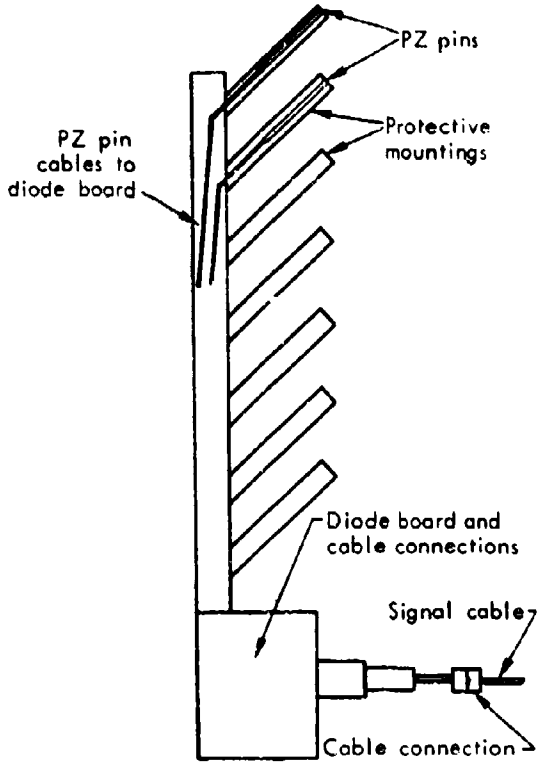

Fig. 4.1. Typical rate stick construction for Phase IIA detonations.

manner, being related to the impedance of the recording instrument and the Curie point of the material. The Curie point in turn is a function of temperature and pressure. The pins therefore cannot be used as pressure transducers. Only the PZ pin polarity may be controlled for pulse identification purposes. PZ pins may be used as position transducers in a manner similar to self-shorting pins. Their chief advantages are that they make input directly into the recording instrument without intermediate circuitry, and they operate at lower pressures. A 40-kbar shock pressure will usually produce a 40-V pulse across 50 Ω with a 50-μsec rise time. The detonation shock wave causes the PZ pin to discharge its voltage signals. The arrival times for all pins on each rate stick were recorded on a Raster oscilloscope. The distance between pins on each rate stick was

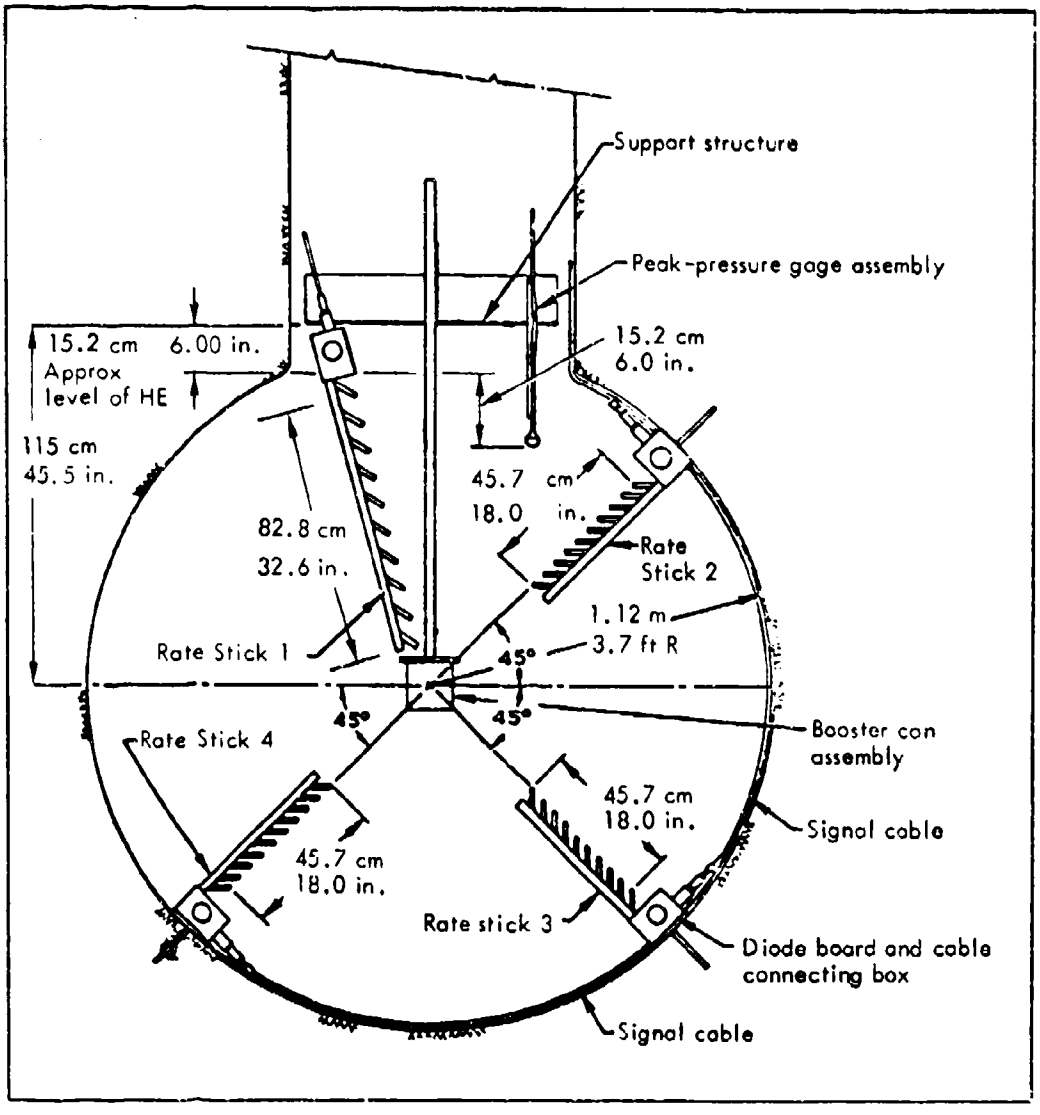

Fig. 4.2. Explosive cavity instrumentation, Phase IIA (typical).

measured and recorded prior to emplacement of the stick. The velocity of the detonating wave was then calculated from the time and distance data. As shown in Fig. 4.2, four rate sticks were placed in a vertical plane in each cavity. The rate sticks numbered 2, 3, and 4 were carefully aligned so that the end of each PZ pin was on a radial line from the center of the charge and at an angle of about 45 deg from the horizontal. Rate Stick 1 was attached to the support ring, which also held and located the charge booster in the center of the cavity.

A plastic gage was used to make single peak pressure measurements near the top of each charge as shown in Fig. 4.2. These plastic gages were mounted on the booster support ring at a distance of about 74 cm (29 in.) from the charge center. In order to operate properly, these gages require a stress pulse that rises above approximately 50 kbar in about 20 nsec. Previous experience with this gage at LLL had shown a record of high reliability.

EXPLOSIVE INSTRUMENTATION RESULTS

The data recorded from each rate stick are listed in Tables 4.1, 4.2, and 4.3 for each detonation and plotted in Fig. 4.3 to show a comparison of the velocities recorded for each rate stick. The velocities recorded by the rate sticks for the first detonation, DOIIA-1 (un-(stemmed at 12.5 m – 41 ft), show excellent reproducibility within the charge and a detonation velocity of about 4 mm/μsec. The pressure gage for this detonation produced a clear signal indicating a peak pressure of about 80 kbar.[8] This level is in general agreement with the expected detonation pressure. The velocities recorded for the second detonation, DOIIA-2 (stemmed at 12.5 m (41 ft)), show significant differences in each quadrant of the explosive and are significantly slower than the velocity measured in the DOIIA-1 detonation. The pressure gage for the detonation produced only noise. Lack of a signal indicates that the detonation wave rise time was too long and/or the pressure level was too low to be recorded.[8] Only Rate Stocks 2 and 3 produced data in the third detonation, DOIIA-3 – stemmed at 6 m (19.7 ft). The loss of Rate Sticks 1 and 4 was discovered prior to detonation and is attributed to failure of the cable connection or of the diode board during explosive loading. The velocities recorded indicate different velocities for the two quadrants although the difference is not as significant as in the DOIIA-2 detonation. The detonation velocities were again slower than the DOIIA-1 detonation. The plastic gage failed to provide a signal on this detonation for the same apparent reason as in the DOIIA-2 detonation.[8]

Possible causes for the erratic behavior of the explosive were considered. The DOIIA-1 detonation was unstemmed and the DOIIA-2 and DOIIA-3 detonations were both fully stemmed. Because the two stemmed detonations produced erratic results, the stemming procedures were examined. The stemming material used to backfill the 0.91-m (3 ft) diameter emplacement holes was a medium matching cement grout. The grout was poured down the emplacement hole with a "Trimie"* with a piece of plywood placed

*A canvas pipe used to guide concrete and limit its freefall distance.

Table 4.1. Rate stick measurements, Diamond Ore IIA-1[9] [DOB—12.5 m (41 ft), unstemmed].

Rate stick	Distance (mm)	Real time (μsec)	Detonation velocity (mm/μsec)
1	114.3	31.4	
	205.6	53.7	4.1
	297.8	76.7	4.0
	389.7	100.0	3.9
	481.7	122.3	4.1
	574.1	142.7	4.5
	666.0	162.1	4.7
	758.0	181.1	4.8
	850.5	200.5	4.7
2	476.3	102.8	
	527.1	115.2	4.1
	577.0	127.0	4.2
	628.0	138.0	4.6
	679.1	148.9	4.7
	729.9	159.3	4.9
	780.2	169.3	5.0
	831.4	179.2	5.2
	882.2	188.8	5.3
	933.3	198.5	5.2
3	609.5	136.2	
	660.1	147.3	4.6
	710.9	158.0	4.8
	761.6	168.1	5.0
	812.8	178.1	5.1
	863.3	187.7	5.2
	914.3	197.4	5.3
	965.2	207.1	5.2
4	625.1	140.2	
	675.4	151.3	4.5
	726.6	161.9	4.8
	777.3	172.2	4.5
	828.5	182.4	5.0
	878.8	192.4	5.0
	929.9	201.1	5.3
	980.5	211.8	5.2

Table 4.2. Rate stick measurements, Diamond Ore IIA-2[9] [DOB = 12.5 m (41 ft), stemmed].

Rate stick	Distance (mm)	Real time[a] (μsec)	Detonation velocity (mm/μsec)
1	95.3	19.5	
	187.0	40.3	4.1
	278.9	78.9	2.4
	371.3	130.0	1.8
	463.3	184.3	1.7
2	368.3	110.1	
	419.3	132.8	2.2
	469.2	156.2	2.1
	520.8	181.0	2.1
3	473.1	147.3	
	524.1	174.1	1.9
	574.3	205.7	1.6
4	495.3	149.9	
	545.4	172.9	2.2
	596.9	197.1	2.1

[a]Additional pins not recorded due to signal arrival after completion of Raster oscilloscope sweep time of 210 msec.

on top of the explosive to prevent the falling grout from penetrating into the explosive. It is suspected that the grout may have penetrated the explosive at various points causing discontinuities that resulted in the erratic detonation velocities. The pressure of the first layer of stemming grout on the explosive was about 0.5 bars (6 psi). This pressure may have been sufficient to cause discontinuities in the density of the explosive, again possibly resulting in the erratic detonation velocities. The explosive itself was also suspected because no detailed early initiation-time laboratory measurements of its detonation characteristics had been made.

Table 4.3. Rate stick measurements, Diamond Ore IIA-3[9] [DOB = 6 m (19.7 ft), stemmed].

Rate stick	Distance (mm)	Real time[a] (μsec)	Detonation velocity (mm/μsec)
1	—[b]	—	—
2	441.3	129.7	
	491.5	142.8	3.8
	541.5	158.0	3.3
	592.7	173.6	3.3
	643.4	188.7	3.4
3	434.9	130.3	
	485.6	141.8	4.4
	536.1	152.9	4.6
	586.8	163.6	4.8
	637.8	173.8	5.0
	688.4	183.6	5.2
	739.1	192.9	5.4
4	—[b]	—	—

[a]Additional pins not recorded due to signal arrival after completion of Raster oscilloscope sweep time of 120 msec.
[b]No data.

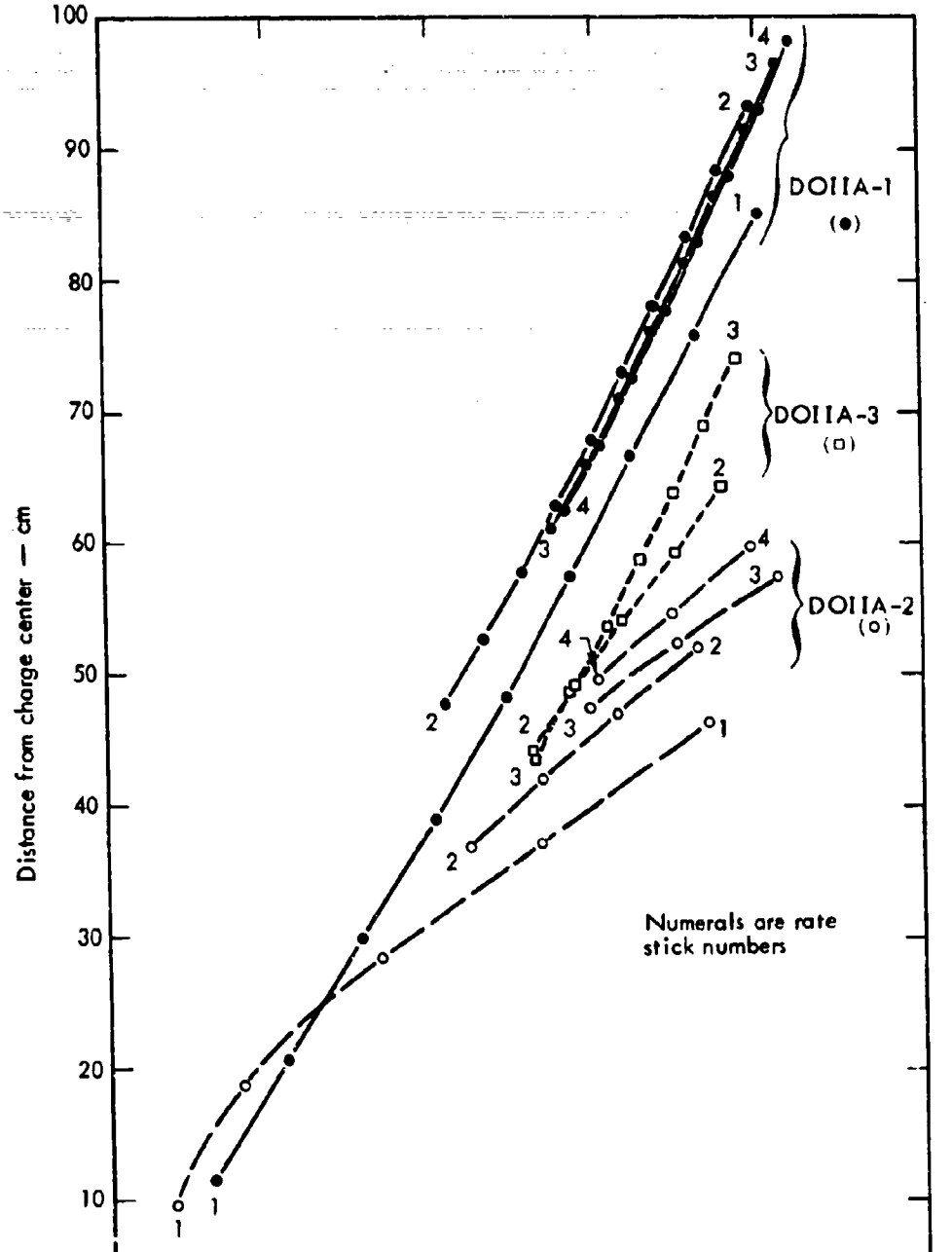

Fig. 4.3. Detonation velocities for slurry explosive detonations in Phase IIA.

Chapter 5

Explosives Equation-of-State and Detonation Velocity Testing

GENERAL

When the large-scale experiments at Fort Peck, Montana, had been completed and the problems in reproducibility of the Diamond Ore slurry explosive had been recognized, a comprehensive series of tests were conducted in an attempt to solve the problems in addition to determining a usable EOS for this slurry explosive. As detailed in Chapter 4, the explosive had performed as expected in the unstemmed detonation but had detonated in an erratic manner in the two Phase IIA stemmed detonations at Fort Peck. Before this apparent stemming dependency could be evaluated, the reproducibility of the Diamond Ore explosive had to be determined. This was to be accomplished in conjunction with the hydrodynamic tests designed to provide data for the EOS, which was required for computer code development. Little previous work had been done in attempting to define the detonation parameters of the ammonium-nitrate-base composite explosives. Some previous work had been done, however, in developing EOS testing techniques for simpler types of composite explosives.[10]

SIX-INCH SPHERE VELOCITY TESTING

The cratering experiments using slurry explosives in the 15.2-cm (6-in.) diameter spheres described in Chapter 3 had been interupted by the large-scale testing at Fort Peck. Upon completion of the DOIIA experiments, this testing was continued. In an attempt to obtain a quick look at the reproducibility of this slurry explosive, detonation velocity measurements were made on 12 of the 15.2-cm (6-in.) spheres using a simple rate stick. These rate sticks were constructed by taping five PZ pins to a micarta rod. A rate stick was placed in each sphere as shown in Fig. 5.1. The first six spheres detonated contained the pure explosive with the second six spheres containing the 10% sand-contaminated explosive. The tests were duplicated with the pure and contaminated explosive to determine

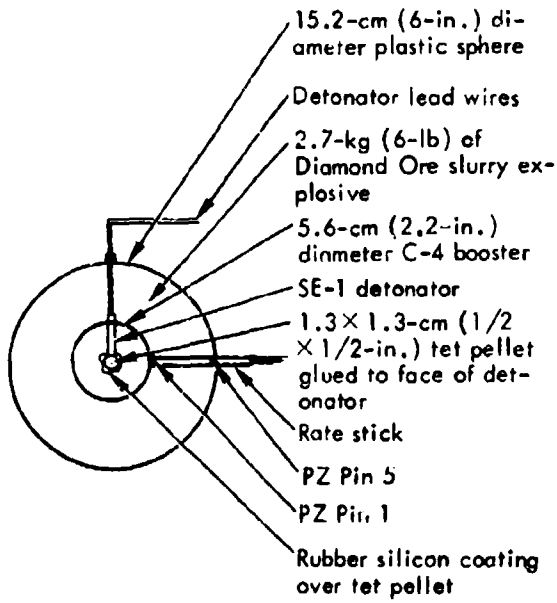

Note: Rate stick was placed with end of rate stick and first self-shorting pin against C-4 booster.

Fig. 5.1. Rate stick placement in 15.2-cm (6-in.) spheres.

Table 5.1. Detonation velocity—15.2-cm (6-in.) cratering spheres.[9]

Event	Explosive	Detonation velocity (mm/μsec)	Comment[a]
DOVR-1	Pure slurry	3.42	OS, ACCEL
DOVR-2	Pure slurry	4.61	SOS, OSC
DOVR-3	Pure slurry	5.76	SOS, DE ACCEL
DOVR-4	Pure slurry	2.99	OS, DE ACCEL
DOVR-5	Pure slurry	?	Spurious signal
DOVR-6	Pure slurry	3.54	OS, DE ACCEL
DOVR-7	Slurry with 10% sand	3.39	OS, DE ACCEL
DOVR-8	Slurry with 10% sand	4.74	OS, DE ACCEL
DOVR-9	Slurry with 10% sand	3.36	OS, OSC
DOVR-10	Slurry with 10% sand	3.71	OS, DE ACCEL
DOVR-11	Slurry with 10% sand	4.67	SOS, DE ACCEL
DOVR-12	Slurry with 10% sand	3.33	DE ACCEL

[a]OS—Overdriven detonation; ACCEL—Accelerating detonation; SOS—Sustained outer drive; OSC—Oscillating detonation; DE ACCEL—Deaccelerating detonation.

possible effects of the sand contamination. The results of tests are shown in Table 5.1.

As indicated by the comment column in Table 5.1, considerable problems were experienced in attempting to measure the detonation velocity this close to the booster. In most cases, the booster appears to have overdriven the explosive, and the detonation wave is decelerating to what would be considered the sustained or true detonation velocity of the explosive. The slurry thickness surrounding the booster was 4.8 cm (1.9 in.). From these data it was concluded that the critical diameter for a sustained detonation for this explosive is considerably larger than the 4.8 cm (1.9 in.) used in these tests. The velocity data obtained from these tests cannot, therefore, be considered as indicative of any significant variations in the detonation velocity of the explosive.

INITIAL EOS TESTING

The EOS for an explosive is a mathematical description of the expansion of detonation products that defines the energy-time release relationship for that explosive (in terms of volume, pressure, and temperature). The detonation of composite explosives is generally defined in two steps: ignition followed by a reaction between the fuel and oxidizer. This reaction produced heat, gases, and solids under high pressures. The heat transfer to the gas and the resulting expansion of the detonation products result in useful work. These chemical reactions occur in less than a microsecond for simple composite explosives but may take many milliseconds for the more complex composite explosives, such as the Diamond Ore water-gelled explosive.[10]

In order to determine the energy-time release relationships for an explosive, a series of "hydro-shots" are conducted. These detonations are conducted under laboratory conditions with the explosive carefully placed in a metal container (cylinder or hemisphere) constructed of a specific metal, usually copper or aluminum, to rigid specifications for container volume, wall thickness, and geometry. Measurements of the volume expansion rate of the container during the very early detonation time are made. Based on the known container wall thickness and the characteristics of the metal, calculations are performed to derive data on energy release vs time. The volume expansion of the container is measured through the use of very high-speed streak photography. The streak camera is focused on a 2.54×10^{-2} mm (1-mil) thick cross section of the container as shown in Fig. 5.2a. As the wall expands, a rotating prism passes the focused image along a length of film at a precise speed. The resulting photograph shows the expansion of a small section of the wall vs time. A schematic of a typical streak camera record is shown in Fig. 5.2b. Other types of instrumentation are often employed to obtain other specific data, such as the corresponding velocity of the detonation wave and the detonation peak pressures at specific points of interest.

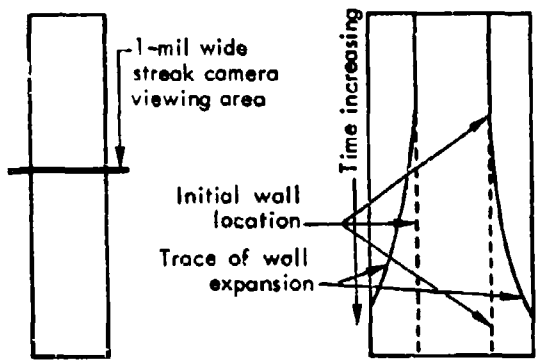

a. Metal cylinder filled with explosive

b. Streak camera record of wall expansion relative to time

Note: Cylinder detonated by plane wave detonator and booster at bottom of cylinder

Fig. 5.2. Cylinder wall expansion testing for equation of state (EOS) data.

The relatively long time for completion of the physical and chemical processes occurring in the detonation of a water-gelled, ammonium-nitrate-based explosive results in size and yield dependence effects on the detonation parameters. In large charges, the detonation velocity and pressure increase until a charge radius is reached where the maximum levels are obtained and the detonation parameters become stabilized.[9] Because of this detonation phenomenon, a total of eight EOS detonations were planned for the Diamond Ore explosive. Table 5.2 lists the size and configuration for each of these shots. Figures 5.3 and 5.4 are drawings of typical shot configurations showing other instrumentation employed. The cylinder tests (two-dimensional) were conducted to insure that the parameters measured in the sphere tests held true for the two-dimensional case. The cylinders were initiated by plane wave lenses to reduce the effects of reflected waves from the cylinder walls. The spheres were initiated by spherical boosters located precisely at the charge center.

In order to duplicate as closely as possible the field conditions at Fort Peck, the Diamond Ore explosive was delivered in a pump truck to the test area, LLL

Table 5.2. EOS test configurations.[9]

Event [a]	Shape	Dimensions L/d or d (cm)	Dimensions L/d or d (in.)	HE	Container material	Booster
KDO-2	Cylinder	5.1 × 30.5	2 × 12	Pure	Copper	P-040[b] and 400 g 9404
KDO-3	Cylinder	5.1 × 30.5	2 × 12	—[c]	Copper	P-040 and 400 g 9404
KDO-4	Cylinder	10.2 × 61.0	4 × 24	Pure	Copper	P-040 and 400 g 9404
KDO-5	Cylinder	20.3 × 122.0	8 × 48	Pure	Copper	P-080[b] and 1600 g 9404
KDO-6	Sphere	20.3	8	Pure	Aluminum	9404 (sphere)
KDO-7	Sphere	20.3	8	Pure	Aluminum	9404 (sphere)
KDO-8	Sphere	61.0	24	Sand	Aluminum	3 lb 9404 (sphere)
KDO-9	Sphere	61.0	24	Sand	Aluminum	125 g 9404 (sphere)

[a] KDO-1 was calibration shot for rate sticks used in Phase IIA detonations at Fort Peck, Mont.
[b] P-040 and P-080 are plane wave lenses.
[c] With 10% sand.

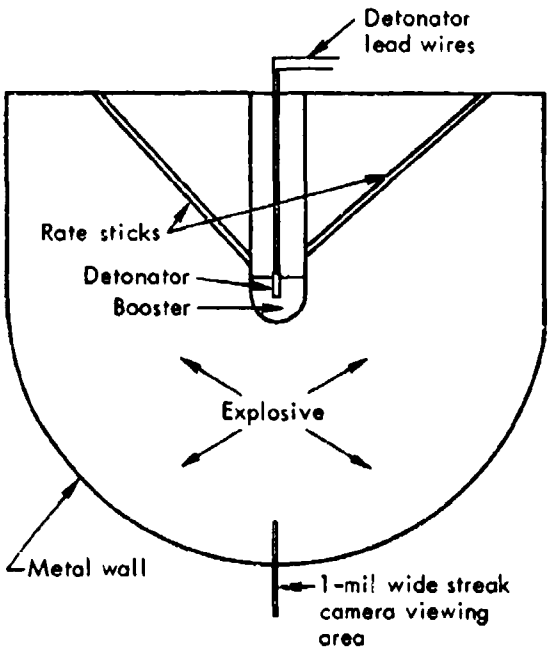

Fig. 5.3. Spherical configuration for EOS testing (typical).

(Site 300). The test containers were filled in the same manner as the charge cavities at Fort Peck; i.e., by pumping directly from the truck through a 5-cm (2-in.) diameter hose. As at Fort Peck, liquid ammonia was used to accelerate the gel formation of the explosive.

The explosive containers were then stored for about two weeks while other final preparations were being made and bunker time for the detonations was obtained. Storage of the explosive-filled containers was accomplished in controlled environment bunkers at Site 300. During periodic inspections of the containers a growth phenomenon was observed. The explosive had expanded and placed the container lids under pressure. When opened, the explosive grew out of the containers as shown in Fig. 5.5. This expansion phenomenon was believed to have been caused by gasification of the ammonia added during filling operations. Containers were x-rayed to determine whether the expansion had produced any voids, because voids would seriously affect the uniformity of the explosive's detonation. Voids of various sizes were found in all containers. The appearance of these voids was believed to be a prime candidate cause of the erratic detonation

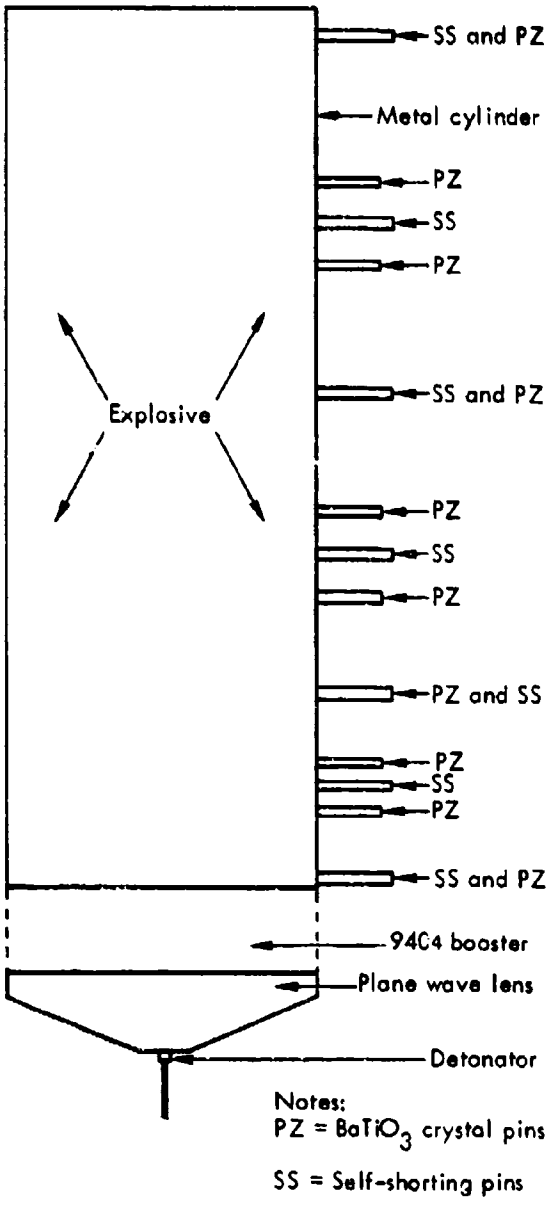

Fig. 5.4. Cylindrical configuration for EOS testing (typical).

velocities experienced at Fort Peck. The first six containers listed in Table 5.2 were detonated in an attempt to obtain EOS data, although the results were expected to be marginal. As stated in Chapter 4, one of the purposes of the Phase IIA detonations was to provide data for use in cratering code development. Without a usable EOS for the Diamond Ore explosive as used at Fort Peck, meaningful calculations for these events could not be conducted. The data obtained from the detonation of these containers are shown in Table 5.3. Densities shown in Table 5.3 were measured just prior to detonation. Attempts at measuring detonation velocities in the cylinder shots were made with two types of pins: standard and self-shorting. The standard PZ pins used previously in rate sticks were backed up by the self-shorting pins. The PZ pins are more sensitive and will report arrival of shock waves that are too small to cause closure of the self-shorting pins. As shown in Fig. 5.4, both types of pins were attached to the exterior wall of the cylinders.

The variation in the densities of the explosive as shown in Table 5.3 are considered significant. The KDO-2 and KDO-3 shot configurations were identical. The effect of the difference in density is demonstrated in the differences in measured detonation wave velocity and in the wall expansion velocities taken from the streak camera photographs. Detonation velocity data were not obtained on the KDO-4 and KDO-5 shots because neither type of pin produced data. The cause is believed to be a lack of sufficient detonation wave pressure to cause gap closure on the self-shorting pins or depolarization of the PZ pins. The KDO-6 and KDO-7 sphere shot configurations were identical. The effects of the differences in density are again evident in the differences in wall expansion velocities. The two detonation velocities given for each sphere shot are the velocities measured

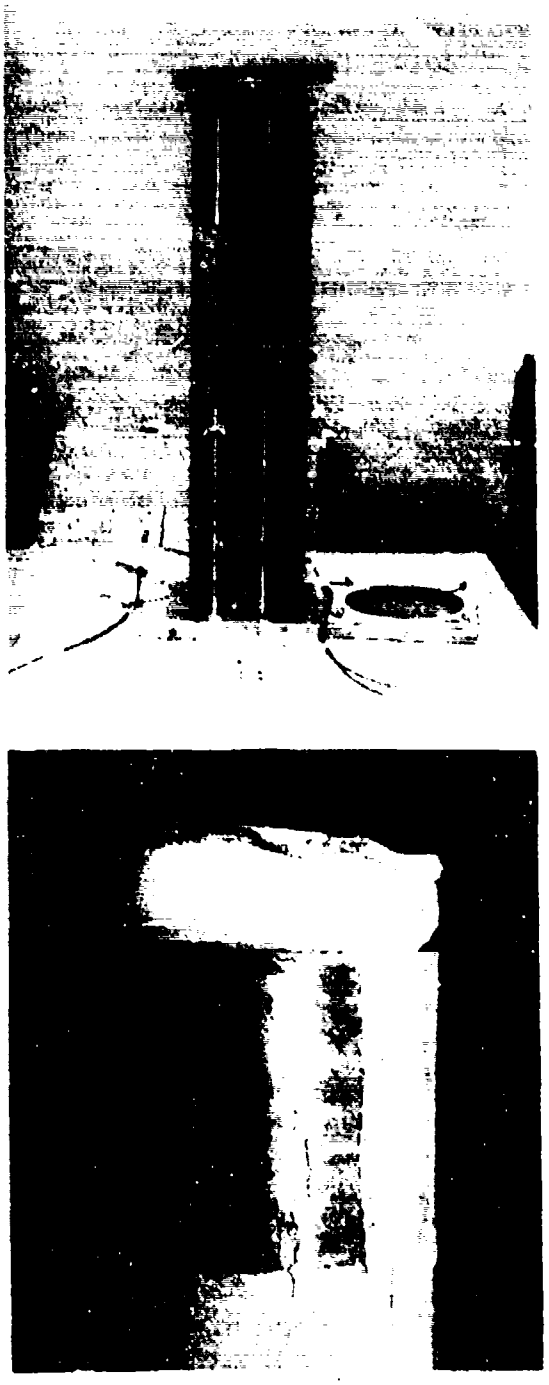

Fig. 5.5. Explosives expansion in EOS cylinder test containers.

by the rate sticks shown in Fig. 5.3. All wall velocities given in Table 5.3 are to be considered suspect because the voids in the explosive caused hot spots in the detonation that in turn caused jetting through the container walls. This jetting destroyed the smooth continuous wall expansion that would have given very accurate data. This jetting is also the reason for the loss of the wall expansion velocity data on the KDO-6 and KDO-7 sphere shots.

Based on these data, the tentative EOS parameters shown in Table 5.4 for the Diamond Ore explosive were calculated and provided to K Division, LLL, and Systems, Science, and Software, Inc., for use in postshot calculations for the Phase IIA detonations. These parameters have a low degree of validity as explained above. The parameters listed in Table 5.4 are used in the Jones-Wilkins-Lee (JWL) equation as follows[11]:

$$P(V_1E) = A(1 - \omega/R_1V)e^{-R_1V} + B(1 - \omega/R_2V)e^{-R_2V} + \omega E/V,$$

The two sets of coefficients are required to describe the two-phase detonation displayed by this type of explosive. The initial reaction coefficients are used to calculate the pressure that, in this case, is released during the initial fast reaction and accounts for about 20.8% (0.02 Mbar cm^3/cm^3) of the total energy (0.096 Mbar cm^3/cm^3) released. In a standard high explosive all of the energy would be released in this (a single) phase. The remaining 79.2% of the energy (0.076 Mbar cm^3/cm^3) for the Diamond Ore explosive is released over a 50-μsec period. The second-phase time-dependent release of energy is linear. This type of phased reaction is shown schematically in

Table 5.3. Initial EOS testing results.[9]

A. Cylinder Shots

Event	Cylinder dimensions (cm)	Cylinder dimensions (in.)	HE	Density (g/cm^3)	Detonation velocity (mm/μsec)	Wall velocity (mm/μsec) $R - R_0 = 19$[a]
KDO-2	5.1 × 30.5	2 × 12	Pure	1.595	4.931	1.06
KDO-3	5.1 × 30.5	2 × 12	With sand	1.403	1.92 (0.85-3.3)	0.70
KDO-4	10.2 × 61.0	4 × 24	Pure	1.315	—	0.75
KDO-5	20.3 × 122.0	8 × 48	Pure	1.452	—	0.93

B. Sphere shots

Event	Sphere dimensions (cm)	Sphere dimensions (in.)	HE	Density (g/cm^3)	Detonation velocity (mm/μsec)	Wall velocity (mm/μsec) $R - R_0 = 20$[a]
KDO-6	20.3	8	Pure	1.549	3.83	1.86
KDO-7	20.3	8	Pure	1.570	—	1.85

[a]Scaled.

Table 5.4. Tentative EOS parameters for Diamond Ore slurry explosives.[9]

Initial Reaction:	
JWL coefficient[a]	CJ-state
A = 1.622 84	ρ_0 = 1.59 g/cm^3
B = 0.002 554 85	D = 0.41 cm/μsec
R_1 = 4.4	P_{CJ} = 0.065 Mbar
R_2 = 1.2	τ = 3.11
ω = 0.32	E_0 = 0.020 Mbar cm^3/cm^3[b]
Completely burned HE:	
JWL coefficient	Idealized CJ-state
A = 4.632 49	ρ_0 = 1.626 g/cm^3
B = 0.012 907	D = 0.763 cm/μsec
R_1 = 4.25	P_{CJ} = 0.250 Mbar
R_2 = 1.0	τ = 2.78
ω = 0.40	E_0 = 0.096 Mbar cm^3/cm^3

[a]Jones-Wilkins-Lee equation.

[b]Mbar cm^3/cm^3 = megabar cubic centimeters per cubic centimer of explosive.

Fig. 5.6 in comparison with a hypothetical standard single phase explosive.

Following this first attempt at formulating an EOS for the Diamond Ore explosive and the identification of the problems involved, a program of step-by-step testing was carried out in an attempt to stabilize the detonation properties by making changes in the composition and manufacturing processes. The solution of the problems and the production of a more accurate and usable EOS were necessary for preshot design calculations for the Diamond Ore Phase IIB experiments planned for October 1972.

COMPOSITION CHANGES AND VELOCITY TESTING

As previously stated the gross changes in the densities and the development of voids in the initial EOS testing were believed to be caused by gasification of the liquid ammonia added to accelerate gel formation in the slurry. Without this ammonia, the explosive will solidify but

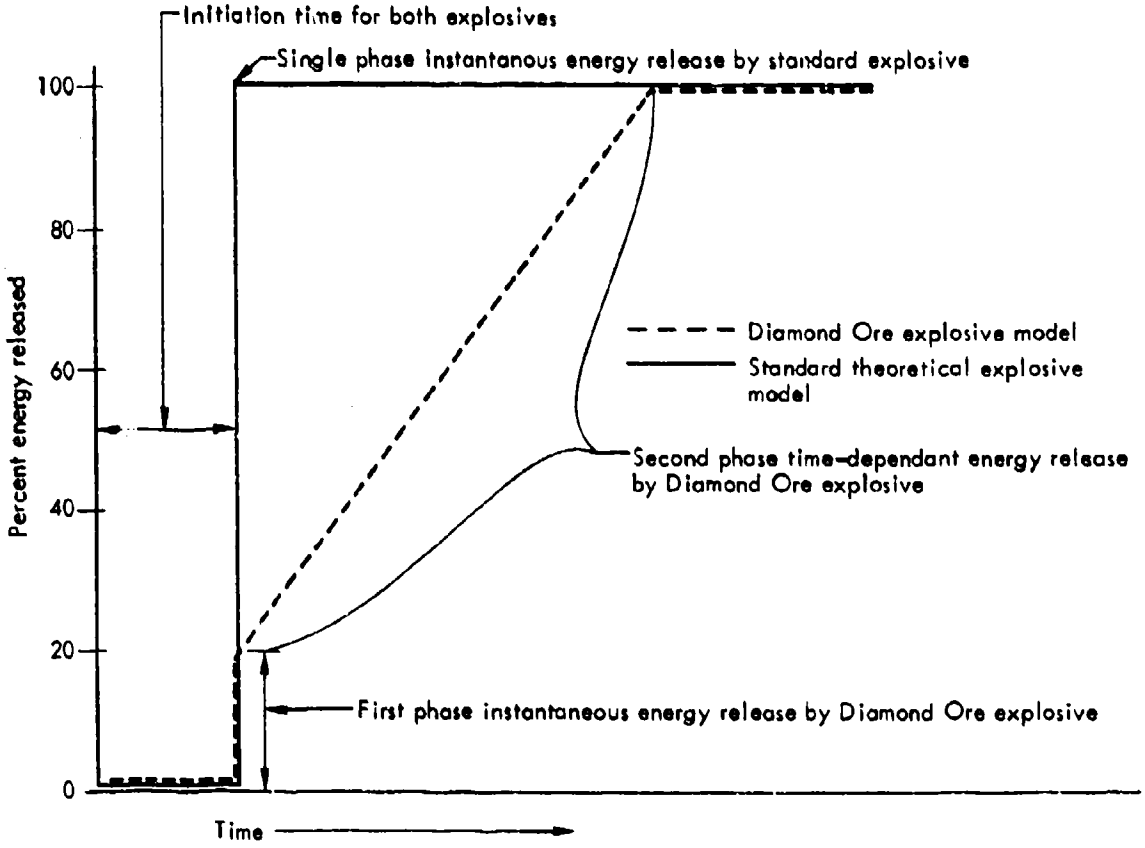

Fig. 5.6. Energy release model for Diamond Ore and theoretical standard explosive.

at a much slower rate. Based on observations of the consistency of the explosive, prior to the addition of the ammonia, it was believed that the explosive without the ammonia was sufficiently viscous to hold the 10% sand in suspension. The manufacturer was asked to deliver amounts of both the pure and sand-contaminated explosive without the ammonia for further testing. These explosives were designated "DIAMOND ORE IIA-1" (pure) and "DIAMOND ORE IIB-1" (sand). Four detonation velocity experiments were conducted with each type of explosive. These experiments were conducted with Polymethylmethacrylate (PMMA) cylinders as shown in Fig. 5.7. The densities and detonation velocities obtained by these experiments are shown in Table 5.5. The absence of the gross variations in the densities measured for each detonation is reflected in the consistency of the detonation velocities. The effect of the 10% sand dilutant on the detonation velocity is also evident. This degree of reproducibility was very encouraging and considered sufficient for the determination of EOS parameters.

Before the remaining two EOS detonations were conducted, a second series of velocity tests was conducted to insure reproducibility between separately

manufactured batches of the same explosive. These tests was conducted with the same charge configurations as the previous series. Four tests were conducted with the pure explosive, designated "DOIIA-2" and the sand-contaminated explosive, designated "DOIIB-2." The results of the series are shown in Table 5.6. Although the densities for both the pure and sand-contaminated explosives were very close to those found in the first series, the detonation velocities were consistently lower. The fact that the detonation velocities were consistently lower for both the pure and contaminated explosive led to a detailed examination of the possible differences in the two test conditions. The only difference found in the two series was the ambient temperature at the times of detonation. The first series was loaded, stored, and detonated at an ambient temperature range of 21 to 24°C (70 to 75°F). The second series was loaded and stored in this same temperature range but was detonated at an ambient temperature of about 38°C (100°F). Chemical analysis of the four explosives indicated no significant change in the composition between the two pure and two contaminated explosives. The detonation of the remaining two EOS tests was again delayed pending resolution of this apparent temperature effect. To evaluate the temperature effect, samples of both of the

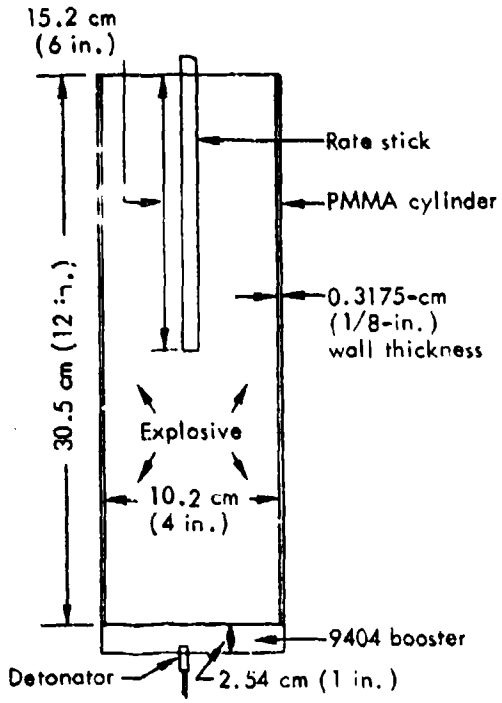

Fig. 5.7. Typical configuration for detonation velocity test.

Table 5.5. Detonation velocity tests (I).[9]

Event	Explosive	Density (g/cm^3)	Average detonation velocities (mm/μsec)
KDO-17	DOIIA-1	1.523	4.23
KDO-18	DOIIA-1	1.517	4.21
KDO-19	DOIIA-1	1.521	4.18
KDO-20	DOIIA-1	1.521	4.23
KDO-21	DOIIB-1	1.585	3.80
KDO-22	DOIIB-1	1.585	3.87
KDO-23	DOIIB-1	1.585	3.82
KDO-24	DOIIB-1	1.593	3.99

Table 5.6. Detonation velocity tests (II).[9]

Event	Explosive	Density (g/cm^3)	Average detonation velocities (mm/μsec)
KDO-25	DOIIA-2	1.532	3.91
KDO-26	DOIIA-2	1.532	3.80
KDO-27	DOIIA-2	1.525	3.92
KDO-28	DOIIA-2	1.522	3.74
KDO-29	DOIIB-2	1.602	3.53
KDO-30	DOIIB-2	1.594	3.42
KDO-31	DOIIB-2	1.596	3.52
KDO-32	DOIIB-2	1.598	3.61

Table 5.7. Detonation velocity tests (III).[10]

Event	Explosive	Density (g/cm^3)	Average detonation velocities (mm/μsec)
KDO-33	DOIIA-1	1.556	4.04
KDO-34	DOIIA-1	1.555	3.94
KDO-35	DOIIA-2	1.522	3.73
KDO-36	DOIIA-2	1.526	3.78
KDO-37	DOIIB-1	1.618	3.79
KDO-38	DOIIB-1	1.592	3.82
KDO-39	DOIIB-2	1.592	3.55
KDO-40	DOIIB-2	1.592	3.39

first two batches were heated to 38°C (100°F) for a period of 4 hr and then allowed to cool. Density changes were measured during this heating cycle and the minor changes observed were attributed to the increased evaporization caused by the temperature effect on the water in the explosive. Detonation velocity tests were then conducted with two samples from each batch of pure and contaminated explosive with the same cylinder configuration as the precious two series (Fig. 5.7). The results of this testing are shown in Table 5.7. The temperature effect is evident in that the detonation velocities were again slower than those in Table 5.5, while the densities remained very close to their pretemperature cycling levels. This series of detonations was conducted with an ambient temperature in the 24 to 27°C (75 to 80°F) range. Because the explosive had been allowed to cool to these ambient temperatures prior to detonation and the velocities continued to be lower, the temperature effect was assumed to be nonreversible.

Discussions were held with Dow Chemical Company to determine the probable cause for this effect. Dow indicated that the particle size distribution of the ammonium nitrate in the explosive is critical to the sensitivity of the explosive. This is especially true in the finer particle size ranges. Raising the temperature of the explosive causes the finer particles to go into solution with the water in the explosive. When the explosive cools, the resulting super-saturated condition causes the ammonium nitrate to precipitate. Although this process is essentially reversible, the precipitant contains ammonium nitrate crystals or particle sizes significantly larger than those that were added during manufacturing. The loss of the fine-size particles will result in a desensitizing of the explosive that could result in a reduction in the detonation velocity.[10] Additional discussions were held with Dow and the Chemistry Department, LLL, where minor changes in the explosive composition were made. The finer-size ammonium nitrate particles were to be replaced by fine-size aluminum particles in an attempt to reduce or to eliminate the temperature cycling effect while maintaining the sensitivity of the explosive. The explosive was to be temperature-cycled to 49°C (120°F) during manufacturing. These explosives were designated "DOIIIA-1" (pure) and "DOIIIB-1" (contaminated).

Sixteen detonation velocity tests were made from two separately manufactured batches of this explosive. The second batch was designated "DOIIIA-2" (pure) and "DOIIIB-2" (contaminated). Two samples of each explosive from each batch were again temperature-cycled to 38°C (100°F) prior to the conduct of the detonation velocity tests. These tests had

the same configurations as the previous tests (Fig. 5.7). Table 5.8 lists the results. In comparison with the DOIIA and DOIIB compositions, the DOIIIA and DOIIIB compositions show a distinct reduction in density and detonation velocity. The reduction in density can be attributed to the reduction in ammonium nitrate and the addition of aluminum particles. The reduction in detonation velocities is attributed to the desensitizing of explosives through the removal of the fine ammonium nitrate particles that was apparently not compensated for by the addition of the fine aluminum particles. In comparing densities and velocities between batches of the same type of DOIII explosives, the temperature effect on the detonation velocities is still evident although not as pronounced. It is apparent that the single temperature cycling during manufacturing was not sufficient to eliminate completely the effects brought on by the dissolving and recrystalization of the ammonium nitrate particles. It should be noted, however, that detonation velocities between different batches of the same explosive with the same temperature cycling history are good. It was therefore decided that if the explosive were temperature-cycled to extremes beyond that expected in normal usage, the reproducibility should be good although some loss in detonation velocity from that experienced in the original composition could be expected.

FINAL EOS TESTING

Discussions were again held with Dow Chemical Company, and a composition "DOIVB" (sand) was established. Because the use of the explosive in modeling detonations and the use of the EOS in design calculations would include only the sand-contaminated explosive, the testing of a pure explosive was discontinued. Although there was concern about the effects of the sand contamination, these were not substantiated and generally speaking, the sand contamination had an apparent stabilizing effect on the explosive. The only changes made to obtain the composition DOIVB explosive were the temperature cycling to 77°C (170°F) during manufacturing and the reduction in the amount of gelling agent by 0.5%. This reduction was made to decrease the viscosity of the explosive and to reduce the chances of air entrapment during loading

Table 5.8. Detonation velocity tests (IV).[9]

Event[a]	Explosive	Density (g/cm^3)	Average detonation velocities (mm/μsec)
KDO-45[b]	DOIIIA-1	1.523	3.67
KDO-46[b]	DOIIIA-1	1.522	3.67
KDO-47	DOIIIA-1	1.527	3.83
KDO-48	DOIIIA-1	1.521	3.68
KDO-49[b]	DOIIIA-2	1.532	3.56
KDO-50[b]	DOIIIA-2	1.525	3.74
KDO-51	DOIIIA-2	1.537	3.83
KDO-52	DOIIIA-2	1.537	3.84
KDO-53[b]	DOIIIB-1	1.580	3.49
KDO-54[b]	DOIIIB-1	1.577	3.43
KDO-55	DOIIIB-1	1.586	3.53
KDO-56	DOIIIB-1	1.587	3.60
KDO-57[b]	DOIIIB-2	1.593	3.49
KDO-58[b]	DOIIIB-2	1.592	3.26
KDO-59	DOIIIB-2	1.594	3.35
KDO-60	DOIIIB-2	1.592	3.35

[a] KDO-41 through KDO-44 were nonrelated HE tests in support of other EERL programs.

[b] Temperature-cycled at Site 300 in addition to cycling of all explosives in manufacturing.

Table 5.9. Final EOS testing results.[9]

Event	Explosive	Density (g/cm^3)	Detonation velocity (mm/μsec)	Wall velocity, R - r = 25 mm (mm/μsec)
KDO-8[a]	DOIVB	1.62	2.35	—
KDO-9[b]	DOIVB	1.626	3.35	0.779

[a]Booster = 5.08-cm (2-in.) sphere of 9404 (125 g).

[b]Booster = 10.2-cm (4-in.) sphere of 9404 (1360 g).

of the final two EOS containers. The KDO-8 and KDO-9 detonations, as shown in Table 5.2, were the only EOS detonations yet to be conducted. Each container was carefully loaded with the DOIVB composition explosive and detonated. The results are listed in Table 5.9. The larger size booster was used in the KDO-9 detonation after the KDO-8 detonation velocity indicated a possible under boosting. The sphere wall velocities were extremely slow. The increase in density of the DOIVB explosive over the previous compositions is attributed to the reduction in entrapped air. Although the resulting data were considered of marginal use for EOS work and only the KDO-9 detonation data were used, JWL coefficients were calculated and are shown in Table 5.10.

Actions taken to stabilize the detonation history of the explosive have resulted in a significant reduction in the explosive energy and sensitivity. Therefore, testing was stopped.

CONCLUSIONS

The lack of consistent results during the testing of Diamond Ore slurry explosive resulted in a decision to abandon the explosive for further EOS type testing. Problems had been anticipated in describing this type of explosive in sufficient detail and accuracy for use in computational work. The complex composition and the effects of variations in these compositions had not previously been thoroughly investigated. Problems in reproducibility were found and their solutions sought. Considerable assistance was provided by the manufacturer, Dow Chemical Company, in understanding and resolving some of the problems encountered. The exhaustive test series was concluded after making significant gains in increasing the reproducibility of the explosive yet without fully understanding the complex causes of these problems. The need to select, test, and determine a usable EOS

Table 5.10. EOS parameters for final Diamond Ore slurry explosives.[9]

Initial reaction:	
A = 1426.63	ρ_0 = 1.626 g/cm^3
B = -0.015 601 9	D = 0.335 cm/μsec
R_1 = 13.0	P_{CJ} = 0.020 Mbar
R_2 = 2.0	τ = 8.124
ω = 0.3	E_0 = 0.026 Mbar cm^3/cm^3
Completely burned HE[a]:	
A = 4.632 5	ρ_0 = 1.626 g/cm^3
B = 0.012 92	D = 0.763 cm/μsec
R_1 = 4.25	P_{CJ} = 0.250 Mbar
R_2 = 1.0	τ = 2.786
ω = 0.40	E_0 = 0.096 Mbar cm^3/cm^3

[a]Second phase energy release is over a period of 670 μsec.

for an explosive for use in the ongoing Diamond Ore program dictated a change in explosives. The results of this test series should in no way be construed as a reflection on the type of economical application of the explosive to use in the construction and mining industry. Even with the apparent microscopic differences in detonation properties, the macroscopic results discussed in Chapter 6 were close to those expected. The Diamond Ore explosive was formulated to meet the extremely strict specifications contained in Appendix A and cannot be considered indicative of formulations applied to commercial construction explosives.

Chapter 6

Gelled Nitromethane Explosive Experiments

GENERAL

The use of nitromethane as an explosive in the Diamond Ore program was considered in the initial planning. It was particularly attractive to the calculational program because it has a well-defined EOS and excellent reproducibility. Nitromethane was the primary explosive used in the Pre-Gondola experiments conducted at Fort Peck, Montana, and data from these tests were to provide the basis for the initial calculational program in Project Diamond Ore. The reproducibility of the detonation characteristics of nitromethane (chemical compound CH_3NO_2) is excellent. Previous testing of nitromethane by the Chemistry Department, LLL, had shown that reproducible detonations were obtained even with the addition of up to 40% by weight of inert materials. There was a corresponding reduction in energy and detonation velocity but these reductions were constant for a given percent of dilution.[9] It was therefore believed that the addition of 10% sand held uniformly in suspension by a small percentage of a gelling agent would result in reproducible detonation parameters. Total inerts would then constitute 15 to 20% and would be well within the 40% limit of the previous testing. The primary disadvantages to the use of pure nitromethane, a liquid manufactured primarily for use as a lacquer solvent, in the Diamond Ore program were the problems encountered in containing it in a subsurface cavity and its inability to maintain the fallout simulation particles in suspension. Containing nitromethane in liquid form requires lining the charge cavity with a material impervious to the solvent. Methods of gelling nitromethane had been unsuccessfully sought during the Pre-Gondola testing. In these tests, gelling was desirable to reduce the seepage from mined charge cavities.

GELLED SYSTEM SELECTION

During the latter phases of the testing of the Diamond Ore aluminized ammonium nitrate slurry explosive, a search was initiated to find a backup explosive. Discussions were held with Commercial Solvents Corporation, the sole producers of nitromethane in the United States, relative to systems and methods of gelling

or thickening nitromethane. Nitrocellulose has been used, but it is a high explosive in itself and when mixed with nitromethane readily forms lumps that are difficult to disperse.[9] This system is not considered practical or safe in terms of the quantities of conditions required for the Diamond Ore program. Polyoxyethylene can be used to thicken nitromethane but a rigid gell is formed which will begin to liquefy after about a week of storage at room temperature.[13] This gell can be further stabilized but the rigid gell produced is not considered compatible with the need to mix, then pump, or pour the gelled nitromethane into a sub-surface cavity. Both of these systems, the nitrocellulose and the polyoxyethylene, lack amine resistance and the gell will break down in the presence of strong amines.[13] Most starches, natural gums, and synthetic polymers used in water gelling systems are ineffective with nitromethane.[13] General Mills, Inc. has been doing development work with a modified guar gum (a cyanoethylether derivative of a galacto-mannan gum) specifically directed at thickening or gelling nitromethane. This gelling agent is identified as XG512 by General Mills. It is a free-flowing white powder that must be quickly dispersed throughout the nitromethane to prevent the formation of lumps that are difficult to disperse.

Samples of the XG512 were obtained and laboratory testing was conducted. Various percentages of the XG512 were mixed with the traced sand and nitromethane. These samples were observed over a period of a few weeks. No liquefaction was observed although perceptible sand-settlement was noted at the end of the second week. The gell that was formed with a mixture of 10% sand, 3% XG512, and 87% nitromethane was selected for further testing. This gell set up in about 90 sec and had the consistency of "thick syrup," allowing it to be pumped.

SAFETY AND FIELD SYSTEM TESTING

Industrial grade nitromethane is relatively insensitive to shock as compared with conventional industrial or military explosives. It cannot be detonated by a No. 8 blasting cap alone. Nitromethane may be detonated, however, if a standard explosive booster of sufficient size is used.[14] There are many ways in which pure nitromethane may be sensitized to make it cap-sensitive. These methods are discussed in Ref. 14. The ease with which nitromethane can be sensitized is of importance to the use of a gelled nitromethane in the Diamond Ore program — not because of a need to sensitize but because of the need to insure that the gelling process did not sensitize the nitromethane. The mixing and pumping operations required to produce the gelled nitromethane were therefore carefully tested prior to use in field operations. Standard drop hammer tests were conducted on the 3/10/87% mixture with negative results. Differential thermal analysis was conducted at atmospheric pressure with no troublesome exothermic reactions found. Further examination indicated that there was no chemical reaction between the XG512 and the nitromethane. The effect of the XG512 can be likened to that of a sponge where the

nitromethane is absorbed and held in a thickened condition. The tracer particles are inert and do not enter into any chemical reaction with either the XG512 or the nitromethane.

Nitromethane is sensitive to detonation from the heat of the compression of gases. This problem has been alleviated by shipping nitromethane in 208-liter (55-gal) drums that are designed to vent if the internal pressure of the drum exceeds about 7 bars (100 psi). This sensitivity is of special importance when nitromethane is to be pumped. The conditions required for accidental detonation from this phenomenon may be produced within the pump itself or in the outlet lines if the flow is abruptly interrupted. In previous experiments where nitromethane was used, the explosive cavity was filled using gravity flow from 208-liter (55-gal) drums. The use of gelled nitromethane requires pumping because of its comparatively high viscosity.

To accomplish field gelling and pumping of the nitromethane, a search was made of the literature to locate commercially available mixing and pumping units that might be used. A compressed-air-driven mixer was chosen. This mixer is the Lighting Model NAG 100 manufactured by Mixing Equipment Company, Rochester, New York. Figure 6.1 is a picture of the unit, which consists of a compressed-air-driven motor, a 0.91-m (3-ft) shaft, and a 19.8-cm (7.8-in.) diameter, 3-blade propeller. The unit clamps to the rim of a 208-liter (55-gal) drum. Testing showed that this unit produced the deep vortex required for rapid and thorough mixing of the sand and XG512 in the nitromethane. The pumping unit selected was also

Fig. 6.1. Nitromethane mixing unit.

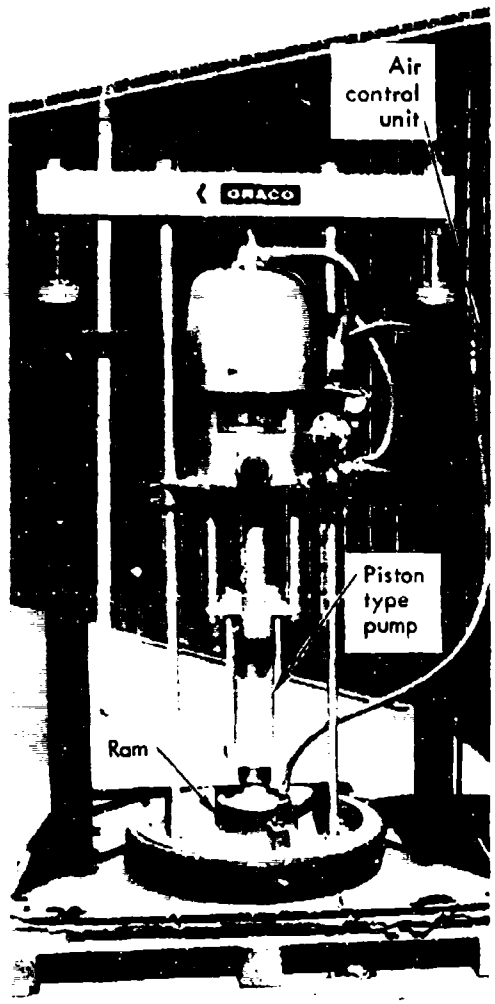

Fig. 6.2. Unit used to pump nitromethane in Diamond Ore testing.

compressed-air-driven. This pump and ram unit is manufactured by Graco, Inc., Minneapolis, Minnesota, and is commonly used to pump heavy automotive greases. The pump is composed of three separate

units as shown in Fig. 6.2. The ram piston fits snugly inside a 208-liter (55-gal) drum and maintains a pressure of about 0.1 bars (1 psi) on the gelled nitromethane. The double action piston pump is mounted to the ram assembly. The air control unit is used to regulate the pressure into both the ram and the pump. The pump produces a 5 to 1 pressure ratio; i.e., for every increment of air pressure input to the pump five times that pressure is applied by the piston. A 181-kg (400-lb) batch of gelled nitromethane was successfully mixed at LLL's Site 300 and used to test the effectiveness and safety of this pumping unit.* The 181-kg (400-lb) test batch was passed through the pump five times. Pumping pressures were varied up to 10 bars (150-psi) without mishap or apparent problems. For safety purposes these tests were conducted under remote control.

EOS TESTING

After the gelling and pumping safety considerations had been satisfied, an EOS test was performed on the 5/10/87% gelled nitromethane. A 5.1-cm (2-in.) diameter (ID), 30.48-cm (12-in.) length copper cylinder with a 0.51-cm (0.2-in.) wall thickness was filled with the gelled nitromethane and detonated with a plane wave generator (PO40) and a 10.2- by 10.2- by 0.13-cm (4- by 4- by 1/2-in.) Comp B booster. Streak photography produced excellent results. From the test data, the energy was calculated at 91.4% (4,406 J/g) of pure nitromethane (4,729 J/g) at a scaled wall expansion of 19 mm. The detonation velocity recorded from PZ pins attached to the cylinder wall was 6.11 mm/μsec. This velocity compares very favorably with the 6.37 mm/μsec for pure nitromethane. Table 6.1 lists the CJ parameters and JWL coefficients calculated for use in EOS calculations by LLL and Systems, Science, and Software, Inc. These parameters are used in the standard JWL EOS equation stated in Chapter 5. As indicated by the single set of parameters, this gelled nitromethane detonates in a single phase in which the energy is released instantaneously as in conventional explosives. This explosive, therefore, does not produce the yield or size effects found in the aluminized ammonium nitrate water-gelled slurry originally studied.

ONE-TON EXPERIMENT

Previous testing with the gelled nitromethane explosive system was directed at determining the feasibility and safety of the gelling and pumping operation. Laboratory tests had also been performed to determine the EOS and the compatibility of the iridium-coated sand with the

Table 6.1. Gelled nitromethane EOS parameters.[9]

JWL[a] coefficients	CJ parameters
A = 2.111	P_σ = 0.125 Mbar
B = 0.047 54	ρ_σ = 1.21 g/cm^3
C = 0.007 95	D = 6.11 cm/μsec
R_1 = 4.3	E_0 = 0.045 Mbar cm^3/cm^3[b]
R_2 = 1.3	τ = 2.614
ω = 0.34	

[a] Jones-Wilkins-Lee equation.

[b] Mbar cm^3/cm^3 = megabar cubic centimeters per cubic centimeter of explosive.

*Examination and disassembly of the pump by the Chemistry Department, LLL, have resulted in certain modifications for safety purposes. The use of the unit in its delivered form for pumping explosives is not recommended.

gelled explosive. No tests could be performed to determine that the higher detonation velocity and pressure of the nitromethane detonation would not influence the fallout simulant. In previous 907-kg (1-ton) events, the fallout simulation was successfully tested with an aluminized ammonium nitrate slurry explosive, but the transient history of the fallout simulant is beyond current analysis and testing was required.

In order to verify the EOS parameters and the fallout simulation technique, a 907-kg (1-ton) gelled nitromethane experiment was conducted on 27 October 1972 in conjunction with the Diamond Ore Phase IIB experiments at Fort Peck, Montana. A separate report will be published on the Phase IIB experiments. The gelled nitromethane 907-kg (1-ton) detonation was designated DOIIB IT-6. As shown in Fig. 6.3, this detonation was conducted at a DOB of approximately 5.5 m (18 ft). The emplacement hole was partially stemmed leaving a 41-cm (16-in.) diameter open access hole. The explosive was placed in an aluminum cylinder of the same design as those used in a series of 907-kg (1-ton) pure nitromethane shots in the Phase IIB experiments. The cavity size and shape, and the size of the unstemmed hole for the series of 907-kg (1-ton) pure nitromethane detonations were scaled down from a Systems, Science, and Software, Inc. design for a 8.4×10^9 J (20-ton) unstemmed modeling detonation. The DOB of 5.5 m (18 ft) was selected as being near the optimum DOB for stemmed 4.2×10^8 J (1-ton) detonations in the Fort Peck Bearpaw shale. As shown in Fig. 6.3, a single rate stick was placed in the container to measure the detonation velocity of the explosive. The mixing and pump units previously mentioned were used to emplace 907-kg (1 ton) of the gelled nitromethane in about 3-1/2 hr.

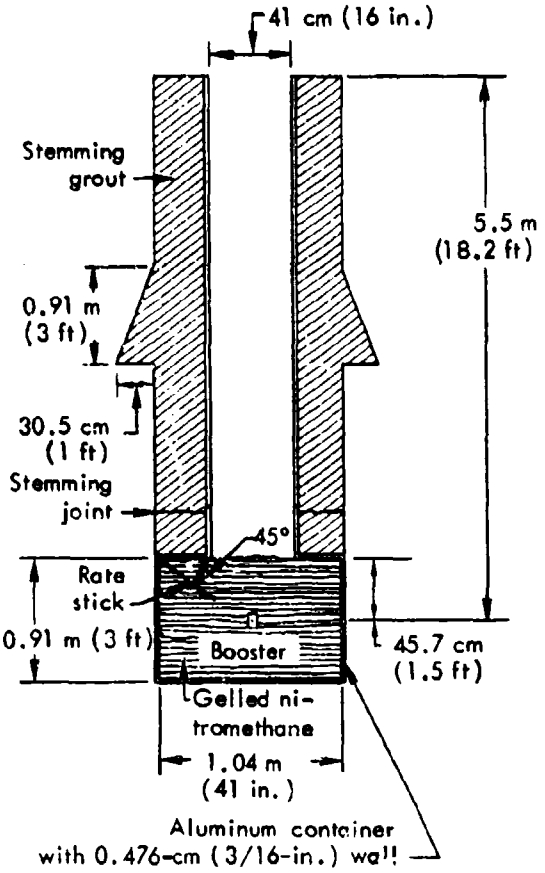

Fig. 6.3. Emplacement configuration for 907-kg (1 ton) of gelled nitromethane (Event DOIIB-IT-6).

The fallout simulation technique is fully documented in Ref. 4. For this fallout simulation, 97 kg (200 lb) of sand (10% of the total amount of explosive weight) containing 80.5 g of iridium was mixed with the explosive. The fallout collection array shown in Figs. 6.4 and 6.5 was used to collect debris samples from the detonation cloud. The 0.61-m^2 (2-ft^2) aluminum trays used on all previous fallout sample tests were employed. The wind data, elevation, direction, and

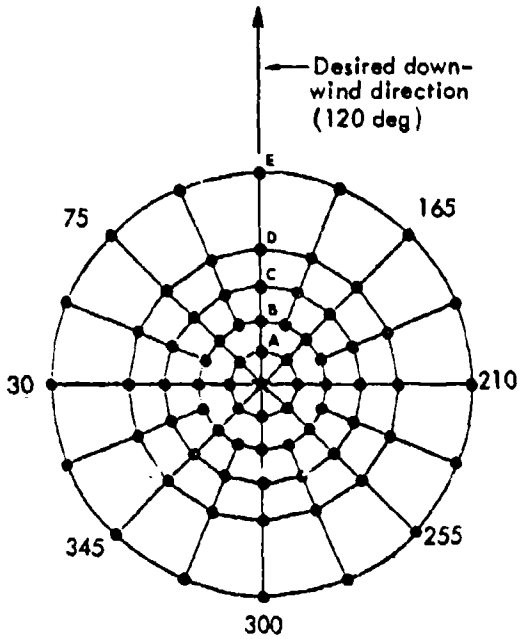

• Debris collector
* SGZ

Arc designation	Distance from SGZ (m)	(yd)
A*	23	25
B*	46	50
C	69	75
D	100	110
E	160	170
F	190	210
G	230	250
H	280	310
I	340	370
J	400	440
K	440	480
L	460	500
M	530	580
N	670	730
O	800	880
P	1,010	1,100
Q	1,190	1,300
R	1,460	1,600
S	1,740	1,900
T	1,830	2,000

*Additional collection trays were located at 5-yd intervals between the A and B circles.

Fig. 6.4. Close-in fallout collection array for DOIIB-IT-6 detonation.

speed required for predicting the downwind direction for this detonation were obtained by a U.S. Air Force "PIEBALL" Team. The DOIIB IT-6 detonation was planned for 1000 hr on 27 October 1972, but was placed on a hold at H-15 min awaiting proper wind conditions. The wind readings taken at about 1145 hr indicated that the detonation cloud debris would be contained within the collection array and the countdown was resumed with the detonation occurring at 1210 hr.

The detonation appeared normal. The rate stick produced a clear record of the detonation wave arrival times. The resulting velocity was calculated to be 6.14 mm/μsec, a figure that compares well with the 6.11 mm/μsec obtained in the EOS testing.

At approximately shot time the winds had begun to change direction and the speed decreased slightly. A minimum wind speed of 8 km/hr (5 mi/hr) was desired to move the debris cloud off this SGZ area and to be compatible with the fallout prediction model. A weather prediction indicating heavy snow for the test area precluded delaying the event to await more favorable winds. Table 6.2 lists the preshot and postshot wind data. These data are plotted in wind hodograph

Table 6.2. IT-6 wind data.

Elevation (m)	(ft)	Time = 1144 hr preshot Direction Out	In	Speed (knots)	Time = 1210 hr postshot Direction Out	In	Speed (knots)
0	0	268	88	2	0	0	0
30	100	273	93	2	281	101	2
60	200	278	98	3	284	104	2
90	300	283	103	3	289	109	3
120	400	286	106	4	291	111	3
150	500	288	108	4	283	103	4
180	600	291	111	5	264	84	4
210	700	296	116	6	251	71	5
240	800	288	108	6	245	65	6
270	900	282	102	7	242	62	6
300	1000	280	100	7	241	61	6

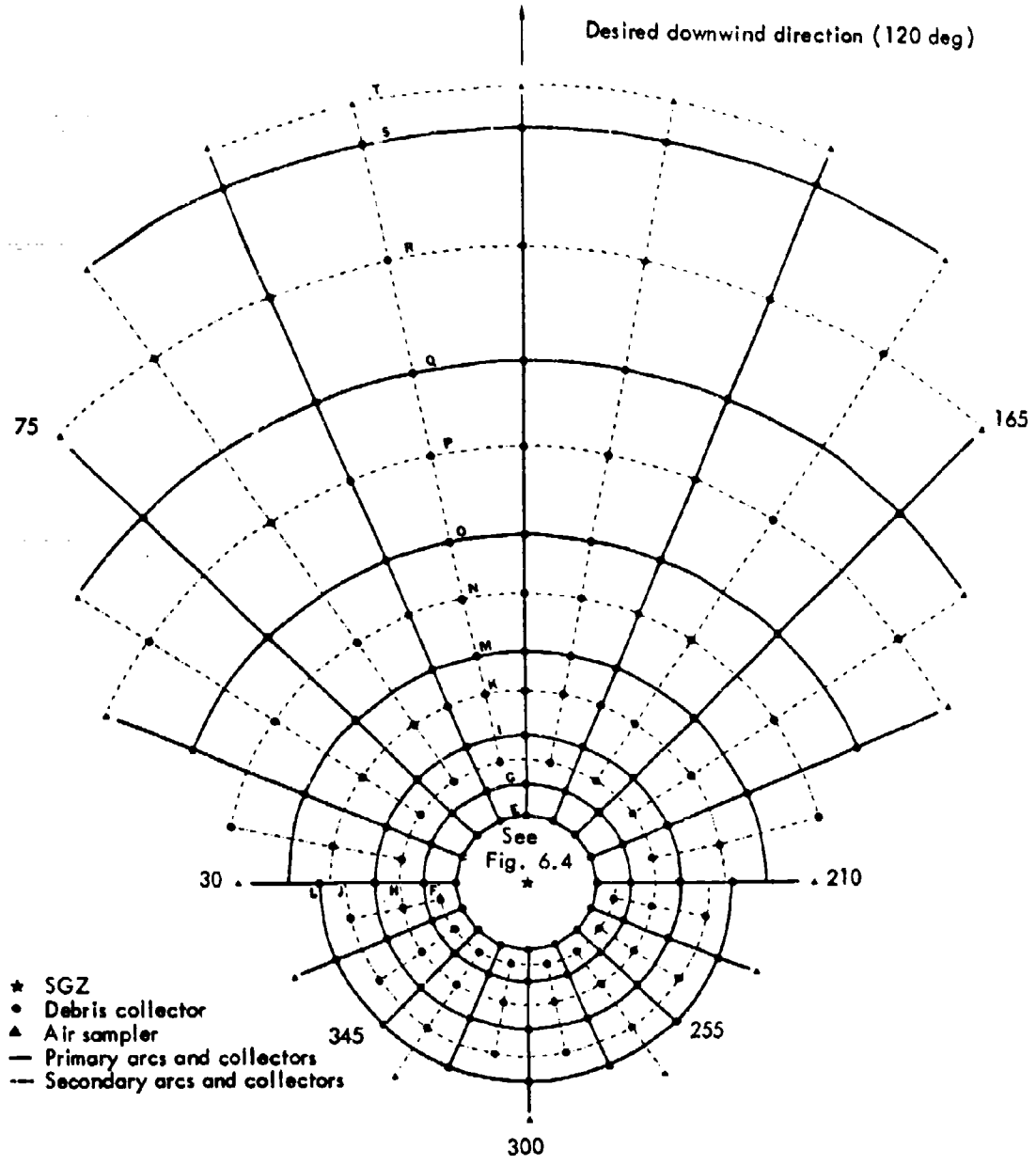

Fig. 6.5. Intermediate-range fallout collection array for DOIIB-IT-6 detonation.

form for comparison purposes with the desired downwind direction in Fig. 6.6.

The contents of each collector tray were sieved for the desired particle sizes and aliquots were incapsulated and irradiated. The samples were allowed to decay for 20 days and then counted in the SRI gamma ray spectrometer. The procedure employed in each step of the above processes is described in Ref. 4. The

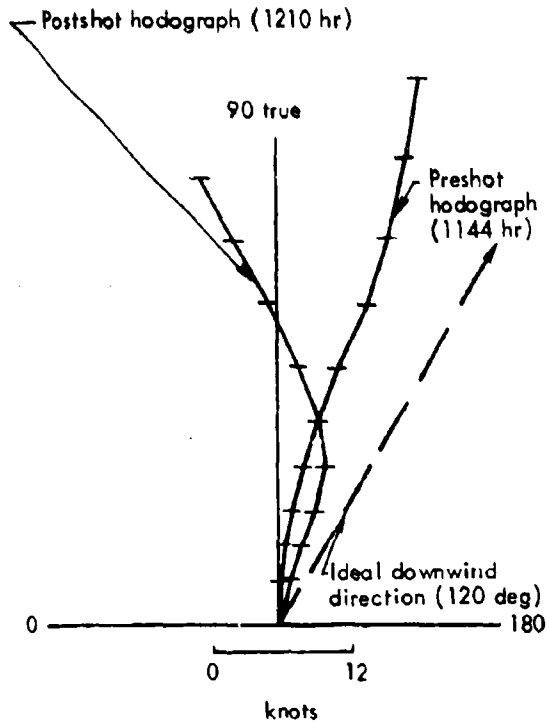

Fig. 6.6. Preshot and postshot wind hodographs for DOIIB-IT-6 detonation.

mass of debris deposited in each tray and the mass of iridium in each tray were computed and are listed in Appendix D.

Mass isodeposition lines are plotted in Fig. 6.7 with the collection array directions and desired hotline indicated. The isodeposition lines for the iridium tracer material are plotted in Fig. 6.8. The effect of both the change in wind direction and speed are evident from this figure. The change in wind direction caused the debris from the cloud to be deposited in the two lobes of the pattern. The low surface wind speed – 0 to 150-m elevation (0 to 500 ft) – caused large amounts of the debris to be deposited in the crater and continuous ejecta areas.

As discussed in Chapter 3, the deposition of fallout is dependent on the winds at the time of detonation. These winds determine the shape and size of the fallout pattern. The vent fraction, f_v, is defined as that portion of the total radioactivity (for a nuclear event) produced by a detonation that is deposited in local area fallout outside the continuous ejecta. Thus, the vent fraction is also dependent on the wind conditions. In this case, the low wind condition produced a small vent fraction because a larger portion of the fallout debris is deposited within the continuous ejecta.

The integration of the total iridium deposited for various radii of continuous ejecta and the effect on the calculated vent fraction are shown in Table 6.3. The limit of continuous ejecta, the range from SGZ where debris ceases to cover continuously the original surface, is at 36.6 m (40 yd). For comparative purposes the apparent crater radius is 7.3 m (23.6 ft) and the radius of the crater lip is 8.1 m (29.4 ft).

Figures 6.9 and 6.10 show the iridium deposition as a function of distance in the upwind-crosswind and downwind direction.

Table 6.3. Effect of various radii of continuous ejecta on vent fraction.

Assumed radius of continuous ejecta (m)	(yd)	Vent fraction (%)
22.9	25	20.04
27.4	30	12.61
32.0	35	8.96
36.6	40	6.77
41.4	45	5.91
45.7	50	4.51
50.3	55	3.98

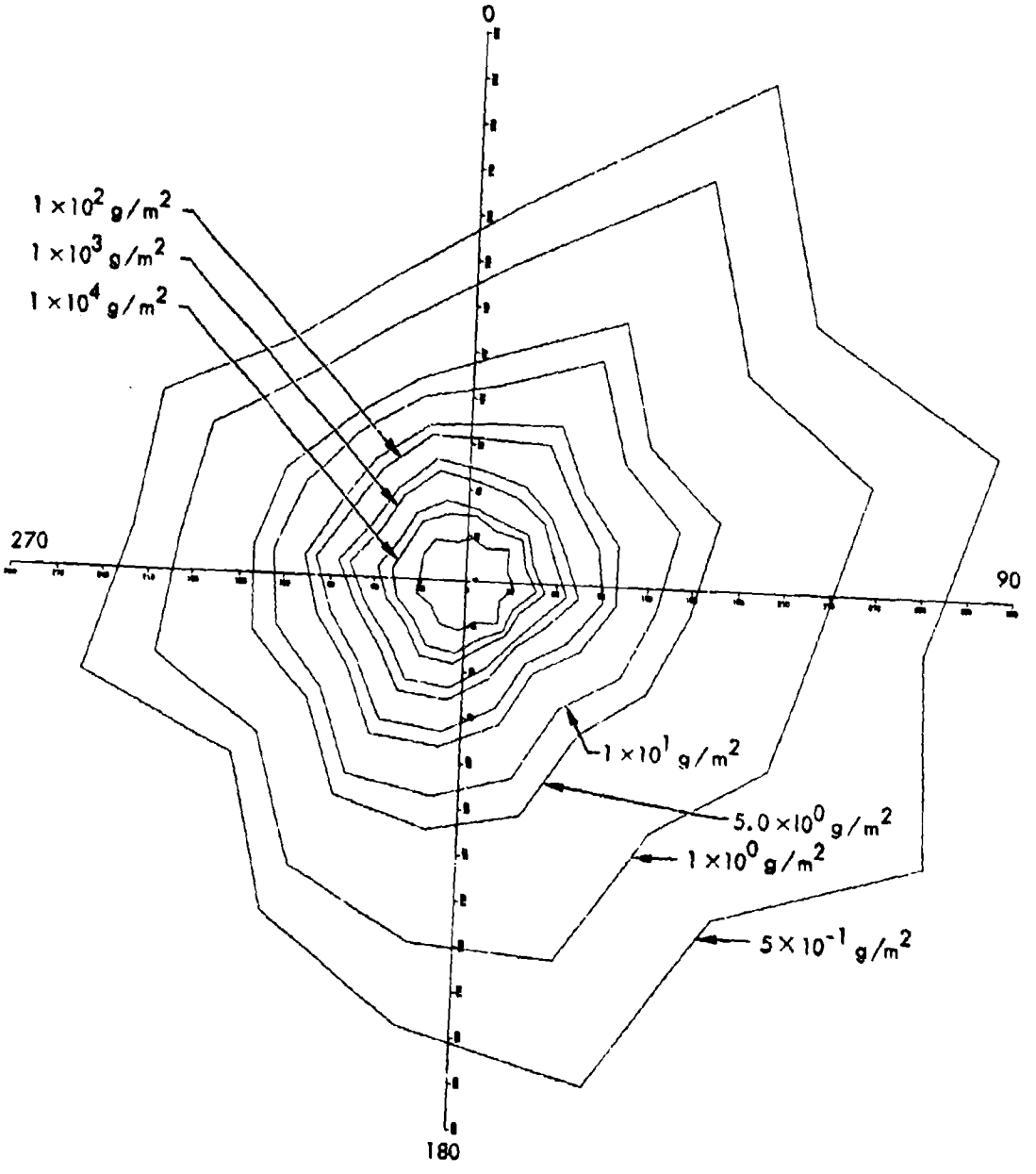

Fig. 6.7. Event DOIIB-IT-6 mass density contours from 5×10^{-1} to 5×10^4 g/m^2.

These curves are later scaled to a common event and compared with nuclear fallout curves. The scaling points on the figure will be explained later. These curves will subsequently be referred to as the "unnormalized" or "unscaled" iridium upwind-crosswind or downwind deposition curves. The curves are obtained from the iridium fallout deposition diagram, Fig. 6.8, by measuring the

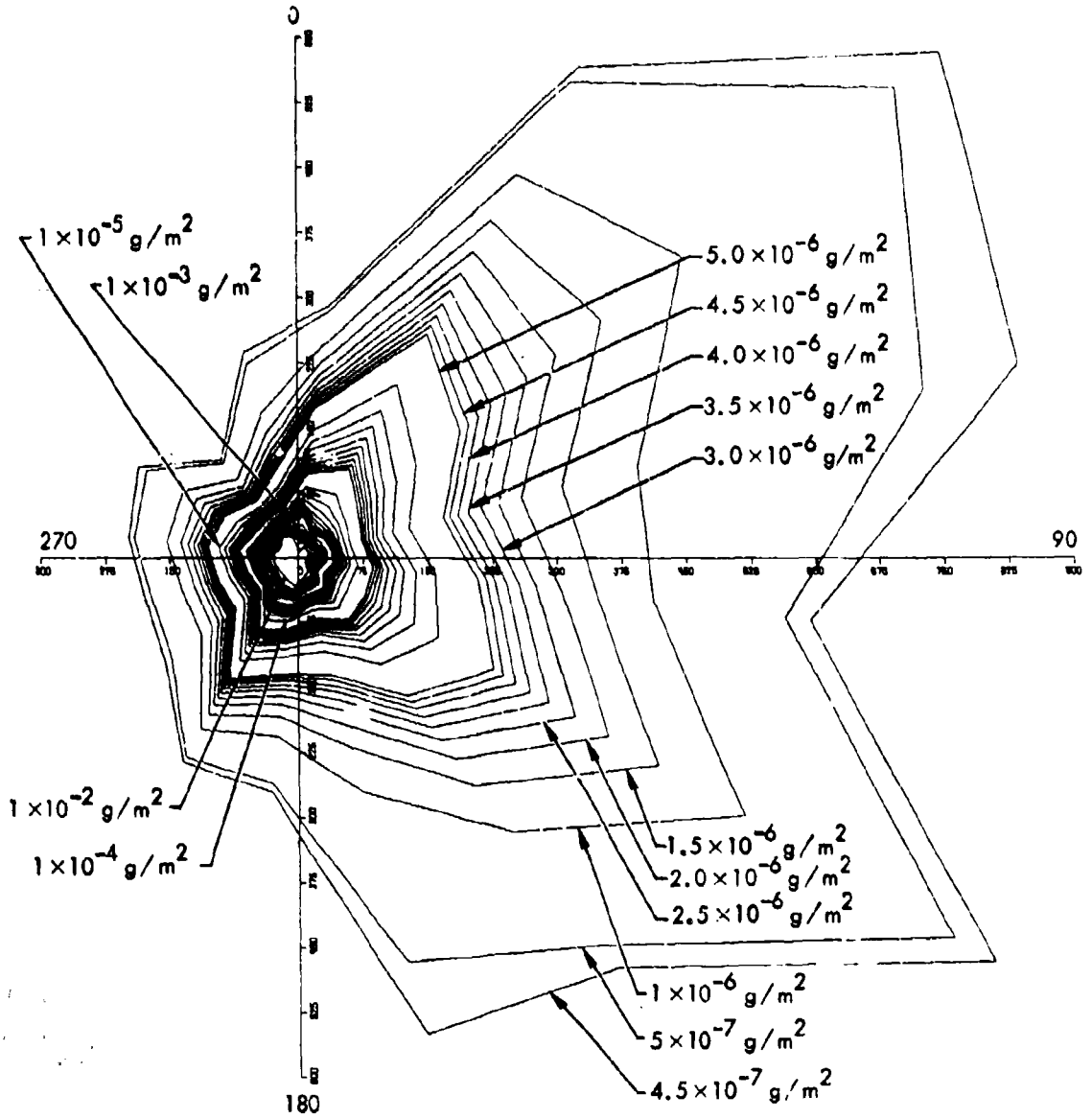

Fig. 6.8. Event DOIIB-IT-6 iridium mass density contours from 1.5×10^{-2} to 4.5×10^{-7} g/m^2.

distance from SGZ to the density contours of interest along either the upwind-crosswind or downwind direction. A "mean" upwind-crosswind unnormalized iridium deposition curve was obtained by averaging the distances for various densities obtained along several rays emanating from the SGZ.

The downwind direction of the iridium deposition pattern reveals two possible "hotlines" (along 52 and 120 deg) and a large shear. Both lines are shown in Fig. 6.10. The hodograph reveals that the first five levels (30.5 m/level; 100 ft/level), which contain the base cloud, are in close agreement with the 120-deg

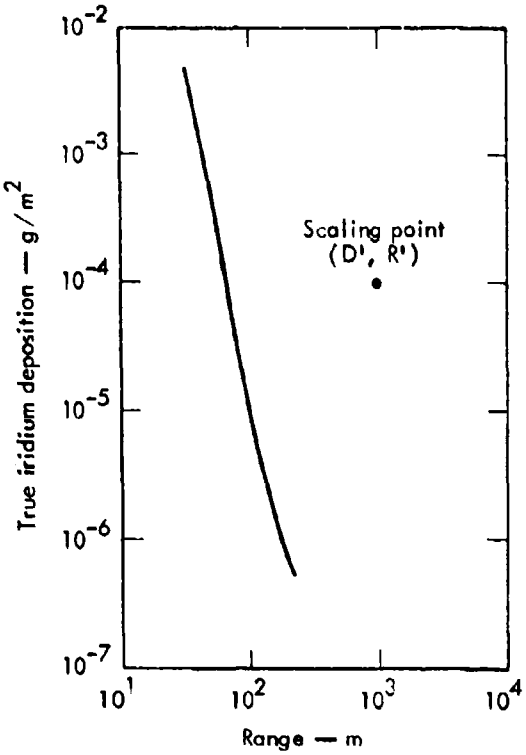

Fig. 6.9. Upwind-crosswind true deposition curve (Event DOIIB-IT-6).

hotline, whereas the wind direction of the succeeding cloud layers, which contain the main cloud, dramatically shifts to the 50-deg hotline. Thus, the measured postshot wind directions and iridium fallout pattern agree and postshot wind data are used in the subsequent analysis.

In the fallout simulation development reported in Ref. 4, the iridium deposition vs distance curves were considered to simulate fallout if (1) the iridium curves when scaled had the same shape as a scaled dose rate vs distance curve for nuclear events, and (2) the scaled curves for upwind-crosswind and downwind iridium deposition were both vertically displaced from the normalized nuclear curve by the same factor. The scaling procedure, detailed in Refs. 4, 15, and 16, is outlined below. For previous tests the displacement factor was determined to be 5×10^4. Said another way, the iridium deposition at a particular range can be converted to a radiation dose rate value in terms of roentgens per hour (R/hr) at H+1 hr by multiplying the iridium deposition in grams per square meter (g^{Ir}/m^2) by 5×10^4.

The scaling procedure used for the iridium fallout simulation events is identical to that used for a nuclear subsurface event. Reference 15 documents the scaling procedure. In subsequent paragraphs and on the figures, the scaled nuclear dose rate vs range is designated as the TR-19 curve.

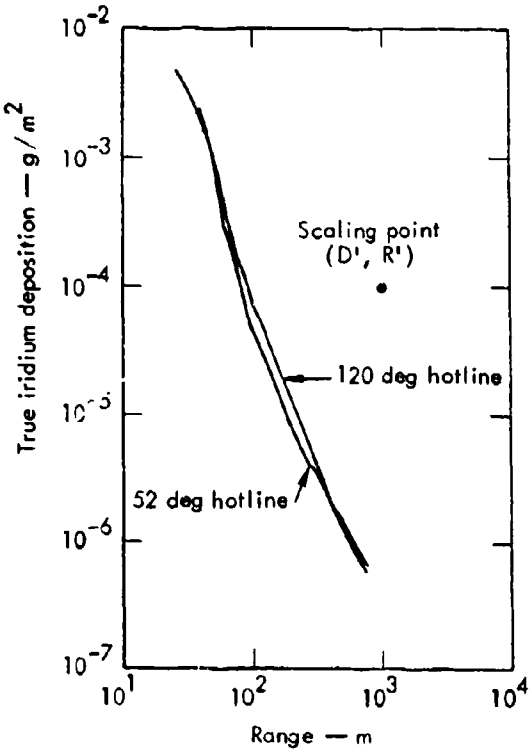

Fig. 6.10. Downwind true deposition curve (Event DOIIB-IT-6).

The scaling model considers the radioactivity to be distributed in two portions of the detonation cloud: the main cloud and the base surge cloud.

The observed exposure rates for any two events are related by physical scaling equations that take into account the major factors controlling fallout deposition. The scaling equations for main cloud downwind deposition are as follows:

$$D_{mc}(R) = \frac{f_{vmc} W_a}{f'_{vmc} W'_a} \times \left(\frac{V'_{eff} H'_{mc}}{V_{eff} H_{mc}}\right)^2 \frac{S'_{eff}}{S_{eff}} D'_{mc}(R'), \quad (1)$$

$$R = R' \left(\frac{V_{eff} H_{mc}}{V'_{eff} H'_{mc}}\right), \quad (2)$$

where:

$D_{mc}(R)$ = external H+1 hr downwind main-cloud-deposited gamma exposure rate (R/hr) [or iridium deposition (g/m^2)].

R = distance or range from SGZ (m); represents downwind hotline distance in this case.

V_{eff} = effective wind speed (m/sec), usually assumed to be the vector-averaged wind velocity up to one-half the main cloud height.

S_{eff} = effective wind shear (deg) over the entire main cloud height.

H_{mc} = main cloud height (m) at stabilization (activity deposited prior to stabilization may be formally considered as part of the total deposition).

W_a = equivalent fission activity yield of the device (tons) [or total amount of iridium tracer (g)].

f_{vmc} = fraction of equivalent fission activity (or of total iridium) vented into the main cloud.

The unprimed quantities represent parameters for the event to which exposure rates and ranges are being scaled, while the primed quantities represent parameters for the event that is being scaled. Generally, the cloud mid-height wind speed, V_{eff}, and the total main cloud height, H_{mc}, for each event are used in the scaling equations (rather than the wind speed and height for each individual cloud layer). It has been demonstrated that this procedure introduces little error into the predictions.

The above scaling description assumes that the main cloud is a tall, thin cylinder with the activity located along its axis. The cloud is comparatively tall, so height is more important than radius in determining the final particle deposition. Since particles must fall from a great height, wind speed appreciably affects their descent. Cloud width is ignored; the pattern width is modified only by the effective wind shear, S_{eff}, which is usually quite significant over typical main cloud heights. Observations of main cloud downwind patterns do indeed show that the

far downwind pattern width is well correlated with the shear.

The scaling equations for base surge cloud upwind-crosswind and downwind deposition reflect the somewhat different factors that control base cloud fallout:

$$D_{bc}(R) = \frac{f_{vbc} W_a}{f'_{vbc} W'_a} \left(\frac{R'_{bc}}{R_{bc}}\right)^2 D'_{bc}(R'), \qquad (3)$$

$$R = R'\left(\frac{R_{bc}}{R'_{bc}}\right), \qquad (4)$$

where:

$D_{bc}(R)$ = external H+1 hr upwind-crosswind or downwind base-cloud-deposited gamma exposure rate (R/hr) [or iridium deposition (g/m^2)]. The upwind-crosswind exposure rate and the downwind exposure rate are two different functions in this case. Thus, there are two different "D_{bc}" functions and two different "D_{bc}" functions for the two directions.

R = distance or range from SGZ (m); represents upwind-crosswind distance or downwind distance.

R_{bc} = radius of base surge cloud (m) at stabilization (activity deposited prior to stabilization may be formally considered as part of the total deposition).

W_a = equivalent fission activity yield of the device (tons) [or total amount or iridium tracer (g)].

f_{vbc} = fraction of equivalent fission activity (or of total iridium) vented into the base cloud.

The unprimed quantities again represent parameters for the event to which exposure rates are being scaled, while the primed quantities represent parameters for the event that is being scaled. Separate functions are not used for the upwind direction and the crosswind direction because nuclear exposure rate functions in these directions were found to be nearly equal.

Once the input parameters for a given event are known, the observed exposure rates may be scaled and compared to any other event of interest. Because data from a considerable number of tests are now available, it is convenient to scale or normalize all events to a standard set of conditions. The conditions selected in the original scaling study[15] were as follows: for main cloud fallout, H_{mc} = 1 m, V_{eff} = 1 m/sec, S_{eff} = 1 deg, $f_{vmc}W_a$ = 4.2×10^9 J (1-ton) fission activity; for base cloud fallout, R_{bc} = 1 m, $f_{vbc}W_a$ = 4.2×10^9 J (1-ton) fission activity. The base cloud wind shears and velocities are implicitly assumed to lie in or near the range of conditions for the nuclear tests [S_{eff}(base cloud) ≈ 5 deg, V_{eff}(base cloud) ≈ 3 to 10 m/sec], although these quantities do not appear in the base cloud scaling equations. Similar standard conditions will be used to normalize the iridium deposition data (see below). Exposure rate functions, $D_{mc}(R)$, that have been scaled to the standard main cloud conditions are termed "normalized main cloud exposure rates." Likewise, exposure rate functions, $D_{bc}(R)$, that have

been scaled to the standard base cloud conditions are known as "normalized base cloud exposure rates." Each normalized exposure rate function for a given event should coincide closely with the same normalized exposure rate function for the other events. The goodness of fit is a test of the physical validity of the scaling relations. Any deviation from a satisfactory fit may give information about physical parameters that have been omitted from the model or about real differences between fallout deposition mechanisms for various events.

The iridium deposition data may be normalized in a manner analogous to the fallout exposure rate data. First, a set of standard conditions to which all events are scaled must be specified. The standard cloud dimensions and wind conditions adopted are the same as those for the nuclear events above. Comparability with the nuclear data is thus achieved. However, the amount of iridium vented into the main cloud or base cloud cannot be directly expressed in terms of equivalent fission yield until a suitable conversion factor is determined. It is necessary to select an arbitrary normalization standard for this parameter. The previous fallout simulation events contained a total activity, W'_a, of 83.5 g of iridium. Therefore, it was decided to scale all data to a standard main cloud or base cloud activity content of 83.5 g:

$$f_{vmc} W_a = 83.5 \text{ g}$$

$$f_{vbc} W_a = 83.5 \text{ g}$$

The actual amount of activity vented into a main cloud or base cloud will be $f'_{vmc} W'_a$ or $f'_{vbc} W'_a$, where W'_a = the amount of iridium placed in the charge.

In order to accomplish the scaling process, a fixed "Scaling Point" must be selected for each observed iridium deposition diagram. The point ($R' = 10^3$ m, $D' = 10^{-4}$ g/m^2) has been chosen for reasons of convenience. This scaling point is marked in Figs. 6.9 and 6.10. The fixed point will translate into normalized or calculated main cloud and base cloud scaling points determined from Eqs. (1) through (4). These points will be called (r_{mc}, d_{mc}) and (r_{bc}, d_{bc}), respectively. Substituting into Eqs. (1) through (4), we obtain the following results:

For the main cloud:

$$d_{mc} = \frac{83.5 \text{ g}}{f'_{vmc} W'_a} \left[\frac{V'_{eff} H'_{mc}}{(1.0 \text{ m/sec})(1.0 \text{ m})} \right]^2 \times \left(\frac{S'_{eff}}{1 \text{ deg}} \right) (10^{-4} \text{ g/m}^2)$$

$$= 10^{-4} \frac{1}{f'_{vmc}} (V'_{eff} H'_{mc})^2 (S'_{eff}); \qquad (5)$$

$$r_{mc} = (10^3 \text{ m}) \left[\frac{(1.0 \text{ m/sec})(1.0 \text{ m})}{V'_{eff} H'_{mc}} \right] = \frac{10^3}{V'_{eff} H'_{mc}}. \qquad (6)$$

For the base cloud:

$$d_{bc} = \frac{83.5 \text{ g}}{f'_{vbc} W'_a} \left(\frac{R'_{bc}}{1.0 \text{ m}} \right)^2 (10^{-4} \text{ g/m}^2)$$

$$= 10^{-4} \frac{1}{f'_{vbc}} (R'_{bc})^2; \qquad (7)$$

$$r_{bc} = (10^3 \text{ m}) \frac{1.0 \text{ m}}{R'_{bc}} = \frac{10^3}{R'_{bc}}. \qquad (8)$$

The units of "r" and "d" are meters and g/m^2, respectively. These scaling points will be used to normalize all iridium deposition curves and to compare the iridium data with normalized fallout exposure rates. Table 6.4 lists the scaling equation parameters used. R'_{bc} and H'_{mc} were obtained from photographic records. S'_{eff} and V'_{eff} are obtained from the post-shot hodograph.

The partition functions, f'_{vmc} and f'_{vbc}, for HE iridium-traced shots at various scaled depths of burial are not known at the present time but can be deduced.[4] It was determined that $f'_{vbc} = 0.75\ f'_v$ and $f'_{vmc} = 0.25\ f'_v$ produced the best scaling results. Previous events showed distribution of $f'_{vbc} = 0.60$ and $f'_{vmc} = 0.40$. The 75-25 split does not seem unreasonable considering the size of the base cloud and the low wind velocity that permitted debris from the main cloud to drop into the base cloud.

Figures 6.11 through 6.18 show IT-6 scaled to the nuclear curves found in TR-19 — Ref. 15 — (divided by 5×10^4, the conversion factor). The scaling points used in these figures are listed in Table 6.4. Two cases are shown for two different ranges of continuous ejecta; 22.9 and 36.6 m (25 and 40 yd). In the case in which $f'_{vbc} = f'_{vmc} = 0.5\ f'_v$, it is evident from Figs. 6.11 to 6.14 that the assumed partition of activity is incorrect. The base cloud curve is high while the main cloud curves (52 and 120 deg hotlines) with respect to the nuclear curve are low. This implies that $f'_{vbc} > f'_{vmc}$ because as $f'_{vbc} \to 100\%$ the base cloud scaling point shifts downward, and as $f'_{vmc} \to 0$, the main cloud scaling point shifts upward. Thus, an assumption of $f'_{vbc} = 0.75\ f'_v$ and $f'_{vmc} = 0.25\ f'_v$ was made. The results are shown in Figs. 6.15 to 6.18. Under this premise the scaled IT-6 curves at both continuous ejecta ranges agree much more closely in both the upward-crosswind and downwind directions.

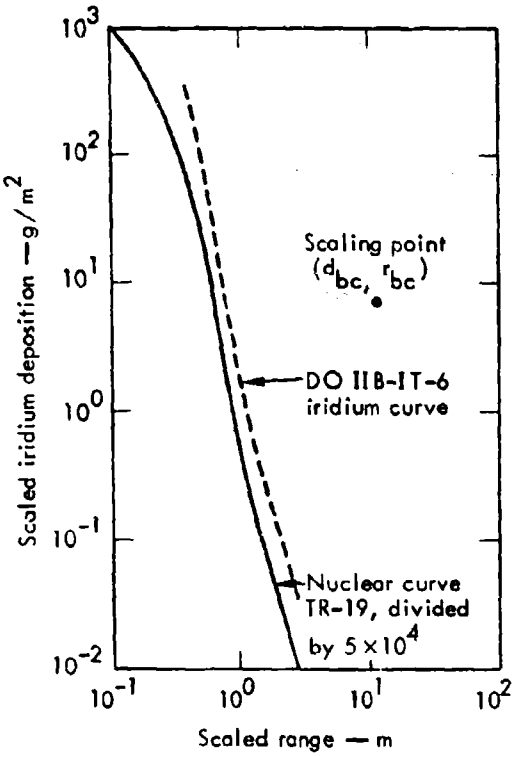

Fig. 6.11. Normalized DOIIB-IT-6 upwind-crosswind deposition using f_v beyond 22.9 m (25 yd) and a 50-50 partition of activity between base and main cloud.

CONCLUSIONS

This test program produced a means of safely gelling nitromethane to a

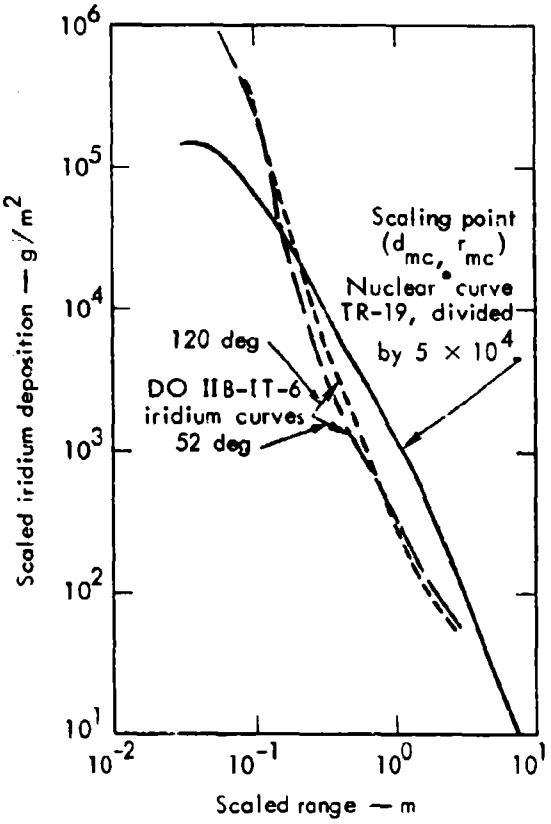

Fig. 6.12. Normalized DOIIB-IT-6 downwind deposition using f_v beyond 22.9 m (25 yd) and a 50-50 partition of activity between base and main cloud.

consistency that would maintain the fallout simulant particles in uniform suspension for a minimum period of two weeks. This two-week period is considered sufficient for the maximum downhole time expected in any future Diamond Ore or ESSEX testing. A means of field mixing and pumping the gelled nitromethane at the 907-kg (1-ton) level was developed and tested. This mixing and pumping system is considered safe. Testing of other mixing and pumping systems is being conducted to increase the system's capacity in view of the multiton yields to be employed in Project ESSEX 1.

An EOS for this gelled nitromethane and traced sand mixture has been produced and documented for use in design calculations by K Division, LLL, and Systems, Science, and Software, Inc. The reproducibility of the explosive has been demonstrated in Laboratory testing at LLL and in a detonation at the 907-kg (1-ton) level. The compatibility of the gelled nitromethane with the fallout simulation program has been demonstrated at the 907-kg (1-ton) level. The sensitivity of the fallout tracing system has not been affected by

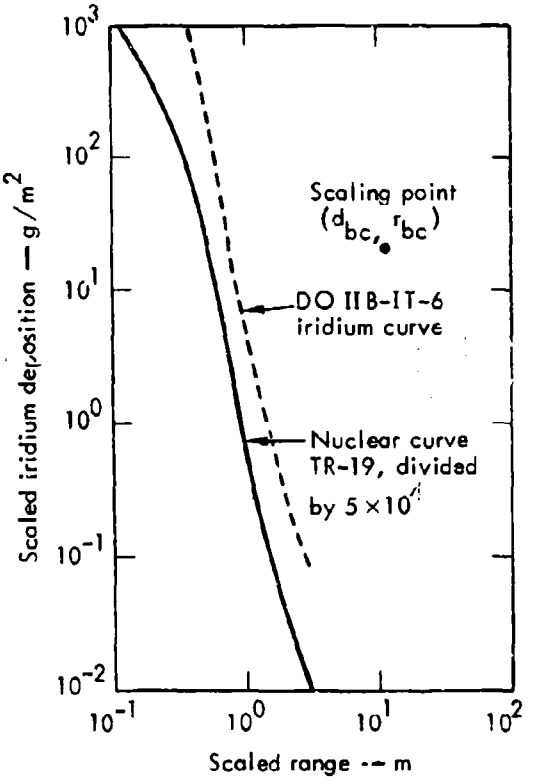

Fig. 6.13. Normalized DOIIB-IT-6 upwind-crosswind deposition using f_v beyond 36.6 m (40 yd) and a 50-50 partition of activity between base and main cloud.

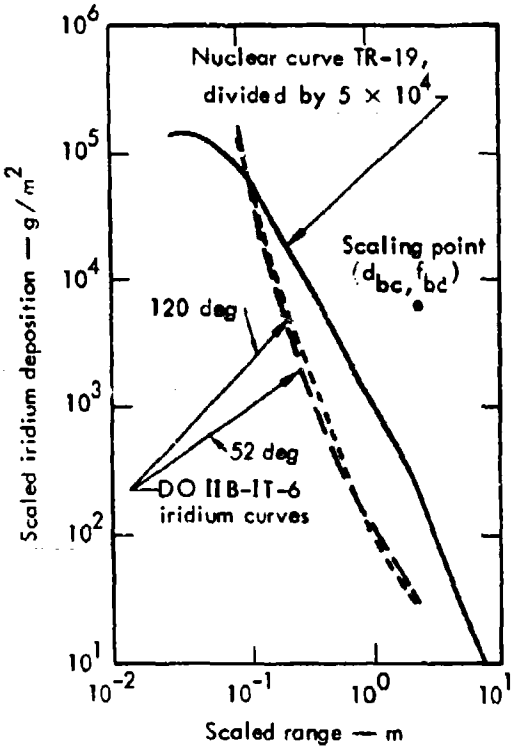

Fig. 6.14. Normalized DOIIB-IT-6 downwind deposition using f_v beyond 36.6 m (40 yd) and a 50-50 partition of activity between base and main cloud.

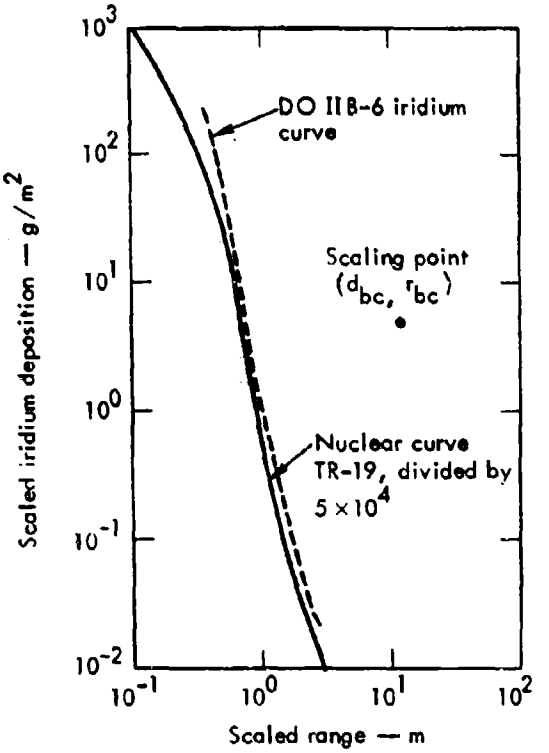

Fig. 6.15. Normalized DOIIB-IT-6 upwind-crosswind deposition using f_v beyond 22.9 m (25 yd) and a 75-25 partition of activity between base and main cloud.

Table 6.4. Scaling parameters used in normalizing IT-6 to nuclear curves.[15]

W'_a = 80.5 g; R'_{bc} = 85 m; S'_{eff} = 34.5 deg; V'_{eff} = 1.41 m/sec.

R_{ejecta} (m)	R_{ejecta} (yd)	f'_v	$f'_v = f'_{vbc} + f'_{vmc}$ f'_{vbc}	f'_{vmc}	Base cloud scaling points d_{bc}	r_{bc}	Main cloud scaling points d_{mc}	r_{mc}
22.9	25	0.200	0.50	0.50	7.33×10^0	1.18×10^1	6.39×10^3	2.38×10^0
36.6	40	0.068	0.50	0.50	2.11×10^1	1.18×10^1	1.82×10^4	2.38×10^0
22.9	25	0.200	0.75	0.25	4.89×10^0	1.18×10^1	1.23×10^4	2.38×10^0
36.6	40	0.068	0.75	0.25	1.44×10^1	1.18×10^1	3.65×10^4	2.38×10^0

its use with this explosive. The problem of determining vent fraction and comparing vent fractions for different types of stemming will be resolved on future tests by specifying both minimum and maximum wind velocities at the time of detonation.

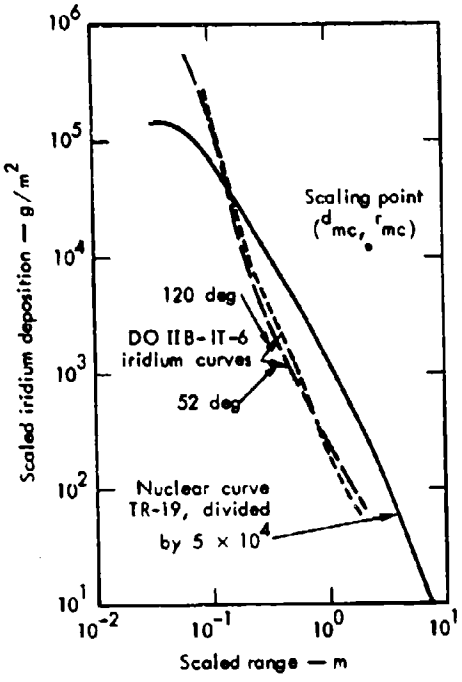

Fig. 6.16. Normalized DOIIB-IT-6 downwind deposition using f_v beyond 22.9 m (25 yd) and a 75-25 partition of activity between base and main cloud.

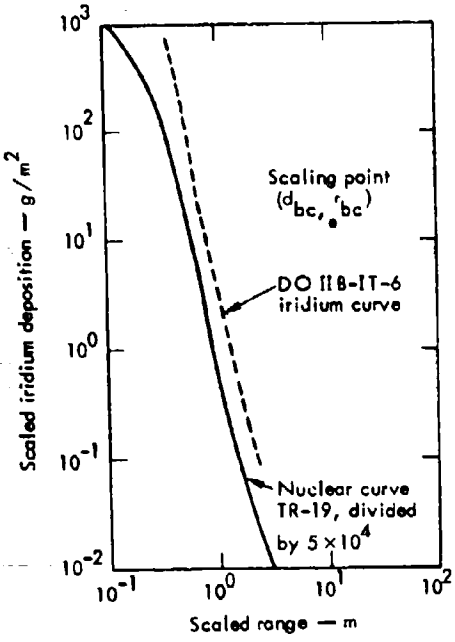

Fig. 6.17. Normalized DOIIB-IT-6 upwind-crosswind deposition using f_v beyond 36.6 m (40 yd) and a 75-25 partition of activity between base and main cloud.

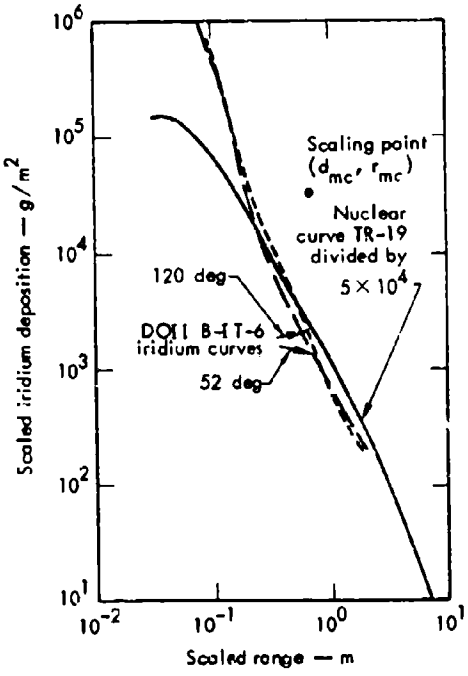

Fig. 6.18. Normalized DOIIB-IT-6 downwind deposition using f_v beyond 36.6 m (40 yd) and a 75-25 partition of activity between base and main cloud.

Chapter 7

Summary and Conclusions

SUMMARY

The Diamond Ore/ESSEX programs are jointly sponsored by the Chief of Engineers and the Defense Nuclear Agency. The Diamond Ore program was initiated in 1970 to determine the effects that different types of emplacement-hole stemming, DOB's, and geologic media will have on the crater size, radioactive fallout, and other collateral effects produced by the subsurface detonation of nuclear cratering devices of subkiloton yields. This purpose was expanded at the beginning of FY 73 to include the study of other targeting effects where cratering may or may not be the primary destruction mechanism. The expanded program was given the name ESSEX, which is an acronym for Effects of Sub-Surface Explosions.

These investigations are being conducted with chemical explosive energy sources designed to simulate nuclear sources. The Diamond Ore program is develop the chemical explosive charge configurations required to model subsurface nuclear detonations. This modeling was to include a means of simulating radioactive fallout. A nominal yield of 84×10^9 J (20 tons) was selected for the model development studies. The model development studies are being conducted through a complimentary series of calculations and field experiments. Calculations are being performed by K-Division, of the Lawrence Livermore Laboratory (LLL) and Systems, Science, and Software, Inc. Two depths of burial are being considered in these model development studies. K-Division, LLL, is performing cratering calculations at a DOB of 12.5 m (41 ft), which is generally considered optimum for the 84×10^9 J (20-ton) yield. Systems, Science, and Softwares, Inc. is conducting cratering calculations at a DOB of 6 m (19.7 ft) or about half of the optimum DOB. Calculations by both agencies are to consider fully stemmed, unstemmed (air-stemmed) and water-stemmed emplacement configurations. Model development is being accomplished through the cratering calculation for a nuclear detonation at the appropriate DOB. Chemical explosive cratering calculations are then conducted in an attempt to match the pressure, velocity, density, and energy depositions predicted by the nuclear calculation. Changes in the chemical explosive yield and shape are made until a good match is achieved between the two predictions. The resulting design for the chemical charge is then field-tested at full scale. Field test data are obtained from instrumentation placed at points of interest to the computational effort. The field data are then compared with the predicted data and changes are made to the charge design as necessary to match the predicted results. After any necessary changes have been made, the chemical explosive model design is ready for employment in various terrain and geologic

conditions to determine the effects of stemming, DOB, and geologic media. Collateral effects data will be gathered and used as input to the specific ESSEX targeting studies.

The cratering calculations require the input of two specific types of data. They are an equation-of-state for the geologic medium and an equation-of-state for the chemical and nuclear explosive. The initial explosive selected for the Diamond Ore experiments was a water-gelled aluminized ammonium nitrate slurry. Dow Chemical Company was selected to supply this explosive through standard competitive bidding procedures based on performance specifications developed by EERL and the Organic Materials Division, Chemistry Department, LLL. Explosive safety testing was conducted at Dow in addition to initial performance testing.

The fallout simulation development program was conducted jointly by EERL and the Stanford Research Institute (SRI). The system developed called for the seeding of the explosive charge with iridium-coated sand of known specific particle sizes. These traced particles were uniformly mixed throughout the explosive at 10% by weight level. The initial testing by Dow included the explosives with this 10% sand level. A series of small-scale 2.7-kg (6-lb) cratering detonations was conducted by LERL in a sand test pit at the LLL Site 300 test facility. Stemmed cratering curves were developed from this testing for both the pure explosive and the sand-contaminated explosive. Any differences in the cratering effectiveness between these two explosives were well within the scatter of the test pit data. Two unstemmed detonations and a water-stemmed detonation were also conducted in this series. As was expected, the water-stemmed crater fell very close to the stemmed curve with the unstemmed detonations indicating reductions in both crater radius and crater depth. All of the sand-contaminated shots included testing of the fallout simulation program. Fallout samples were collected from each of these shots. Samples from the water-stemmed, unstemmed, and two stemmed detonations, all at about optimum DOB, were processed for determination of fallout data. Identical vent fractions were obtained for the two stemmed detonations demonstrating the reproducibility of the fallout simulation system. The unstemmed and water-stemmed detonations produced a significantly higher vent fraction than the stemmed detonations. This might have been assumed considering the immediate venting of the detonation produced by the open emplacement hole and the apparent lower stemming efficiency of water. The water-stemmed detonation produced the largest vent fraction numerical value. Because vent fraction is defined as the sum of material vented and deposited in the focal fallout area, vent fraction should not be interpreted as meaning the total of the vented material. The vent fraction values were not compared to actual nuclear vent fractions from nuclear cratering tests at NTS, because no attempt was made to model nuclear test phenomena, such as the use of detailed and keyed stemming designs or the matching of uphole velocities or reactions in the unstemmed or water-stemmed cases. The difference in these vent fractions does however demonstrate the sensitivity

of the fallout simulation system for the various stemming conditions.

The fallout simulation system was also tested at the 4.2×10^9 J (1-ton) level in conjunction with the Middle Course II experiments at Trinidad, Colorado. Results of these tests with various types of stemming demonstrated the same vent fraction trends as were found in the Site 300 2.7-kg (6-lb) tests.

In order to obtain field data to do code development work, three heavily instrumented 9,070-kg (10-ton) detonations were conducted at Fort Peck, Montana, in October 1971. These detonations included a fully stemmed and an unstemmed detonation at a DOB of 12.5 m (41 ft), and a fully stemmed detonation at a DOB of 6 m (19.7 ft). Detonation velocity measurements were made in each quadrant of each 9,070-kg (10-ton) sphere. These measurements for the first detonation indicate that all four quadrants of the explosive detonated uniformly and at about the predicted velocity. The same measurements in the second detonation [DOB of 12.5 m (41 ft) stemmed] and in the third detonation [DOB of 6 m (19.7 ft) stemmed] indicated not only a generally slower detonation than the first shot, but significant variations were noted within each charge. This lack of reproducibility in this explosive was verified in subsequent EOS testing by the Chemistry Department, LLL. Attempts were made to stabilize the detonation characteristics through a series of formulation changes. After exhaustive testing, the explosive was stabilized but was also desensitized to a point where it was not considered applicable to the Diamond Ore program.

During this testing a search for a backup explosive was conducted. This search was directed at a means of gelling or thickening nitromethane to a consistency that would hold the fallout simulant particles in uniform suspension. A modified guar gum (XG512), being developed for the express purpose of gelling nitromethane, was obtained from General Mills, Inc. Laboratory testing by the LLL Chemistry Department decided on a mixture of 3% gum, 10% sand, and 87% nitromethane. This mixture was sufficiently thick to maintain the sand in suspension for a two-week period. Safety and EOS testing was conducted on the 3/10/87% mixture, and a system for the field mixing and down-hole emplacement was developed and tested. This system was then used in the conduct of a 907-kg (1-ton) unstemmed gelled nitromethane experiment at a DOB of 5.5 m (18 ft) at Fort Peck, Montana, in October 1972. Detonation velocity measurements taken in this 907-kg (1-ton) detonation verified the laboratory-obtained velocities. This 907-kg (1-ton) detonation also included a test of the fallout simulation program. This testing indicated no compatibility problems between the two systems. Wind conditions experienced during this test prevented the calculation of a realistic vent fraction. A report dealing with the other cratering test conducted at Fort Peck in October 1972 will be published.

CONCLUSIONS

The water-gelled aluminized ammonium nitrate slurry extensively tested in

the Diamond Ore program is not suitable for use in scientific work where reproducibility in the micro/millisecond time frame is necessary. The size/yield dependency effects caused by the relatively wide detonation front exhibited by this explosive should be expected in other complex composite explosives. The reproducibility problems on the microscopic scale do not affect the use of these explosives in commercial applications where the macroscopic scale is of interest.

The gelled nitromethane, composed of 3% by weight of the gelling agent, XG512-guar gum, 10% trace sand, and 87% nitromethane, is a high-energy, reproducible and economic explosive suitable for use in the Diamond Ore/ESSEX program. An equation-of-state suitable for use in the calculation programs was defined for this explosive by the Chemistry Department at LLL. This explosive is also compatible with the fallout simulation program.

The fallout simulation program as developed jointly by EERL and SRI meets the objectives of the Diamond Ore program in that it allows determination of a vent fraction for various emplacement configurations to include the type of stemming, DOB, and effects of unstemmed hole sizes. This system also simulates radioactive fallout in that iridium mass deposition curves can be scaled to the upwind-crosswind and downwind dose rate curves from nuclear detonations.

Appendix A
Explosives Contract Specifications

This appendix contains a verbatim copy of the specifications section of the Project Diamond Ore explosives contract as awarded to the Dow Chemical Company. Specifications are included for the explosive, manufacturer testing, and certification, and for the supply of specific quantities of the explosive to NCG (now EERL). The certifications provided by the manufacturer contained information regarded as proprietary. This information is therefore not published in this report. Requests for this information should be directed to the manufacturer.

SECTION F

Project DIAMOND ORE -- SPECIFICATIONS

F-1 Project Description

A. Introduction. Project DIAMOND ORE is a three phase program developed by the Nuclear Cratering Group (NCG) to study the problem of simulating a nuclear detonation using chemical slurry explosives. The principal objectives of the program are: (1) to model the cratering characteristics of a nuclear detonation, and (2) to simulate the radioactive fallout from a nuclear detonation. To simulate the radioactive fallout, it is envisioned that a non-radioactive tracer element will be coated on sand particles, and the sand particles mixed uniformly with the chemical explosive. Following detonation, the sand contaminant will be collected in fallout trays. The collected samples will be irradiated in a nuclear reactor to activate the tracer element on the sand particles. The levels of induced activity in the collected samples will then define a fallout pattern.

Project DIAMOND ORE will be conducted in three phases. Phase I will include the chemical explosive selection, selection of the sand contamination level necessary for collection, and small-scale (approximately six-pound spherical charges) chemical explosive testing performed by the selected manufacturer and by NCG. At the present time, it is not known what percentage weight level of sand contaminant can be used to both (1) permit high order detonation of the approximately six-pound spherical charge, and (2) permit physical detection of the sand following collection of fallout samples, prior to irradiation. In Phase I equation-of-state testing will be performed by the Lawrence Radiation Laboratory (LRL) on both the selected pure explosive and the pure explosive with the chosen level of sand contamination.

Phase II will include two large scale nuclear test simulations (large chemical explosive detonations containing the tracers) to be performed

at Fort Peck, Montana, during the fall of 1971, plus an undetermined number of large-scale nuclear test simulations to be conducted during the spring or summer of 1972. Phase III will consist of between two to eight large-scale nuclear test simulations to be conducted during Fiscal Year 1973.

B. Explosive Specifications. The pure explosive selected for Phases I and II will be a slurry which must meet the following performance specifications:

1. The minimum energy density (mass density times theoretical heat of detonation) shall be 2850 cal/cc. The theoretical heat of detonation shall be calculated by taking the difference in heats of formation between products and reactants, assuming complete reaction of the reactants.

2. The minimum density after gelling shall be 1.50 gm/cc.

3. The minimum detonation velocity shall be 5000 m/sec.

4. The slurry explosive shall have a critical diameter such that a 6-inch diameter sphere of explosive with 10.0% sand contamination (i.e., 90.0% by weight explosive and 10.0% by weight sand contaminant) will have a high order detonation using a No. 8 blasting cap and 150 gm of pentolite booster.

5. Sensitivity: The pure explosive shall be no more sensitive or hazardous than tritonal (80% TNT, 20% Al).

6. Gelling: The pure explosive shall be homogeneous throughout and shall gell to a consistency that will support a 6-foot high column of gravelly sand in a 3-foot diameter drill hole without intermixing. Any cover employed by the Contractor to prevent intermixing is subject to final approval by the Contracting Officer. Prior to gelling, the explosive shall be sufficiently liquid to allow pumping through a 2-inch inside diameter hose 100 feet long at a rate of at least 100 lbs/min.

7. Filling explosives containers: The Nuclear Cratering Group will furnish a total of 250 translucent plastic (PVC) hemispheres for all spherical charges to be manufactured. (This includes 56 extra hemispheres.) Each

plastic (PVC) hemisphere is 0.030 inches thick, 6.0 inches in diameter with a 0.5-inch flange. The plastic hemispheres shall be filled such that the gelled explosive is level with the flange on the hemisphere. Two such hemispheres, when mated together to form a sphere, shall have no voids. In addition, a sufficient number of test assembly containers will be supplied by LRL through NCG for filling. No extra test assembly containers will be included. Specific data as to size and shape of these test containers will be furnished later.

8. Sand contaminant: The sand contaminant will be supplied by NCG. It will range in particle size from 125 μ to 175 μ. The sand contaminant shall be mixed uniformly throughout the explosive in the quantity specified by item number. The sand contaminant will be shipped in three separate shipments for use in Explosive Lots 1 through 3. Sand Shipment No. 1 will contain 25 pounds in one 5-gallon container. This quantity is double the amount of sand required. Quantities for Sand Shipment Nos. 2 and 3 will be determined at a later date. A sufficient excess will be included.

9. The spherical charges of a given item shall have a density and weight variation no greater than three percent.

10. The explosive shall be chemically compatible with the furnished PVC plastic hemispheres such that 12 months storage of the explosive in the hemispheres will not cause any degradation of the explosive or the hemispheres.

C. Research Proposal

Each vendor shall submit a firm fixed price bid for the services to be performed as listed in the Schedule hereof. The proposal shall contain the information detailed below:

1. Company Background Information

a. Description of Research Facilities: Each vendor shall include a

description of its research facilities to be used for the testing and production of the required explosive.

b. Statement of Previous and Current Experience in the Slurry Explosive Field.

c. Principal Investigator: Each vendor shall provide a resume for the principal investigator on the project.

2. Technical Specifications to be Provided. The proposed explosive must meet all the performance and handling specifications listed in paragraph IB. The following information shall be furnished by the vendor:

a. Chemical formulation of explosive in percentage by weight described in terms of common chemical names and not in terms of special company designations. This shall include the amount and composition of all gelling events. This information will be regarded as proprietary and classified "For Official Use Only."

b. The particle size distribution of all components comprising the explosive. In addition, the expected particle size distribution of all components after gelling.

c. Minimum energy release as calculated by taking the difference in heats of formation between products and reactants, assuming complete reaction of the reactants.

d. Minimum density after gelling.

e. Shock, bubble, and total energy in calories per gram of explosive (booster energy is subtracted out).

f. Cap sensitivity.

g. Minimum pentolite booster required for high order detonation.

D. Explosive Selection. Award of a contract will be on the basis of the lowest bid price for the services to be performed as listed in the Schedule.

1. Testing - Part 1. The vendor shall manufacture spherical charges of the pure explosive (Item 1) and spherical charges of explosive with several percentage weights of contamination (Items 2 through 6), as detailed in the Schedule. The vendor shall also manufacture pure explosive for the filling of test assembly containers to be used in equation-of-state testing by LRL (see the Schedule). The test assembly containers will be furnished by LRL through NCG. The manufacturer shall conduct the following tests:

Underwater Tests: Three underwater tests shall be conducted on each of the explosive Items 1 through 6 to determine:

(a) Shock energy

(b) Bubble energy

(c) Total energy

All energies shall be reported in cal/gm of pure explosive; i.e., the contamination and booster shall be subtracted out. The explosive charges to be used in these tests shall be spherical and constructed as specified in paragraph IB7. The charges shall be center detonated with a No. 8 blasting cap and a 150 gm pentolite booster. The test results shall be reproducible to within five percent for each level of contamination.

2. Certification - Part 1. The results of the underwater tests will be analyzed by NCG to determine the percentage level of contamination to be used in subsequent experimental work. The level of contamination will be selected from Items 2 through 6. The following certification shall be furnished by the vendor upon completion of the underwater tests detailed in paragraph ID1:

a. Chemical formulation of explosive in percentage by weight described in terms of common chemical names and not in terms of special company nations. This shall include the amount and composition of all gelling agents. This information is required for equation-of-state testing by NCG and will be regarded as proprietary and classified "For Official Use Only."

b. The particle size distribution of all components comprising the explosive. In addition, the actual or expected particle size distribution of all components after gelling.

c. Measured gelled density of pure and contaminated explosives, grams per cc.

d. Shock, bubble, and total energy in calories per gram of pure explosive for all tests listed in paragraph ID1.

3. Testing - Part 2. Following the selection of the percentage level of contamination by NCG, the vendor shall manufacture the spherical charges and samples to be used for equation-of-state testing as detailed in the Schedule. The vendor shall conduct the following tests on the final selected item:

a. Cap sensitivity tests: Conduct six (6) tests: three (3) each with a No. 6 and a No. 8 blasting cap. Each charge shall be spherical and constructed as specified in paragraph IB7. Results shall be reported as:

(1) Explodes

(2) Ignites

(3) No reaction

b. Minimum booster tests: Performance of these tests is contingent on results of the cap sensitivity tests in paragraph ID3a. Minimum booster tests shall be conducted only if the cap sensitivity tests are negative (i.e., ignites or no reaction). Two tests shall be conducted per booster size. The explosive charges to be used in these tests shall be spherical and constructed as specified in paragraph IB7. Charges will be center detonated. Results shall be reported as grams of pentolite and cap size required to obtain a reproducible high order detonations.

4. Certification - Part 2. The following certification shall be provided upon completion of the tests specified in paragraph ID3:

a. Cap sensitivity - see paragraph ID3a.

b. Minimum Pentolite Booster - see paragraph ID3b.

c. Measured gelled density of selected contaminated explosive, grams per cc.

5. Equation-of-state testing. The vendor agrees to permit equation-of-state testing to be performed on the explosives specified in the Schedule.

Testing will be accomplished by the Lawrence Radiation Laboratory or an independent organization under contract to NCG or to the Lawrence Radiation Laboratory.

6. Shipment of spherical charges and filled test assembly containers. The spherical explosive charges to be furnished NCG as specified in the Schedule will be shipped as hemispheres. Each hemisphere shall be suitably labelled with the batch number with a permanent marking. The exposed surfaces of the explosive in hemispheres are to be covered with "Saran Wrap" or suitable equivalent to prevent evaporation. Contracting Officer's authorized representative will orally furnish shipping instructions. Shipment of the filled test assembly containers shall be made to the same location. Advance notice of shipping and estimated arrival date should be furnished the Contact Officer.

E. Field Experiments. The explosive lot No. 3 (see the Schedule) is tentatively scheduled for use at Fort Peck, Montana in September or October 1971. Additional information on the field experiment will be supplied at a later date. The Contractor shall note the following:

1. Unit price: The price quoted for this lot shall be for delivery of the slurry explosive downhole.

2. Emplacement: The slurry may be delivered to the job site either in bulk or prepackaged. The slurry shall be capable of emplacement by pumping or tremie into the charge cavity through a 4-inch diameter combination fill and vent line or open access hole. The discharge end of the delivery hose or tremie shall be kept below the rising pool level of the explosives at all

times. The quantity of blasting agent shall be measured by count of the packaged materials, by weighing or by metering, at the option of the Contractor. The measurement unit shall be in pounds. If the material is weighed or metered, the measuring system shall be calibrated in the presence of a representative of the Contracting Officer. The tolerance of the measuring system shall be within 3 percent of the value indicated on the recording device.

3. Emplacement Bulk Density: The Contractor shall make a minimum of one density measurement per emplacement hole to determine the density of the blasting agent being emplaced. After emplacement, the density of the explosive shall be within 5 percent of the average density as determined experimentally.

F. Additional Information

1. Contact Officer: Captain Richard J. Meisinger shall be designated as Contact Officer at NCG.

2. Notice of Possible Additional Explosives Requirements: NCG may purchase quantities of the selected contaminated explosive in 12 to 100-ton lots in the third and fourth quarters FY 72 and FY 73. Procurement of the possible additional quantity will be from the successful Contractor under this procurement.

Appendix B

Specifications for Test Medium at Site 300 Test Pit

General:

EERL operates an explosive test facility at the LLL Site 300 test facility. The EERL test facility is composed of a firing bunker and indoor and outdoor firing tables. The use of this test facility allows for the conduct of small-scale testing of explosives under controlled conditions. The outdoor table was used for the small-scale cratering tests discussed in Chapter 3. The remainder of this appendix describes the test medium and its reconditioning during the Diamond Ore 6-lb cratering series.

Sand Gradation:

The PCA gravel pit concrete sand used at Site 300 has the following gradation:

U.S. standard sieve size	Percentage passing by weight
#4	97-100
#8	73- 88
#16	53- 68
#30	38- 48
#50	15- 25
#100	2- 10
#200	5

Moisture Content:

Field compaction tests completed by the South Pacific Division Soils Testing Laboratory showed that eleven passes of a vibratory compactor over a 7-in. lift of loose sand with a moisture content of 6% would yield a consistent density. On the basis of these tests, a specification requiring an average moisture content of 6% and an average dry density of 112.0 lb/ft^3 was initially adopted. However, it was found that the sand arriving at the site had a moisture content higher than the 6% that had been adopted. Tests were then conducted with the moisture content set at 8%. It was found that, at a moisture content of 8%, after 11 passes of a vibratory compactor, the sand yielded an average dry density of 112.0 lb/ft^3. Therefore, because of the difficulty involved in drying the sand and the results found in the Site 300 tests, it was decided to establish the moisture content at 8%.

Sand Placement:

After every shot all disturbed sand was removed and new sand was placed in the pit in 7-in. layers. The sand was then tested for moisture content by means of a speedy moisture meter. After the sand had been brought to the acceptable moisture

content, limits of 7.8 to 8.2%, it was compacted by means of 11 passes of a small vibratory compactor. Wet density tests, with a Reinhard rubber balloon density tester, were then used to measure the compaction. The sand was to be within the limits of 119.5-120.5 lb/ft^3 wet density. If the density was below standards, the lift was recompacted until it met requirements.

Appendix C

Multiton Cratering Experiments (Phase IIA)

BACKGROUND AND PURPOSE

As stated in Chapter 2, the original planning for Project Diamond Ore inincluded several 18,140-kg (20-ton) chemical explosive detonations at the Nevada Test Site. This plan was significantly altered with the addition of the computational programs to be conducted by Systems, Science, and Software, Inc., and by K Division, LLL. One of the requirements of the calculational programs was a detailed definition and understanding of the constitutive relationships of the medium in which the modeling calculations and detonations were to occur. Due to the large amount of equation-of-state (EOS) type information available for the Bearpaw shale at Fort Peck, Montana, this site was selected for the Phase II model development experiments. Fort Peck had been the location of the Pre-Gondola series of cratering experiments in the late 1960's and was available for the conduct of additional large-scale chemical explosive testing. In addition to the existence of EOS data, this medium was ideally suited for numerical modeling calculations because of geologic uniformity. The geologic profiles of this area typically show a thin layer of topsoil overlaying a weathered clay shale. The weathering of the shale decreases with depth to an unweathered shale that extends to great depths. The geographic location of Fort Peck and the test area is shown in Fig. C.1.

The first large-scale experiments at Fort Peck, Montana, in the Diamond Ore program were three 9,070-kg (10-ton) detonations (Phase IIA) conducted in October 1971. Two of the detonations were at a DOB of 12.5 m (41 ft) with one shot unstemmed (DOIIA-1) and one shot stemmed (DOIIA-2). The third detonation had a DOB of 6 m (19.7 ft) (DOIIA-3) and was stemmed.

These detonations were highly instrumented to provide data to aid in code development work being conducted by LLL and Systems, Science, and Softwares, Inc. The detonations would also provide a first look at the effects of stemming in multiton yields. The explosive EOS testing was not completed by the time the Phase IIA detonations were conducted. Therefore the charge designs were based on the energy test data provided by the manufacturer as described in Chapter 3. The explosive charges in Phase IIA were instrumented to allow for the determination of explosive EOS data in multiton detonations as discussed in Chapter 4.

The two-dimensional codes discussed in Chapter 2 had not been used to calculate cratering detonations with the two-phase EOS found in the Diamond Ore slurry explosives. As neither chemical nor nuclear unstemmed cratering detonations had been previousiy conducted, there existed no standard by which to judge the validity of the calculational techniques. The purpose of the Phase IIA experiments was then to provide the field data required

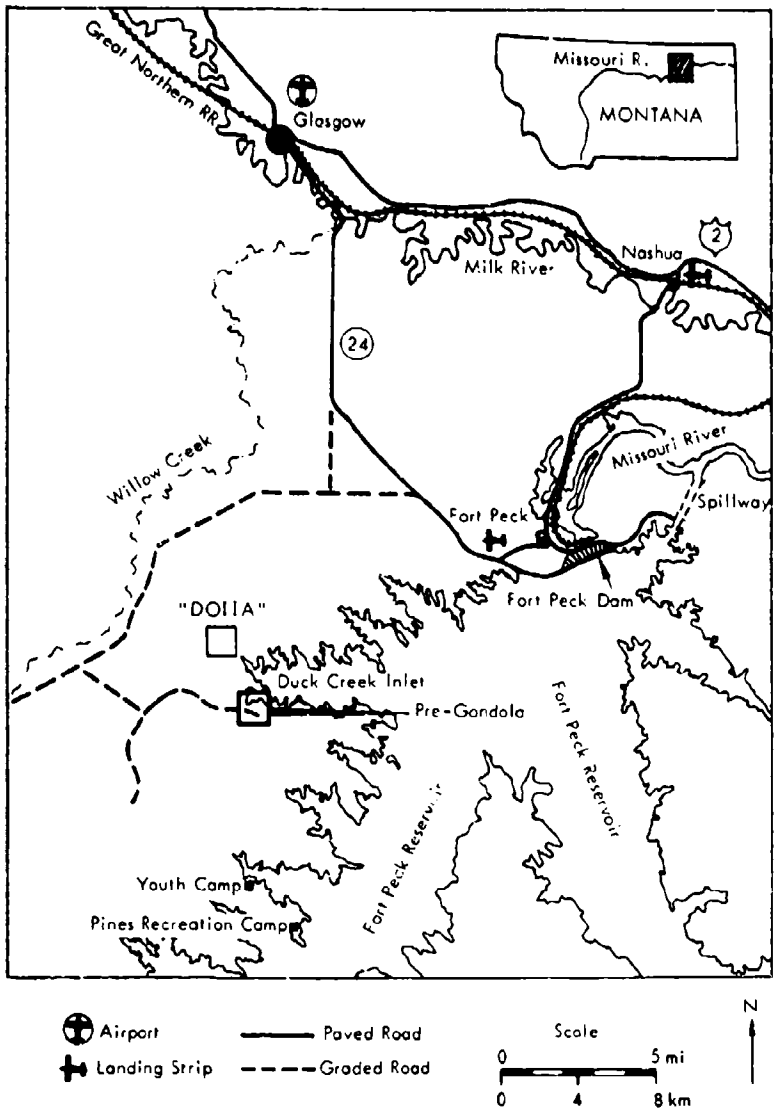

Fig. C.1. Diamond Ore site location.

to aid in both code development in the use of a two-stage explosive EOS and in code verification and development for the modeling of the unstemmed configuration. These experiments were also to provide a first look at the differences in effects from stemmed and unstemmed cratering detonations at the multiton yield level.

TEST AREA DESCRIPTION

The Diamond Ore Phase IIA site was located in the Duck Creek Inlet area adjacent to the Fort Peck Reservoir in Section 34, T26N, R39E, Valley County, Montana (Fig. C.1). There were no inhabited dwellings within 6.4 km (4 mi) of

the test site. As shown in Fig. C.1, the Diamond Ore test area was about 3.2 km (2 mi) northeast of the Pre-Gondola test site. The three surface ground zeroes (SGZ), were located on the edge of a broad, flat valley. This area was selected after extensive seismic refraction surveys were conducted. The relatively flat valley floor was needed for fallout collection activities planned for future testing. The test site contained sparse vegetation that supported only limited cattle grazing which is managed by the Department of Interior, Bureau of Land Management. The test site lies on land controlled by the Corps of Engineers, but also falls within the Charles M. Russell Wildlife Refuge. This refuge is administered by the Department of Interior, Bureau of Sport Fisheries and Wildlife. The Fort Peck site is located in the Bearpaw shale, a highly compacted, uncemented clay shale of the Cretaceous Age. Where the Bearpaw shale outcrops, it forms either badlands or a terrain with moderately steep to gentle slopes. The shale at the Diamond Ore site is uniform, dark grey, highly compacted and uncemented. It contains infrequent calcareous and iron-manganese concretions up to several feet in diameter, and wavy, light-grey-to-yellow bentonite layers up to several inches thick. Several joint sets with inconsistent orientation occur at spacings at 0.15 to 0.91 m (0.5 to 3 ft), and numerous hairline cracks are visible between the major joints. The shale is weathered to depths of 3 to 9 m (10 to 30 ft). The effects of weathering include increased fracture frequency and opening of joints. The surface layers of the weathered shale are highly fragmented. Alternate wetting and drying cycles have produced a further breakdown of the surface shale particles to form a fat clay.

The layering determined by preshot seismic refraction surveys of each SGZ is shown in Fig. C.2. Cores were drilled at each SGZ to a depth of 15.2 m (50 ft). Core logs and the results of laboratory testing of these core samples are shown for each SGZ in Figs. C.3, C.4, and C.5. The equation-of-state of this medium is documented in Ref. 5 and will be used in the design for the next test series.

EXPERIMENT DESIGN

As previously stated, the Phase IIA experiments preceded the calculational efforts by Systems, Science, and Software, Inc., and LLL to aid in actual code development. The only explosive data available for design of the experiments were the explosive energy data from the manufacturer's performance testing described in Chapter 3. It was desirable to have the explosive charge as close to the final modeling charge yields as possible. It was also desirable to have all three explosive charges identical to demonstrate the effects of varying the type of stemming and DOB. Based on the initial studies described in Chapter 2, a 67.2×10^9 J (16-ton) TNT-equivalent explosive energy yield was selected.* This yield was based on the expected loss of about 20% 84 $\times 10^9$ J (20-ton) nuclear explosive energy in cavity vaporization.[2] This TNT energy requirement converts to a Diamond Ore

*Recent calculations by K Division, LLL, indicate that a more realistic yield for the stemmed case is 42×10^9 J (10 tons).

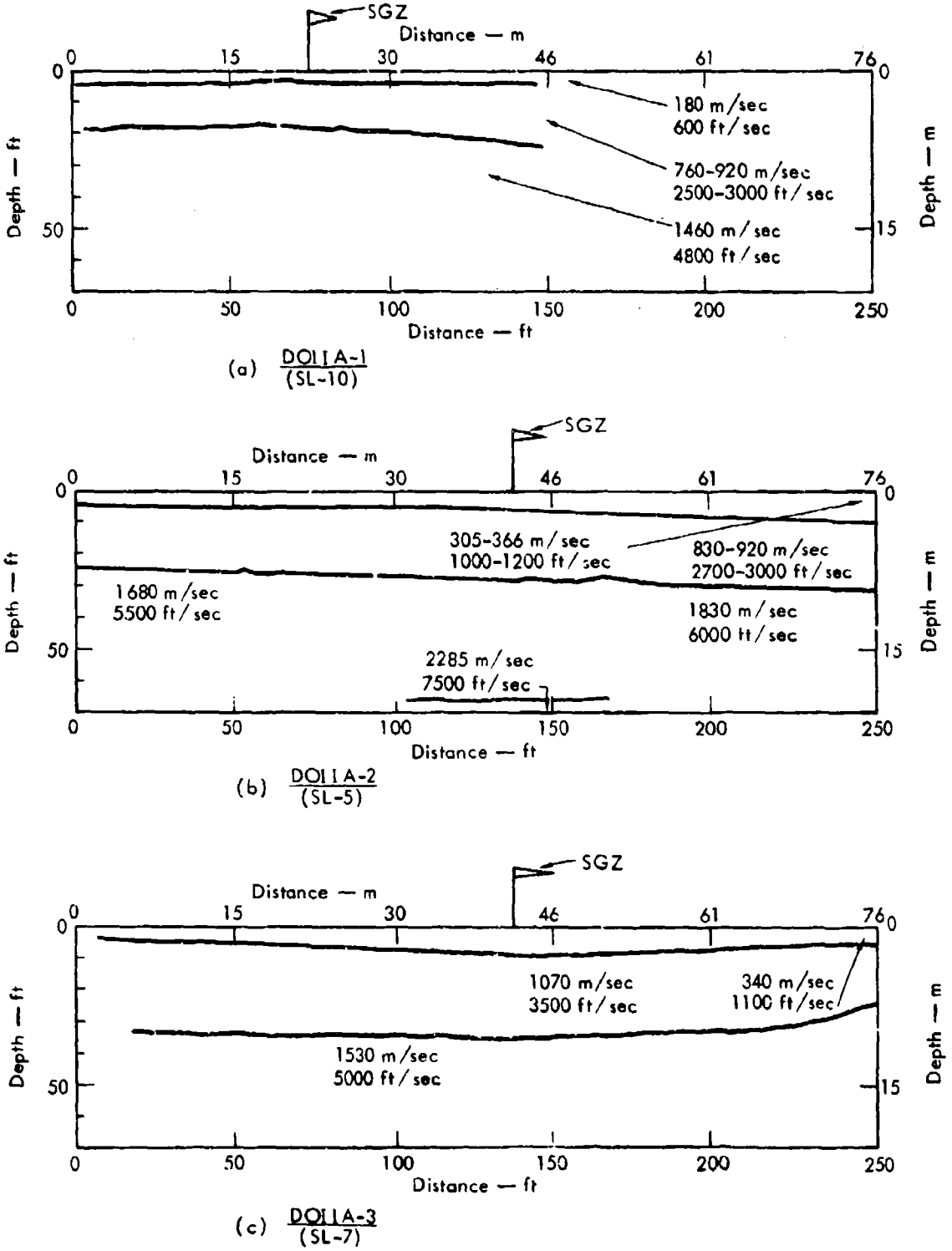

Fig. C.2. Seismic refraction survey results for DOIIA surface ground zeroes.

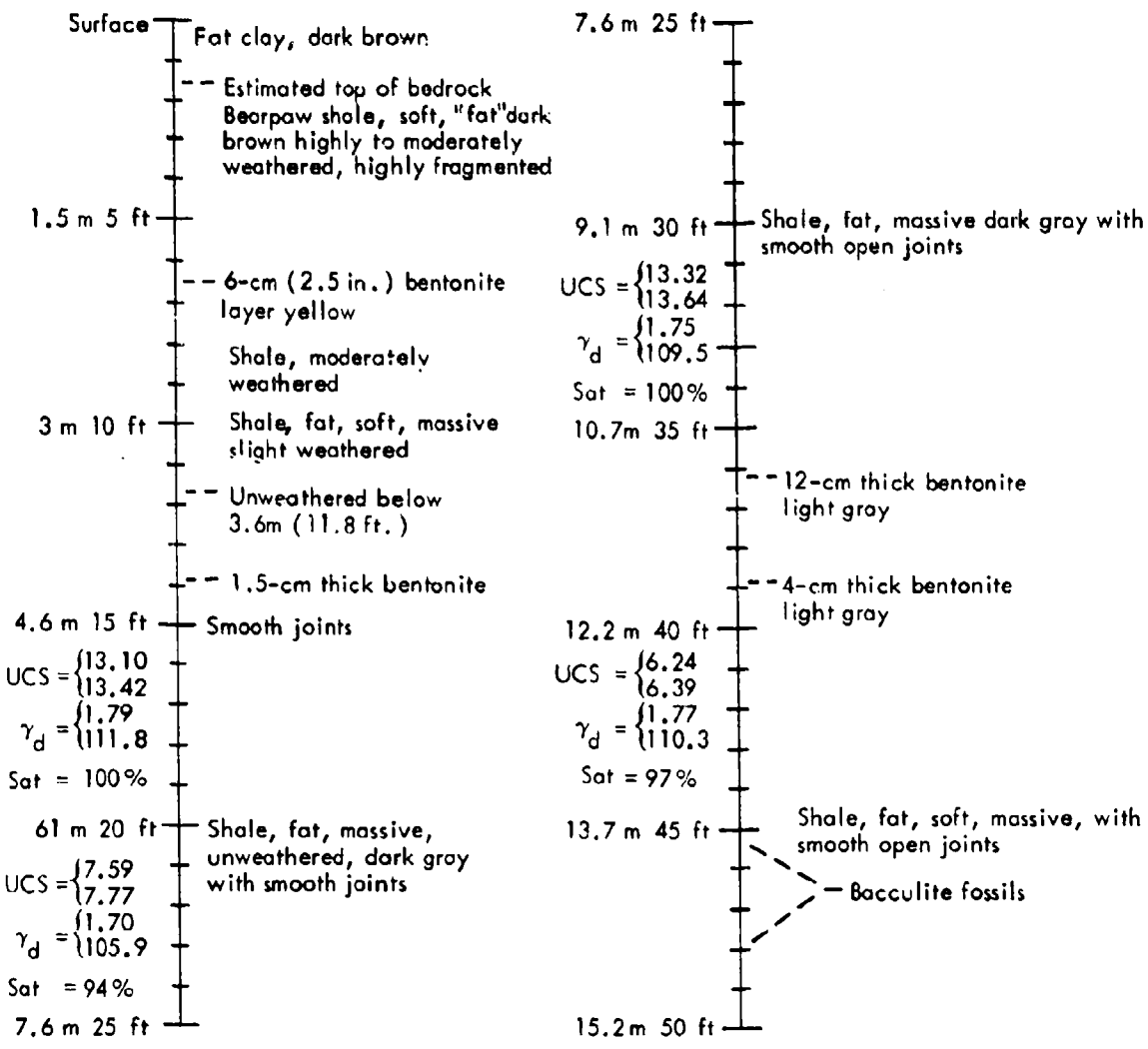

Note: Laboratory test data given to left of elevation line with geologic description given to the right. UCS=Unconfined Compressive Strength in kg/cm^2 and $tons/ft^2$; γ_d = dry density in g/cm^3 and lb/ft^3; Sat=Saturation in percent.

Fig. C.3. Drilling log and laboratory test data for DOIIA-1.

slurry explosive charge weight of 9,070-kg (10 tons) for the pure explosive. The explosive charges were placed in mined, spherical cavities having a diameter of 2.3 m (7.6 ft). In an attempt to maintain explosive continuity throughout Diamond Ore experiments, the explosive was later changed to include the 10% sand contamination. The sand added to the explosive was not coated with the iridium trace element because no tracer program was to be conducted in multiton detonations until the final modeling detonations. The addition of the 10% sand reduced the effective energy yield for each 9,070-kg (10-ton) slurry charge to about 58.3×10^9 J (14 tons) of TNT.

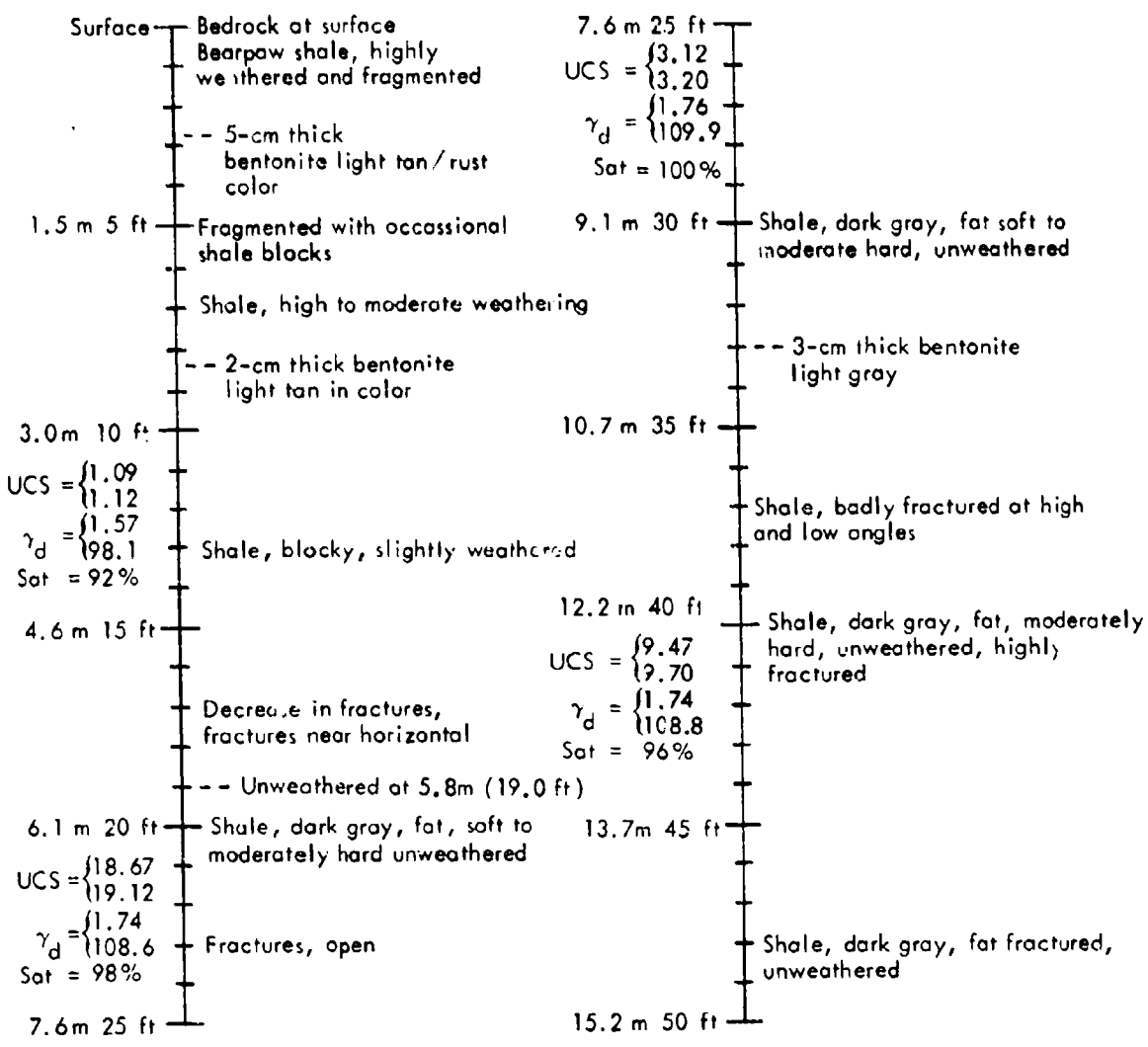

Note: Laboratory test data given to the left of elevation line with geologic description given to the right. UCS = Unconfined Compressive strength in kg / cm^2 and tons / ft^2; γ_d = dry density in g/cm^3 and lb/ft^3; Sat = Saturation in percent.

Fig. C.4. Drilling log and laboratory test data for DOIIA-2.

The stemming in the 12.5 m (41-ft) DOB and 6-m (19.7 ft) DOB detonations was done with a media matching grout designed for use in the Pre-Gondola experiments by the Concrete Laboratory of the Waterways Experiment Station. Stemming for the 12.5-m DOB detonation was keyed into the surrounding medium in much the same manner as the Pre-Gondola and previous NTS nuclear detonations had been (see Fig. C.6). Because of its shallower DOB, the 6-m detonation was not keyed. The 12.5-m DOB unstemmed detonation was to have the full 0.91 m (3 ft) diameter access hole left open (air-stemmed or unstemmed).

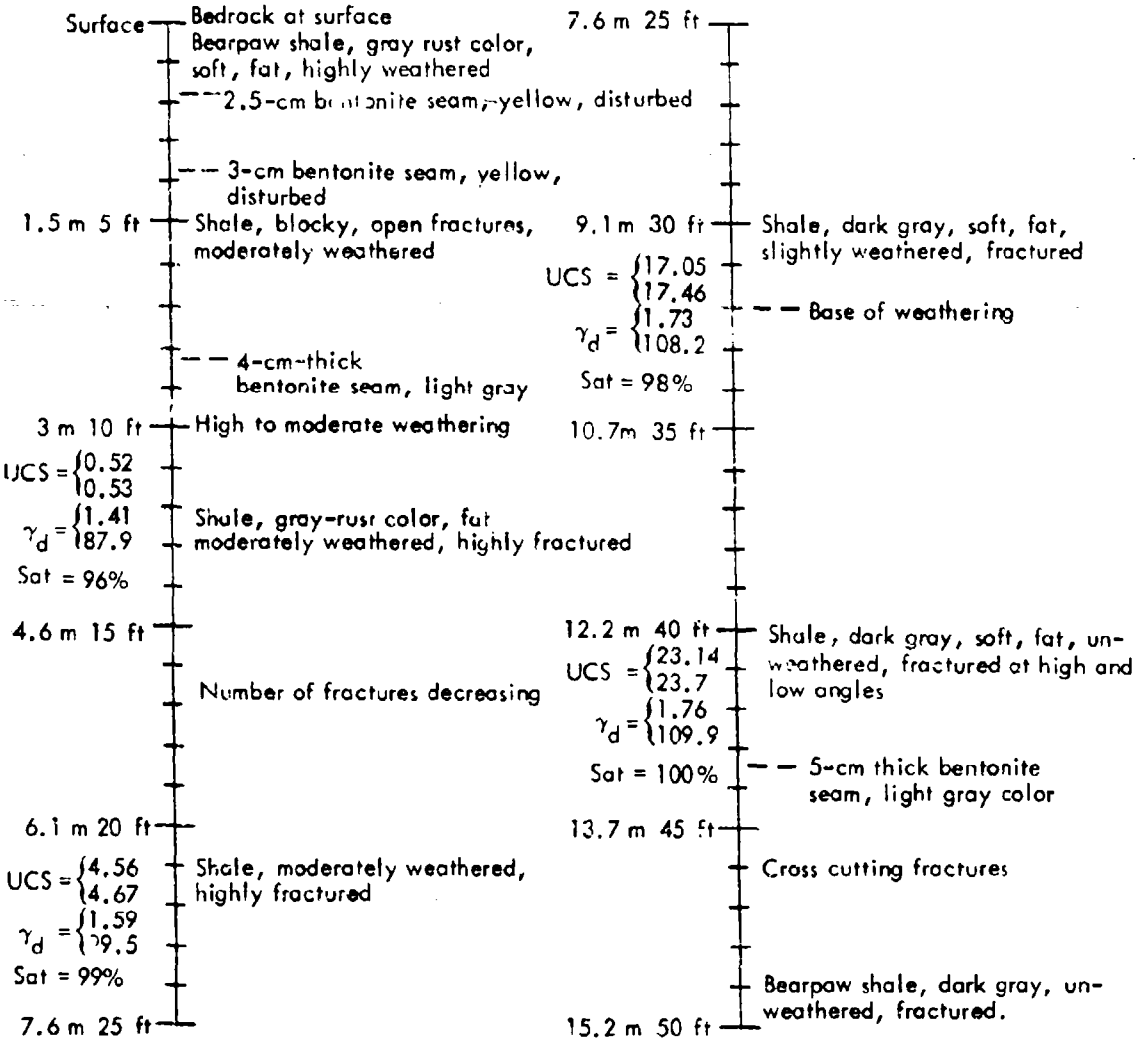

Note: Laboratory test data given to the left of elevation line with geologic description given to the right. UCS = unconfined compressive strength in kg/cm^2 and $tons/ft^2$, γ_d = dry density in g/cm^3 and lb/ft^3. Sat = saturation in percent.

Fig. C.5. Drilling log and laboratory test data for DOHA-3.

INSTRUMENTATION PLAN

Close-in measurements were planned to provide the required data for code development and verification and to determine the detonation history of the explosive. Other measurements and technical programs were directed toward making a comparison of the effects that the different types of stemming and different DOB's would have on the resulting craters and collateral effects.

The requirements for the close-in code verification measurements were developed by LLL and Systems, Science, and Software, Inc. These stress and

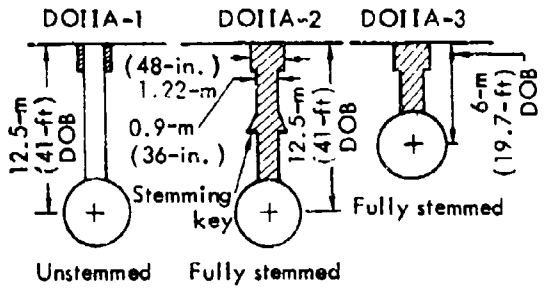

Fig. C.6. DOIIA stemming configurations.

velocity measurements were taken within and adjacent to the predicted crater during crater formation. The resulting stress and velocity levels could then be compared directly with those predicted by a calculation of the same detonation. Figures C.7, C.8, and C.9 show the linear array of close-in instrumentation used for each Phase IIA detonation. Close-in subsurface instrumentation was not conducted on the 6-m (19.7-ft) DOB detonation because this same data would be available from the 12-m (39.3-ft) DOB stemmed detonation at very early times prior to the occurrence of free surface effects. The Explosives Instrumentation Program is discussed in Chapter 4. All close-in instrumentation was conducted by LLL.

The comparative effects measurement programs included high-speed photography of each detonation, airblast measments, ground shock measurements, and

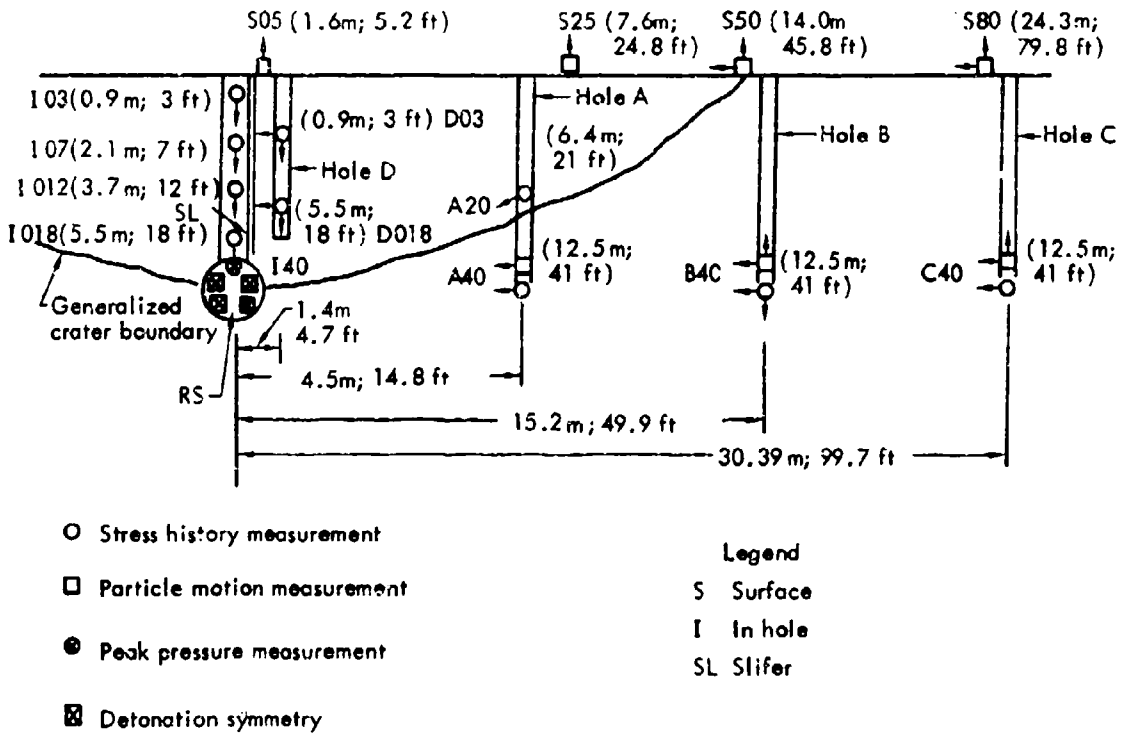

Fig. C.7. Close-in instrumentation for DOIIA-1.

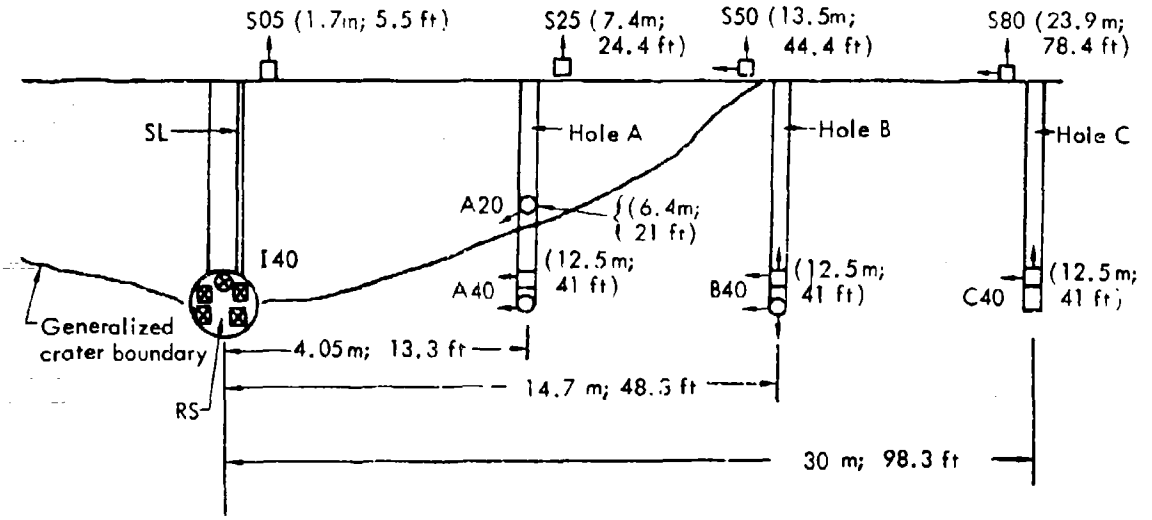

(SGZ) NOTE: Cavity center offset approximately 45.7 cm (18 in.) toward gages

○ Stress history measurement

□ Particle motion measurement

⊗ Peak pressure measurement

⊠ Detonation symmetry

Legend

S Surface

I In hole

SL Slifer

Fig. C.8. Close-in instrumentation for DOIIA-2.

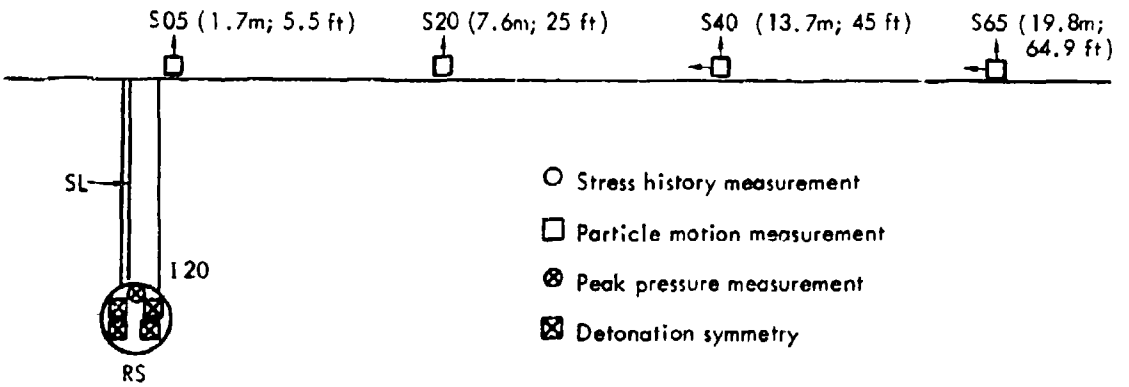

Fig. C.9. Close-in instrumentation for DOIIA-3.

preshot and postshot aerial mapping of the craters. Conventional ground survey techniques were also used to determine preliminary crater dimensions and to assist in obtaining data on missile ranges and distributions. Postshot investigations

to determi. ejecta distribution were conducted utilizing the NCG point-count technique described in Ref. 17. These comparative effects programs were conducted with EERL in-house capabilities; the survey and topographical mapping support was provided by the Omaha District Engineer and Fort Peck Area Engineer.

FIELD LAYOUT AND CONSTRUCTION

Figure C.10 is a topographic map showing the general site layout for the Phase IIA experiments. The LLL Recording Trailer Park (RTP) No. 1 was used for the DOIIA-1 and DOIIA-2 detonations and the RTP No. 2 was used for the DOIIA-3 detonation. The Control Point (CP) and camera station remained in the same location for all three detonations. Cables were run directly from the RTP's to each SGZ.

An area 122 m^2 (400 ft^2) was cleared of vegetation around each SGZ. Explosive cavities were mined from access shafts that were drilled at a diameter of 1.07 m (3.5 ft) for the first 2.13 m (7 ft) and then at 0.91 m (3 ft) for the remaining required depth. Corrugated metal pipe (CMP) 1.07 m (3.5 ft) in diameter was installed in the first 2.13 m (7 ft) of the access hole. A 0.91-m (3 ft) diameter CMP was then hung in the remaining depth of the access hole for safety purposes during mining and instrumentation emplacement activities. This 0.91-m (3-ft)-diameter CMP was removed after all activities were completed in the explosive cavity except explosive emplacement. After mining, the explosive cavities were brought to required tolerances with Shotcrete. Cavity radii were measured with conventional survey techniques. The cavity volumes for all three shots were calculated with the surveyed cavity radii. After loading, explosive volumes were corrected for incomplete filling of the cavity. The resulting explosive volumes were in agreement with the volume calculated from the suppliers pumping data (assuming a specific gravity of 1.56). The yields were then determined using a specific gravity of 1.56 and a specific energy release of 5,926 J/g. The results are shown in Table C.1.

The explosive was delivered to the site by Dow Chemical Company in tank trucks. The slurry was transferred from the tank trucks to a pump truck and then pumped into each cavity. A metering device on the pump truck was used to measure the amount pumped into each cavity. Liquid ammonia used to accelerate gelling was added on the outlet side of the pump through a tube located in the center of the outlet line.

Instrumentation holes were drilled at the locations shown previously in Fig. C.7, C.8, and C.9 Instrumentation packages were mounted on plastic pipe and aligned in each instrument hole. The instrument holes were then grouted with an LLL instrumentation grout commonly used at NTS and previously used for Pre-Gondola at Fort Peck. Surface motion instruments were placed in formed holes, which were then filled with the same instrumentation grout. The surface of these grout pads were then color-coded for postshot identification. All rate sticks and the boosters were emplaced prior to the filling of the cavity with explosive. Cables from each rate stick were placed against the cavity wall to insure that they were

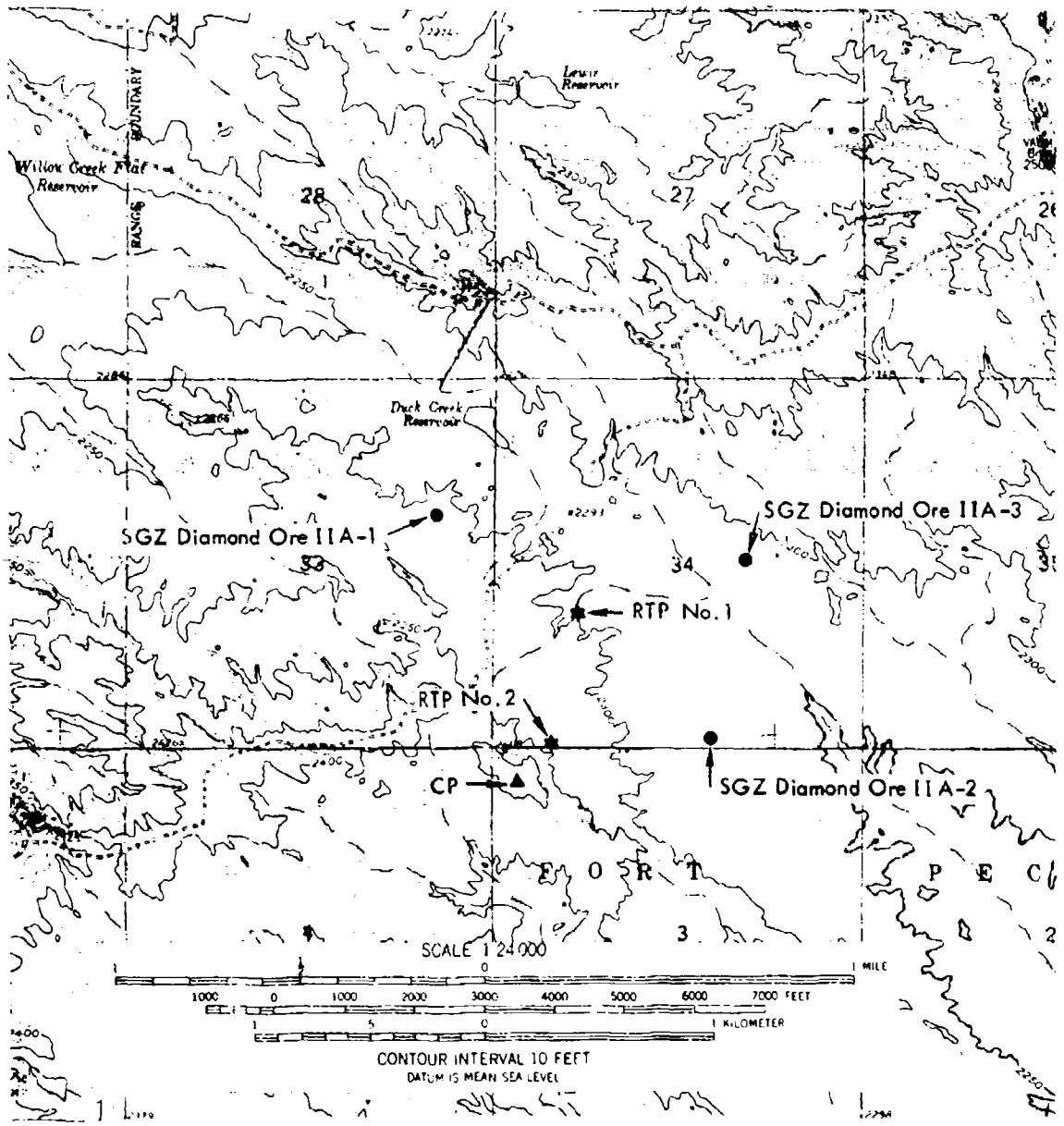

Fig. C.10. Surface Ground Zero (SGZ), Control Point (CP), and Recording Trailer Park (RTP) locations.

not destroyed by the detonation before the pin closure signals were transmitted.

The access holes for the DOIIA-2 and DOIIA-3 detonations were stemmed in successive layers after each cavity had been loaded with explosives. The 1.22-m (4 ft) diameter portion of the Diamond Ore IIA-1 access hole was stemmed to 0.91 m (3 ft) with the same Shotcrete used to shape the explosive cavities (see Fig. C-6).

Table C.1. Explosive yield determinations.

Dimension	DOIIA-1		DOIIA-2		DOIIA-3	
Survey volume (m^3) (ft^3)	6.17 ± 0.6	218 ± 21	5.72 ± 0.54	202 ± 19	6.14 ± 0.74	217 ± 26
Survey radius (m) (ft)	1.14 ± 0.36	(3.73 ± 1.2)	1.11 ± 3.35	(3.63 ± 11)	1.14 ± 4.57	(3.73 ± 15)
Explosive volume (m^3) (ft^3)	6.09 ± 0.6	215 ± 21	5.69 ± 0.54	201 ± 19	5.27 ± 0.74	186 ± 26
Volume pumped (m^3) (ft^3)	5.91	208.6	5.91	208.6	5.79	204.4
Yield[a] (J) (tons)	56.28×10^9 $\pm 5.46 \times 10^9$	13.4 ± 1.3	52.5×10^9 $\pm 5.04 \times 10^9$	12.5 ± 1.2	48.72×10^9 $\pm 6.72 \times 10^9$	11.6 ± 1.6

[a] 1-ton yield = 10^9 cal = 4.2×10^9 joules.

CHARGE DETONATION

Each charge was fired from a standard LLL timing and firing system located at the CP. Each charge was initiated by an SE-1 detonator and a 4.54-kg (10-lb) cylindrical C-4 booster, which contained two SE-1 detonators with only one being fired at zero time. Zero time signals were sent to the LLL instrumentation trailer and the airblast recording stations. A flashbulb was also fired near each SGZ at zero time. The high-speed photography cameras were started automatically by the timing and firing system at 2 sec before zero time. The detonation schedule was as follows:

DOIIA-1	1000.00 hr MDT	19 October 71
DOIIA-2	1200.00 hr MDT	22 October 71
DOIIA-3	1000.00 hr MDT	29 October 71

Initial observations of each detonation indicated that the explosive had performed as expected except for the appearance of hot spots or large glowing or burning orange masses in the cloud and ejecta during each detonation. The number of observed iridescent masses increased with each detonation. The results of the explosive instrumentation are discussed in Chapter 4.

HIGH-SPEED PHOTOGRAPHY

Two high-speed cameras were used to photograph each detonation at frame rates of 50 and 1,000 ft/sec. Figures C.11, C.12, and C.13 are detonation sequences for each experiment. Studies of these films have produced the following data: the unstemmed DOIIA-1 detonation vented within the first millisecond. The explosive gas venting and the glow from the zero time flashbulb appeared in the same frame. The venting appears to have been interrupted by a possible closure of the access hole at about 90 msec. This closure phenomenon was also witnessed in the 907-kg (1-ton) partially stemmed detonation (M-16) in the Middle Course II experiments.[7] Venting occurred in the DOIIA-2 detonation at about 130 msec and at about 29 msec in the DOIIA-3 detonation. Venting at these late times is not expected to have any significant effect on overall crater sizes.

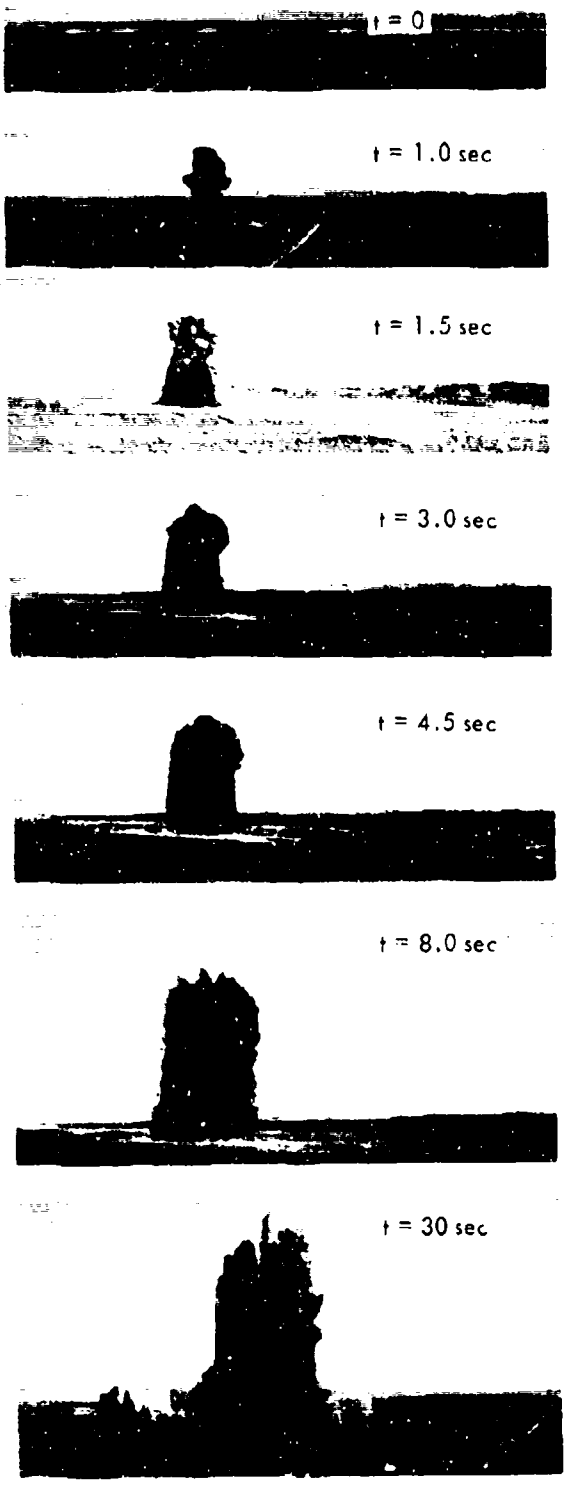

Fig. C.11. Detonation sequence for DOIIA-1.

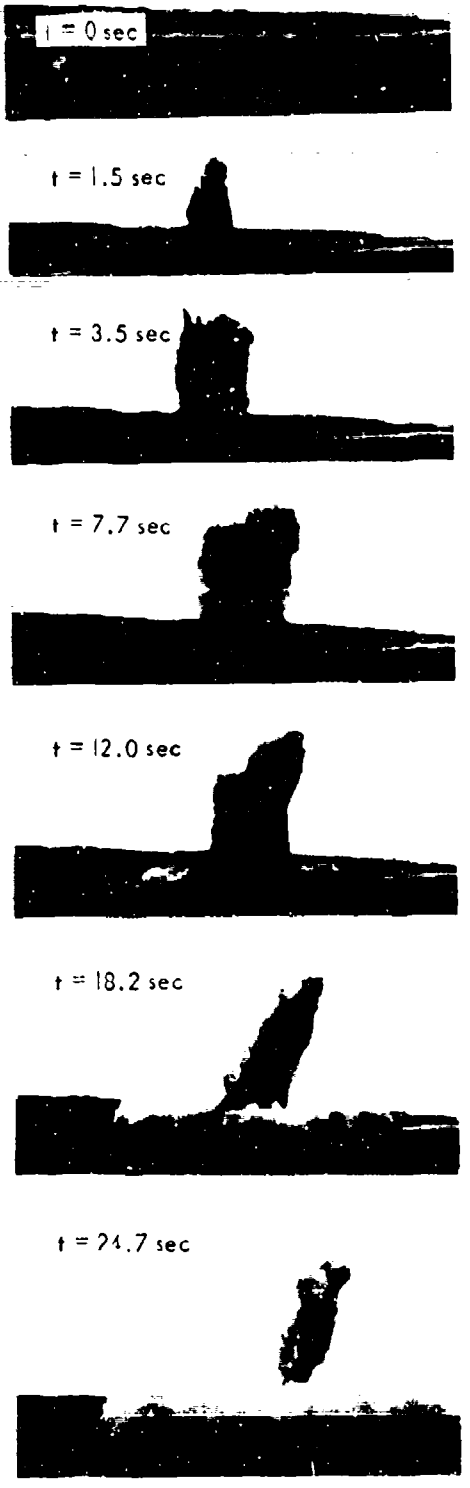

Fig. C.12. Detonation sequence for DOIIA-2.

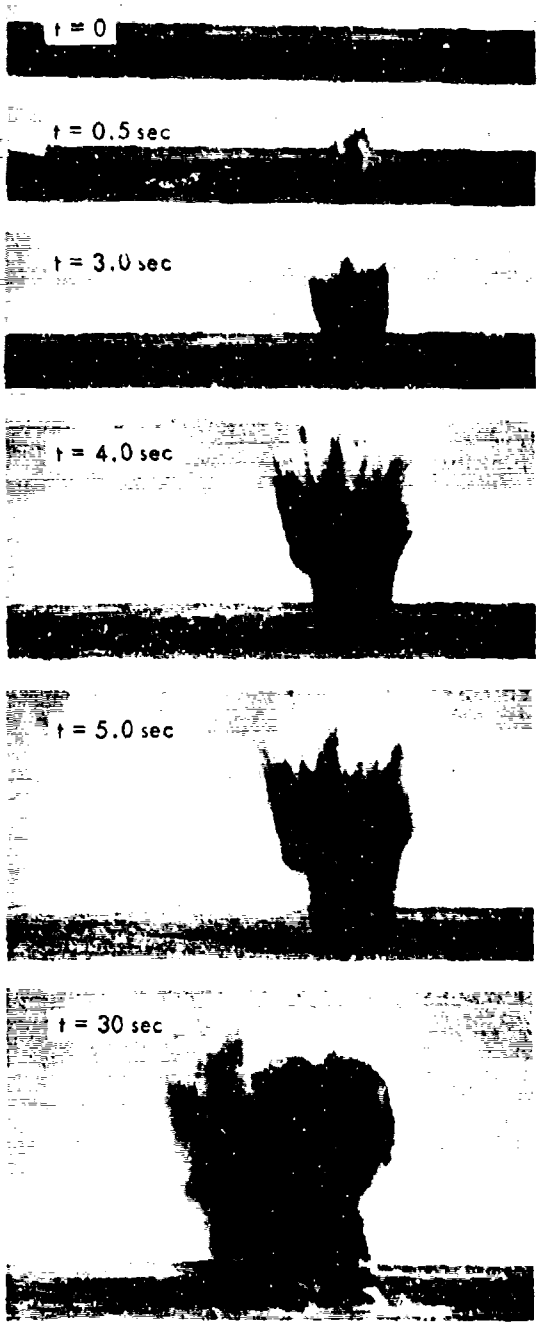

Fig. 6.13. Detonation sequence for DOIIA-3.

The hot spots or burning orange masses that appeared in the detonation cloud were observed on the photography. They are believed to have been masses of burning explosive. They appeared in the time frames as follows: DOIIA-1, 1.9 to 3.6 sec; DOIIA-2, 4.0 to 8.5 sec, and DOIIA-3, 0.4 to 7.9 sec. Discussions with Dow representatives on the site indicated that these iridescent objects are common in the detonation of large quantities of slurry explosive. Photographic reference targets were placed 23 m (75 ft) apart at 61 m (200 ft) in front of each SGZ. These reference targets provided a scale upon which to make mound growth and venting velocity measurements. No correction has been made for the parallax caused by this configuration but it is less than 4%. The vertical velocities measured in this manner are as listed in Table C.2. The very high vent velocity in the DOIIA-1 detonation is attributed to the unstemmed emplacement hole. The differences in the vent velocities in the two stemmed cases are attributed to the earlier venting (29 msec for DOIIA-3 vs 130 msec for DOIIA-2) of the DOIIA-3 detonation when the cavity gas pressure was higher. This earlier vent in turn is attributed primarily to the shallower DOB but also may have been caused by the lack of a stemming key and/or the faster detonation velocity in the DOIIA-3

Table C.2. Velocity data from high-speed photography.

Event	Vent velocity	Mound velocity
DOIIA-1 (m/sec)	1,500	60
(ft/sec)	5,000	~200
DOIIA-2 (m/sec)	180	50
(ft/sec)	600	160
DOIIA-3 (m/sec)	450	180
(ft/sec)	1,500	600

experiment. The initial mound growth velocities are determined by the spalling effect of the shock front as it is reflected at the ground surface. The closeness of the values for the mound velocities in the two 12.5-m (41-ft) DOB cases (DOIIA-1 and DOIIA-2) indicates similar shock front phenomena even though stemming conditions differed. The small differences in these mound velocities may have been caused by the differences in energy release time of the two detonations. The higher mound velocity in the shallower 6-m (19.7-ft) detonation (DOIIA-3) is attributed to the higher energy and particle velocities found in the shock wave when it reaches the surface. These higher levels are attributed to the shorter distance over which the shock wave has traveled in reaching the ground surface.

CRATER DIMENSIONS

Crater dimensions were initially obtained from conventional ground surveys conducted before and after each detonation. Two orthogonal profiles were surveyed at each SGZ. These dimensions have been replaced by those obtained from preshot and postshot aerial photography taken at each SGZ. Topographic maps were produced with standard photogrammetric techniques and then contour maps (isopachs) showing elevation charges between preshot and postshot ground surfaces were drawn. Orthogonal profiles were then obtained from these isopachs for each crater. These results are shown in Figs. C.14, C.15, and C.16 for the DOIIA-1 shot; in Figs. C.17, C.18, and C.19 for the DOIIA-2 shot; and Figs. C.20, C.21, and C.22 for the DOIIA-3 shot. The crater measurements obtained from these maps are listed in Table C.3. The apparent crater radii, R_a, were obtained from the planimetry of the area of the zero contours in Figs. C.15, C.18, and C.21. The apparent crater depths represent the maximum negative elevations shown on the isopachs. The apparent height of the crater lip, H_{al}, is the average lip height taken again from the isopachs. The radius of the apparent crater lip, R_{al}, was calculated from the planimetered area contained within the maximum positive elevations in each crater lip. The apparent crater volumes, V_a, are calculated from the planimetered area of each 1.52-m (5-ft) contour. The radii of the continuous ejecta, R_{ec}, were calculated from the planimetered area of the continuous ejecta as shown on the postshot aerial photographs of each SGZ. The limits of the continuous ejecta were marked on the ground after each detonation so as to be visible on the aerial photography. These limits are readily apparent in Figs. C.23, C.24, and C.25. The maximum missile ranges were obtained from field survey data.

While it is realized that comparison of the crater characteristics produced by the detonations must be made with caution due to the behavior of the slurry explosives previously discussed, certain features are worthy of note. The two 12.5-m DOB detonations (DOIIA-1, 2) produced significantly different craters. Previous calculations and studies had indicated that about a 10% degradation in crater size was to be expected in an unstemmed detonation. Although the apparent depths and radii are very close to each other, the unstemmed detonation

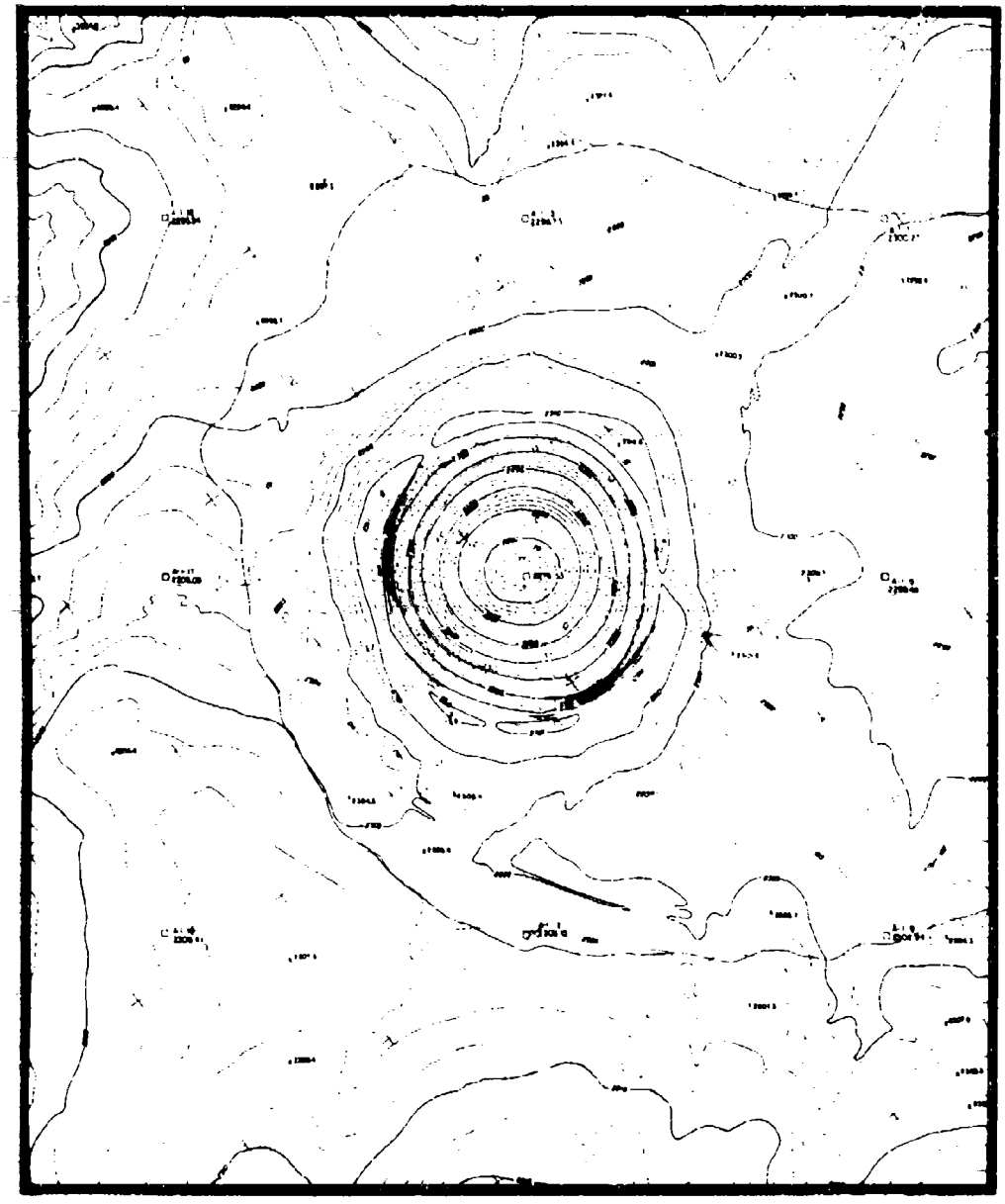

Fig. C.14. DOIIA-1 postshot topographic map.

excavated a significantly larger volume of material, 19.4% more. This volume difference results from a difference in the shape of the two craters. The unstemmed crater has a more rounded, less steep profile resulting in a larger volume (see Figs. C.16 and C.19) This bowl shape in the unstemmed crater is attributed

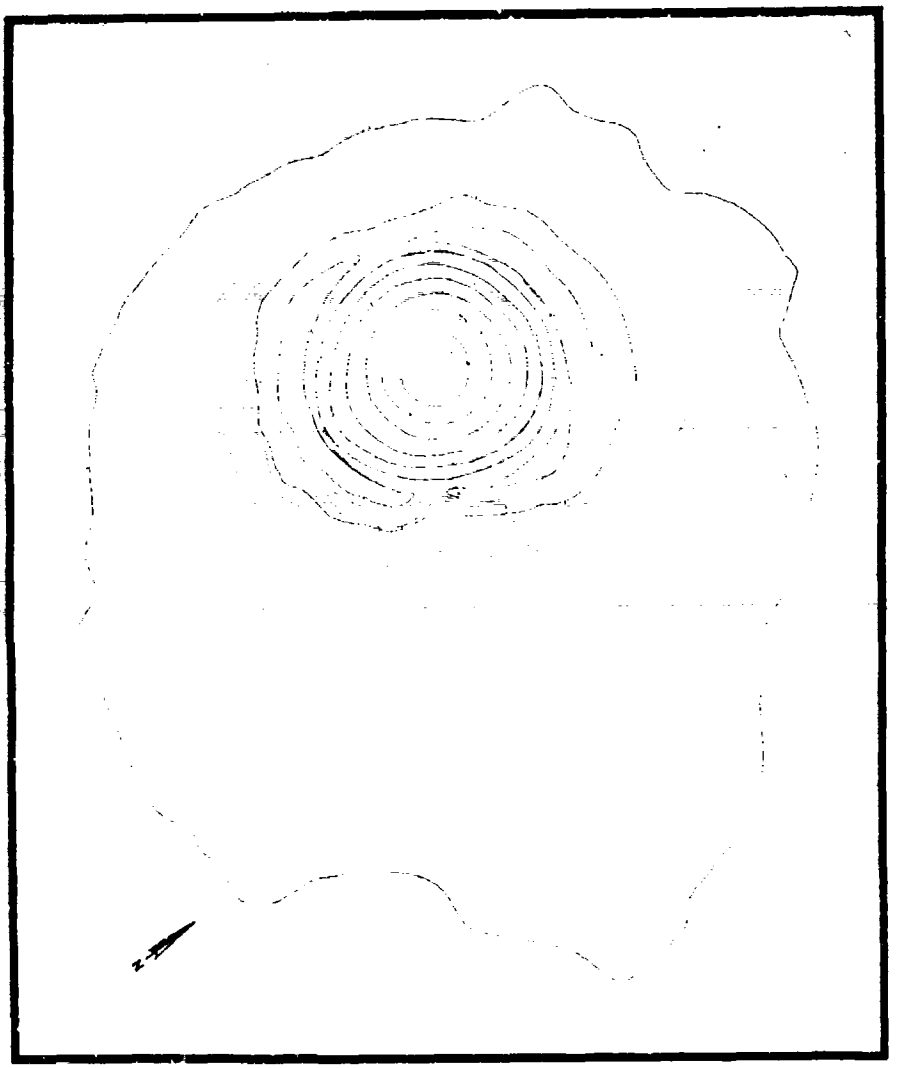

Fig. C.15. DOIIA-1 isopach.

to the horizontal pressure effects of the gases escaping up the access hole. A portion of the difference in volume in the two craters may also be attributed to a bench located in the northeast wall of the DOIIA-2 crater (Fig. C.18). This anomaly would cause a reduction in the crater volume. The difference in crater size may also have been caused by the differences in the time release of explosive energy of the two detonations; the smaller DOIIA-2 crater being produced by the slower detonation. This volume difference in the DOIIA-1 and DOIIA-2 craters is not significant, however, in a comparison with the DOIIA-3 crater. This crater, from a charge detonated at a DOB of 6 m (19.7 ft), is significantly

Table C.3. Diamond Ore IIA crater measurements.

Dimensions	DOIIA-1 (m)	DOIIA-1 (ft)	DOIIA-2 (m)	DOIIA-2 (ft)	DOIIA-3 (m)	DOIIA-3 (ft)
DOB	12.5	41	12.5	41	6	19.7
Apparent radius, R_a[a]	20.6	67.6	19.84	65.1	19	62.3
Apparent depth, D_a	7.3	24.0	7.01	23.0	9.45	31.0
Lip height, H_{al}[a]	3.4	11.0	3.81	12.5	2.3	7.5
Lip crest radius, R_{al}[a]	25.8	84.7	25.02	82.1	22.71	74.5
Apparent volume, V_a	4,350[b]	5,690[c]	3,640[b]	4,760[c]	4,400[b]	5,760[c]
Radius of the continuous ejecta, R_{ec}[a]	81	267	84	275	89	293
Continuous ejecta, R_{ec}— maximum	116	382	98	322	105	344
minimum	46	152	63	208	55	182
Lip height, H_{al}— maximum	4.0	13	4.3	14	2.7	9
minimum	2.4	8	3.3	11	1.8	6
Maximum missile range	317	1,040	338	1,110	665	2,180

[a]These values are averages.
[b]m^3.
[c]yd^3.

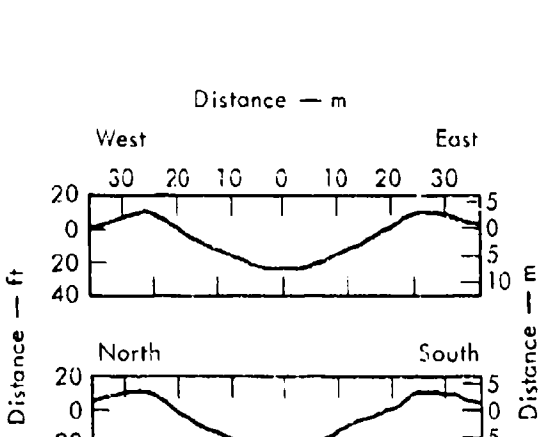

Fig. C.16. DOIIA-1 crater profiles.

larger than the crater from the stemmed detonation at 12.5-m (41-ft) DOB, which had been considered near optimum. Its apparent radius is about 8% smaller than either of the other craters, while its depth is almost 30% greater. This significant difference in depth in the DOIIA-3 crater is reflected in an apparent crater volume that is 21% greater than the DOIIA-2 crater volume. This explosive charge detonated slower than the DOIIA-1 charge, yet faster than the DOIIA-2 charge. A possible explanation for this deeper crater and larger excavated volume lies in the geologic profile of the DOIIA-3 SGZ as shown in Fig. C.5. This detonation occurred completely within the unweathered shale that was significantly weaker than the shale at and immediately above the other two detonations. Also of significance is the difference in maximum missile range. The shallower DOIIA-3 detonation produced a maximum range of about double that of the other two detonations.

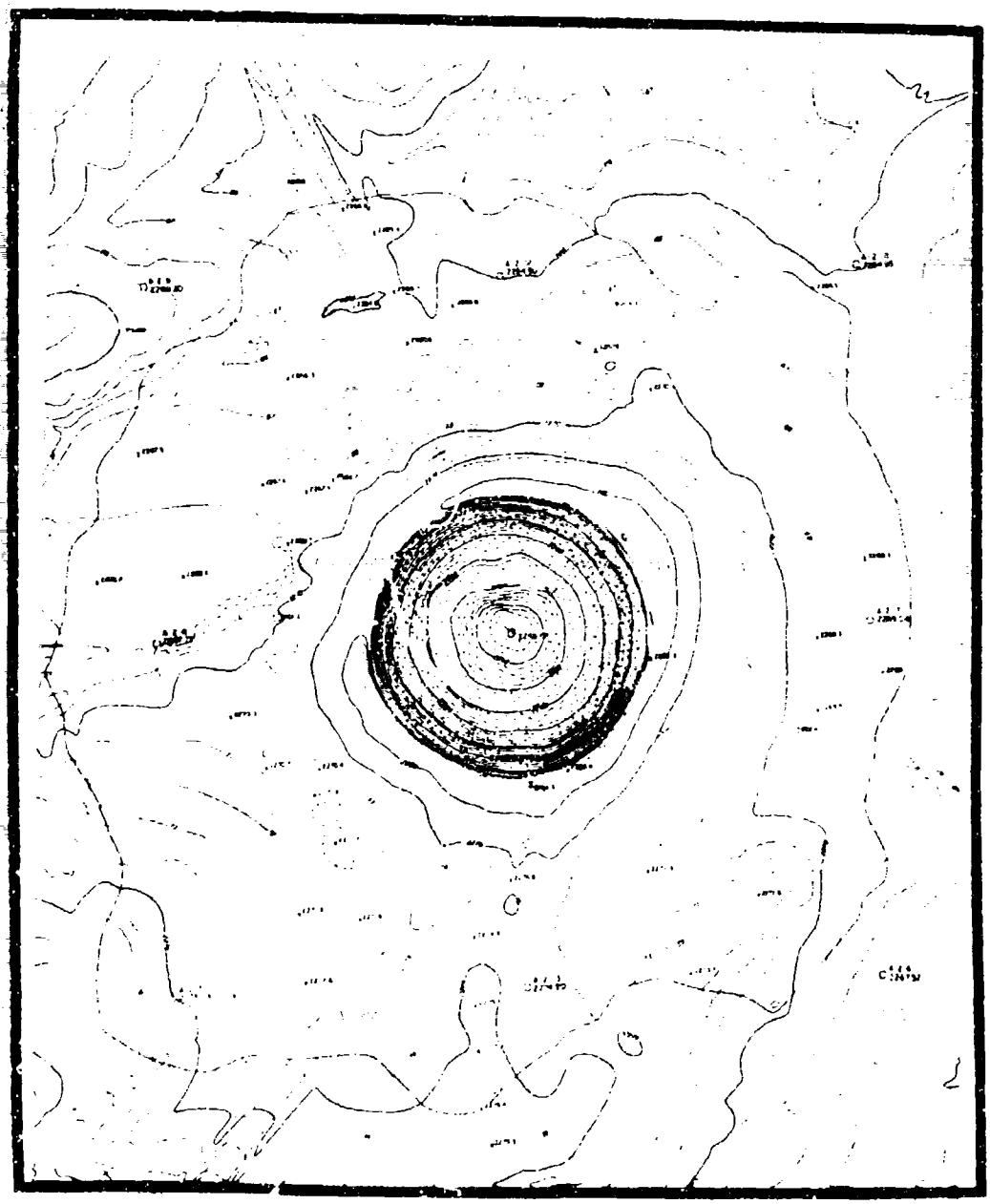

Fig. C.17. DOIIA-2 postshot topographic map.

This larger range was expected as the shallower detonation produces higher surface velocities with relatively higher horizontal velocity components. The major portion of the missiles come from the surface and near-surface area above the detonation. Figure C.26 is the cratering curve developed from the Pre-Gondola experiments at Fort Peck.[18] Each of the four Pre-Gondola detonations had a yield of about 84×10^9 J (20 tons). The three DO Phase IIA detonations are plotted for

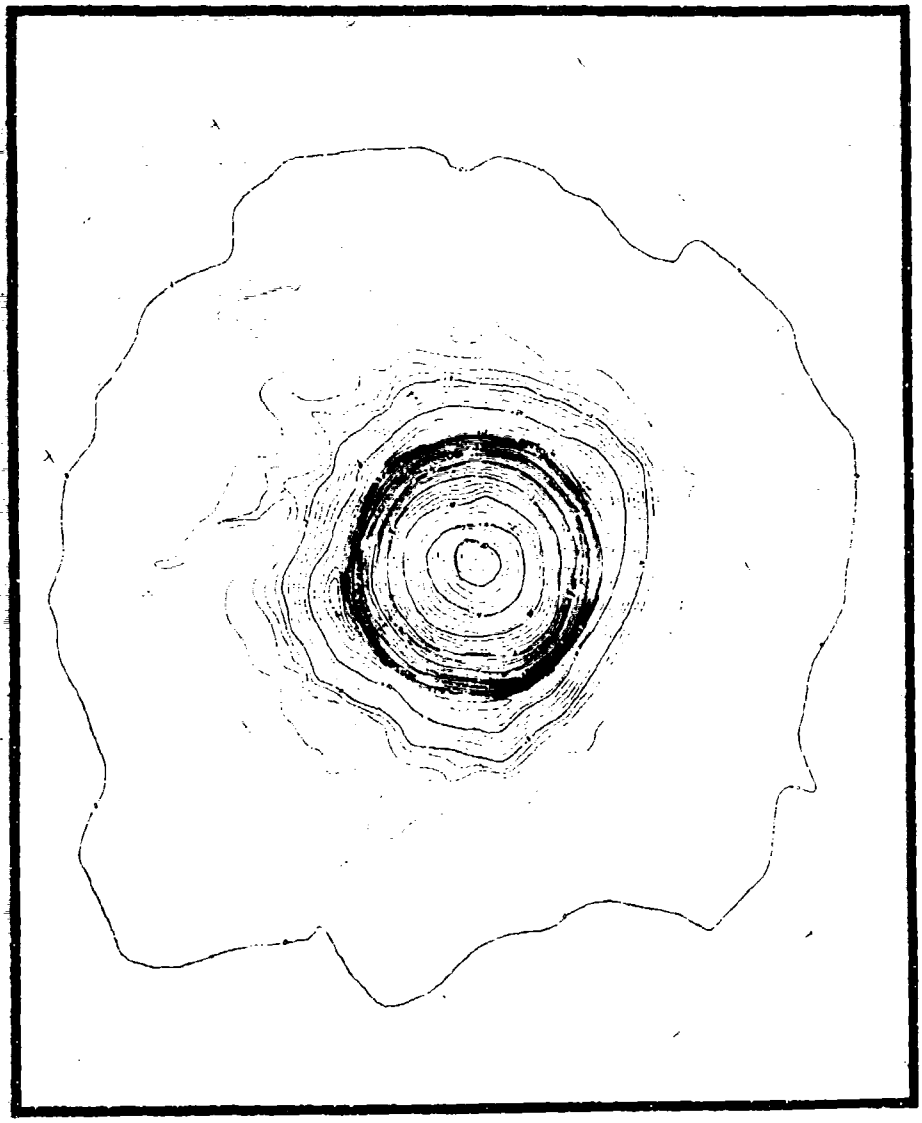

Fig. C.18. DOIIA-2 isopach.

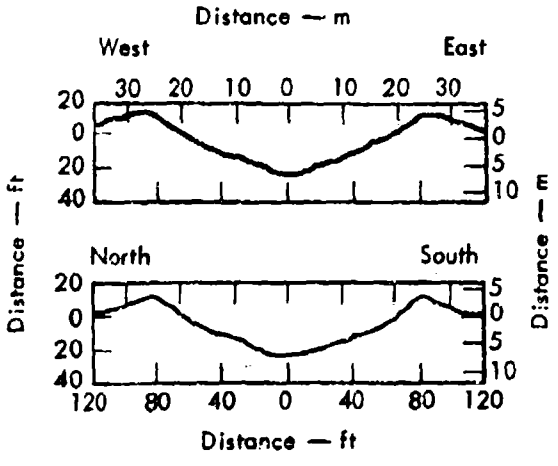

comparison purposes with an assumed yield of 58.8×10^9 J (14 tons).

CLOSE-IN INSTRUMENTATION RESULTS

As stated previously, the close-in instrumentation program for the three

Fig. C.19. DOIIA-2 crater profiles.

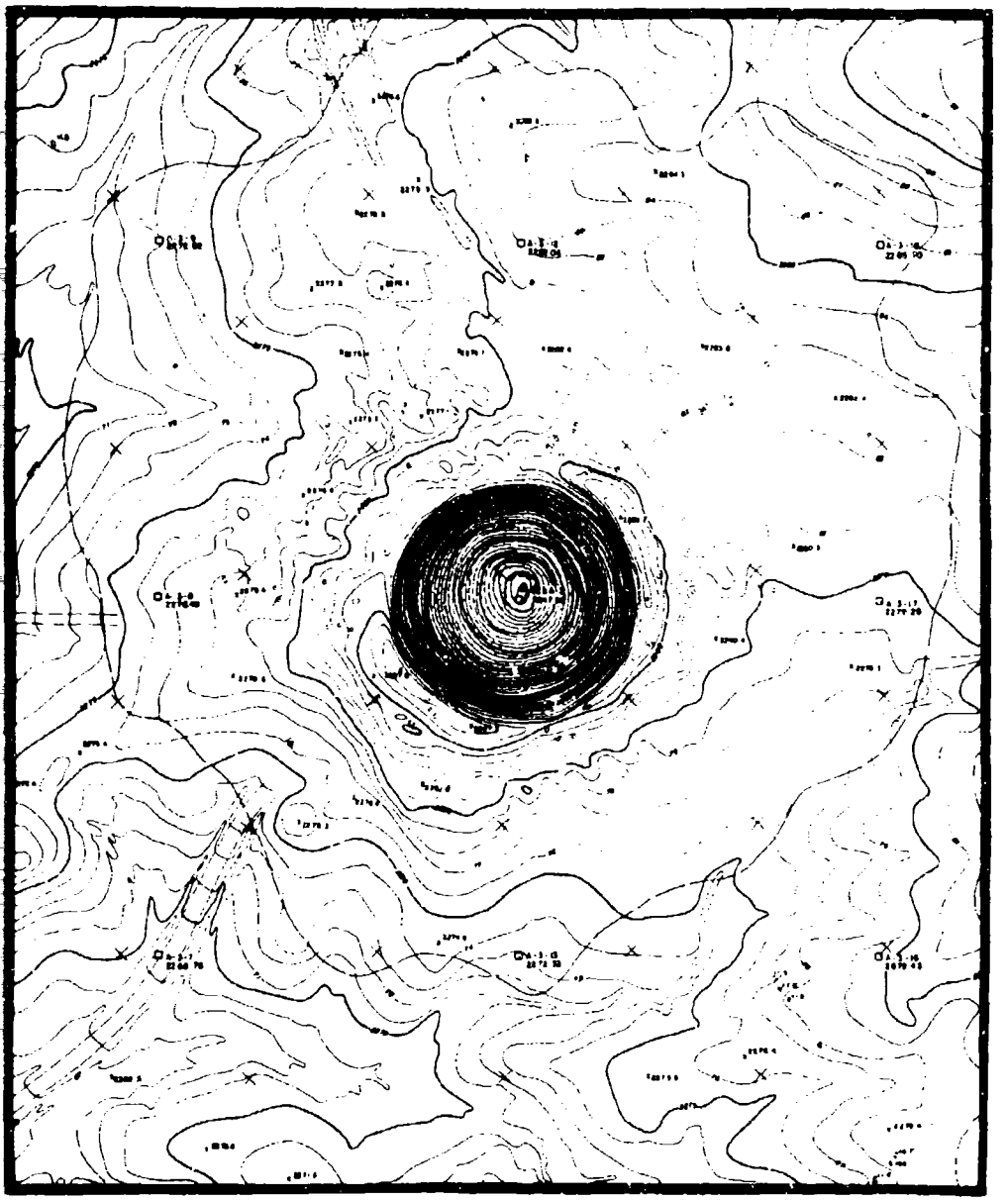

Fig. C.20. DOIIA-3 postshot topographic map.

Phase IIA detonations was the responsibility of LLL. This section presents the results of this program. Detailed information as to the type of gage, electrical circuitry, and recording equipment employed and the wave forms recorded are contained in Ref. 8. Figures C.7, C.8, and C.9 show the location and type of measurements attempted on each detonation.

Time of Shock Arrival Measurements (TOA)

In the DO Phase IIA experiments, arrival times of the shock wave were

measured principally in four regions: (1) within the aluminized ammonium nitrate slurry explosive to measure detonation velocity and to evaluate the explosive performance, (2) along the shot horizon at instrument holes A, B, and C to provide verification of the constitutive relations used in one-dimensional studies with the SOC code, (3) along the ground surface to be used as a means of relating the SOC calculations to the observed surface motion, and (4) within and adjacent to the emplacement hole of the 12.5-m (41-ft) unstemmed shot to measure the shock velocity. Although most of the TOA data was a byproduct of instrumentation designed to provide stress, velocity, or acceleration time histories, rate sticks within the explosive and slifers within the open and grouted emplacement holes were designed to provide only arrival time data. The detonation velocity measurements made within the explosive have been discussed in a previous section. Table C.4 lists the shock and seismic velocities calculated using the TOA data from the various sources.

Shot Horizon TOA Measurements

The arrival times recorded by the shot level stress, velocity, and acceleration gages in instrument holes A, B, and C for the stemmed and unstemmed 12.5-m (41-ft) events are given in Table C.5 and plotted in Fig. C.27. No shot-level measurements were made on the stemmed 6-m (19.7-ft) event. The observed shock velocities of 2.00 m/msec (see Table C.4) agree closely with those observed in the Pre-Gondola I experiments[18] but are considerably higher than suggested by the preshot seismic refraction surveys (Fig. C.2). The Bearpaw clay shale constitutive relations developed from the Pre-Gondola data[5] give rise to a calculated shock velocity of 1.96 m/msec when used in the SOC code.

Table C.4. Summary of shock velocity measurements.[9a]

Gage location	DOIIA-1 Unstemmed—12.5 m			DOIIA-2 Stemmed—12.5 m			DOIIA-3 Stemmed—6 m		
	Source	Velocity (m/msec)	Remarks	Source	Velocity (m/msec)	Remarks	Source	Velocity (m/msec)	Remarks
At shot level in Bearpaw shale	A, B, C	2.00 ± 0.04	—	A, B, C	2.00 ± 0.05	—	—	—	—
	Seismic	1.5	Preshot	Seismic	1.8	Preshot	Seismic	1.1	Preshot
	HS	1.8	Long range	HS	1.6	Long range	HS	1.7	Long range
Surface	S	0.77 ± 0.05	—	S	1.07 ± 0.09	—	S	0.64 ± 0.07	—
	Seismic	0.82	Preshot average	Seismic	0.91	Preshot average	Seismic	0.61	Preshot average
Emplacement hole	Slifer	3.4	Air	Slifer	1.7	Grout	Slifer	1.8	Grout
	I	~3.4 ± 0.1	—	—	—	—	—	—	—
Air shock	HS	0.77	Near SGZ	—	—	—	HS	0.36	Near SGZ
	HS	0.33	Long range	—	—	—	HS	0.34	Long range

[a]Notation: RS = rate stick; HS = high-speed photography; A, B, C = instrument hole gages (see Figs. C.7 and C.8); I = emplacement hole gages; S = surface gages.

Table C.5. Recorded arrival times.[8]

Gage location	DOIIA-1 Unstemmed—12.5 m Station	Distance (m)	Gage[a]	TOA (m/sec)	DOIIA-2 Stemmed—12.5 m Station	Distance (m)	Gage[a]	TOA (m/sec)	DOIIA-3 Stemmed—6 m Station	Distance (m)	Gage[a]	TOA (m/sec)
Shot level	A40	4.51	AC-R	1.64	A40	4.05	AC-R	1.88	—	—	—	—
			ST-R	1.58			ST-R	1.48				
	A20	7.59	ST-R	3.52	A20	7.31	ST-R	3.55	—	—	—	—
	B40	15.15	VE-R	—	B40	14.72	AC-T	7.01	—	—	—	—
			VE-T	7.47			VE-R	7.71				
			ST-R	6.95			ST-R	6.86				
			ST-T	7.09			ST-T	7.05				
	C40	30.39	AC-T	—	C40	29.96	AC-T	14.64	—	—	—	—
			VE-R	14.5			VE-R	—				
			STR-R	—								
Surface	S05	12.59	AC-V	8.34	S05	12.62	AC-V	9.32	S05	6.22	AC-V	3.25
	S25	14.60	VE-V	12.5	S25		VE-V	—	S20	9.69	AC-V	5.56
	S50	18.75	VE-V	18	S50	18.41	VE-V	—	S40	14.97	VE-V	—
			AC-HR	18.07			AC-HR	16.53			VE-HR	—
	S80	27.34	AC-V	27.1	S80	26.97	AC-V	22.96	S65	30.66	AC-V	22.47
			AC-HR	28.9			AC-HR	23.07			AC-HR	25.73
Emplacement hole	I40	1.1	P	0.24	I40	—	P	—	I40	—	P	—
	I18	7.01	ST-R	1.91								
	I12	8.84	ST-R	2.43								
	I07	10.36	ST-R	2.86								
	I08	11.58	ST-R	3.28								
Hole D	D18	6.86	ST-V	2.95								
			ST-HR	2.95								
	D08	11.36	ST-V	10.0								
			ST-HR	6.4								

[a]Notation: AC = accelerometer; HR = horizontal radial; VE = velocity gage; ST = stress gage; STR = strain gage; P = pressure; V = vertical; R = radial; T = tangential.

Surface TOA Measurements

The observed surface arrival times for the three events are recorded in Table C.5 and plotted in Fig. C.27. The noncoincidence of the surface arrival time curves for the shots indicates a substantial difference in the constitutive properties of the upper geologic layers of each shot point. This is supported by the preshot boring logs and seismic refraction surveys (Figs. C.2 through C.5). Some refraction is clearly evident because the curves do not pass through the origin in Fig. C.27. In spite of the refraction, the slope of the lines correlates well with the media-weighted seismic velocities estimated from the preshot seismic survey. These estimates assumed straight-line source-to-surface shock propagation.

The surface TOA data are particularly valuable because they provide, via the Buckingham-Pi[19] theorem, an effective means of relating the observed surface velocities, stresses, and accelerations to the same quantities calculated at shot depth with the SOC code. Surface TOA data will be discussed in more detail later.

Emplacement Hole TOA Measurements

TOA data for the open emplacement hole of the 12.5-m (41-ft) unstemmed shot were obtained from four stress gages located in the emplacement hole at 0.91 to 5.5 m (3 to 18 ft) from the ground surface (Fig. C.7). These data were supplemented by a slifer and by two pairs of stress gages located in an adjacent

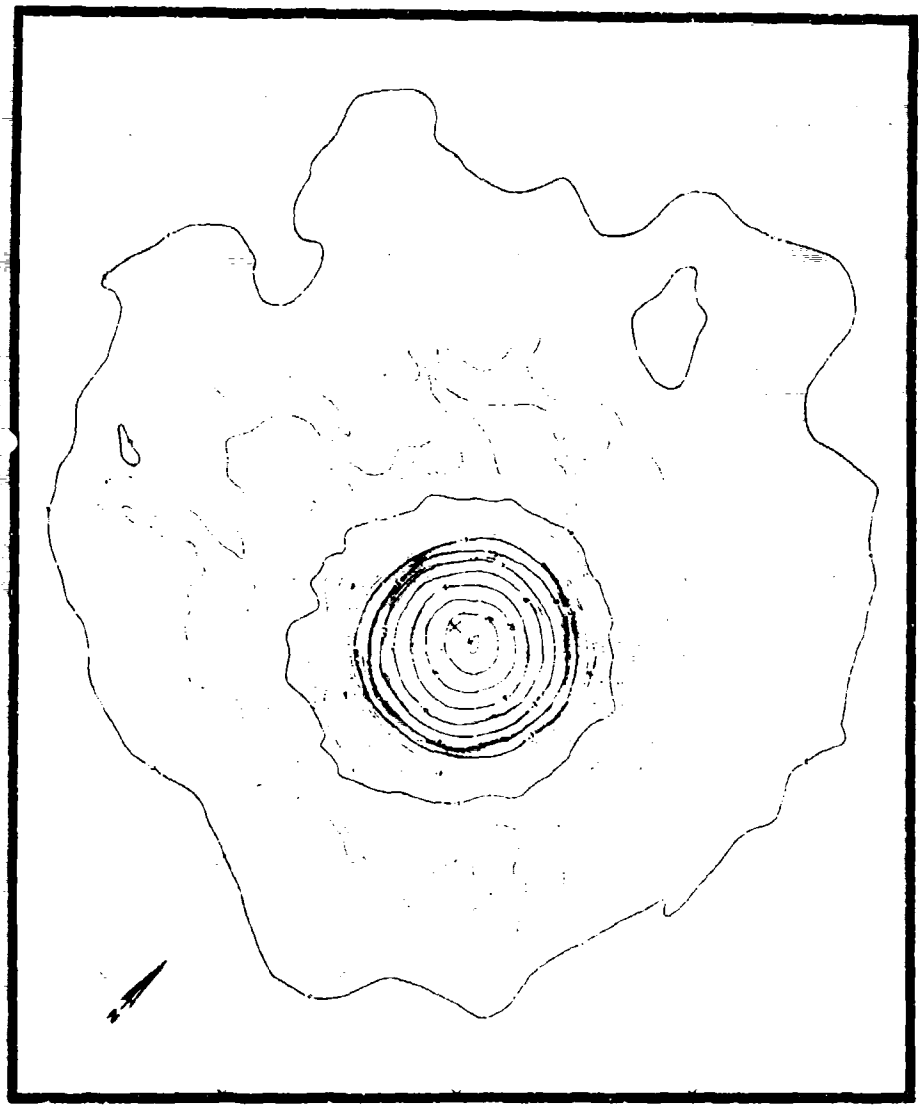

Fig. C.21. DOIIA-3 isopach.

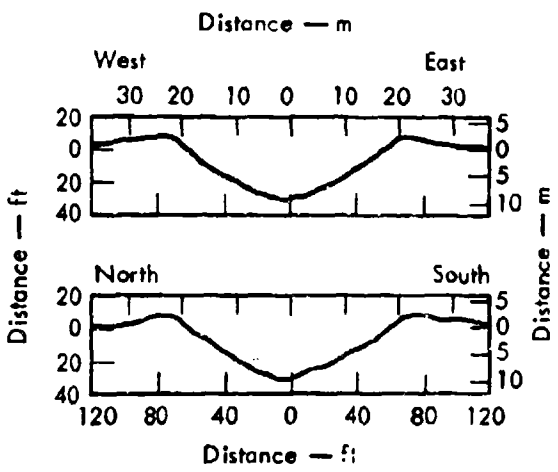

borehole (D). Slifer systems were also situated within the grout stemming material of the 12.5- and 6-m (41- and 19.7-ft) stemmed events (Figs. C.8 and C.9).

The shock velocities determined from the slifers in the unstemmed and grouted emplacement holes have been recorded in Table C.4. In the case of the open emplacement hole of DOIIA-1, the slifer

Fig. C.22. DOIIA-3 crater profiles.

Fig. C. 23. Aerial photo composite of DOIIA-1 crater.

Fig. C. 25. Aerial photo composite of DOIIA-3 crater.

velocity is in complete agreement with that obtained from the stress gages. In the free atmosphere near SGZ, the air-shock velocity was observed to diminish to 0.77 m/msec as was indicated by high-speed photography. The TOA data for the stress gages in Hole-D (located parallel to but 1.4 m (4.7 ft) from the emplacement hole) do not give a clear indication of whether the shock first reached these gages via the emplacement hole. At Station DO3, the 10-msec arrival of the vertical stress component and

Fig. C. 24. Aerial photo composite of DOIIA-2 crater.

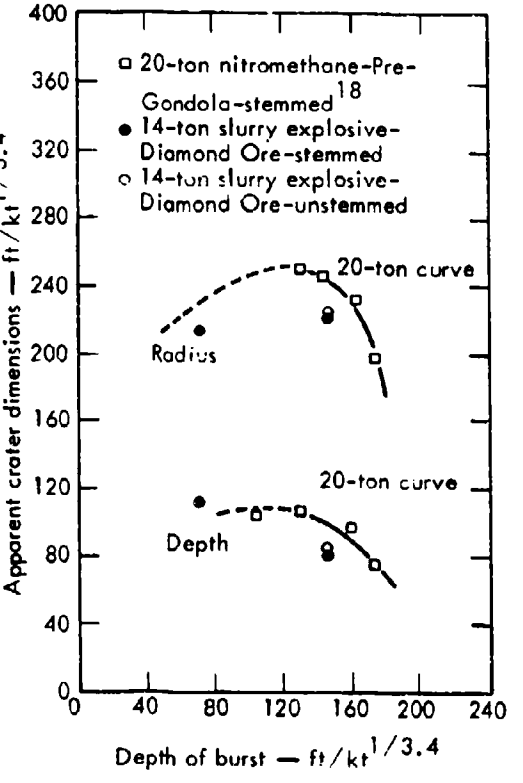

Fig. C 26. Cratering curves for Fort Peck Bearpaw shale.

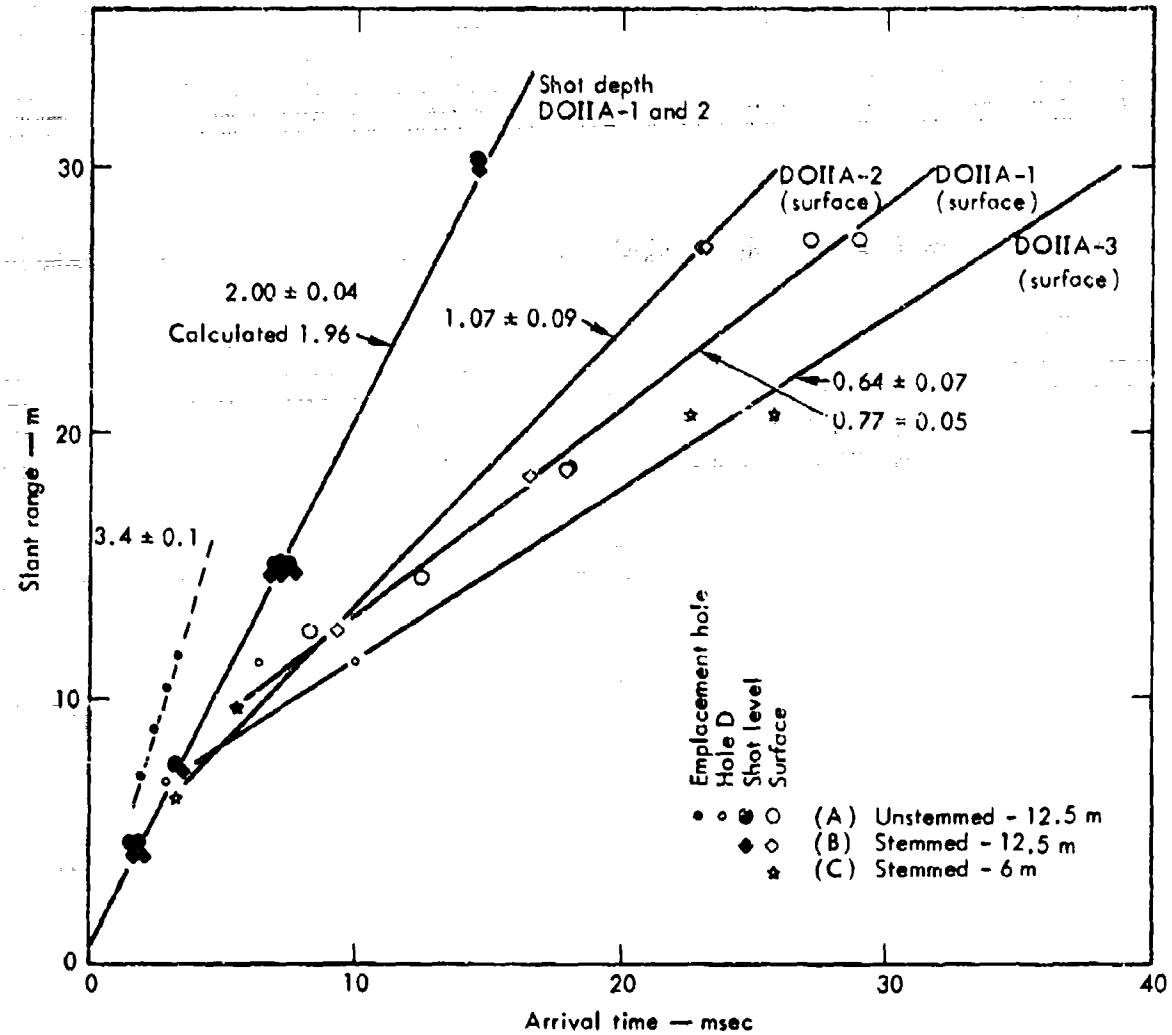

Fig. C.27. Shock arrival times.

the 6.4-msec arrival of the horizontal component would seem to suggest a cylindrical wave propagating from the emplacement hole. This would, however, imply a 3.6-msec relaxation time for the material—this does not seem reasonable. One must therefore conclude that one of these values is in error, probably the 10 msec value.

The slifer velocities for the grout in the two stemmed events were higher than the shock velocities in the undisturbed medium. This is supported by the high-speed photography, which showed spallation occurring at the grout surface 1 to 2 msec before the surrounding Bearpaw shale surface. The failure to completely match grout and medium properties may have contributed to the stemming failures that occurred at 130 msec for DOIIA-2 and 29 msec for DOIIA-3. These failures were, however, sufficiently late in time to have negligible effect on the cratering process.

Stress, Pressure, and Strain Measurements

Stress history measurements were made on the 12.5-m (41-ft) unstemmed

and stemmed experiments only. On these events, stress transducers were situated at shot level in instrument holes A and B and at half shot depth in hole A. In addition, a strain measurement was attempted in hole C for the unstemmed shot. For the unstemmed shot, four transducers were placed in the open emplacement hole and four more in the adjacent parallel hole D (see Figs. C.7 and C.8).

Shot-Level Stress History Measurements

All shot-level stress gages on the two 12.5-m (41-ft) events failed to yield correct stress histories for time intervals greater than a few milliseconds, although signals were received from the surface-mounted, voltage-controlled oscillator for several hundred milliseconds. In most cases, the recorded signal rose to a first peak and then flattened out or continued to rise discontinuously over several hundred milliseconds. As the shock front should be of only a very few milliseconds duration, this behavior was clearly not representative of the physical situation.

In a few records, the first peak was followed by a slight decrease before flattening, suggesting that gage failure occurred upon release from peak load conditions. If it is assumed that most of the gages failed at, or shortly after, the peak, then the first peak can be taken to correspond to the shock peak. Interpreted in this fashion, the peak stresses behaved in a consistent manner. These values are tabulated (Table C.6) and displayed graphically in Fig. C.28. In the case of the stress gage at station A40 (and also I18) on the unstemmed event, a different type of failure occurred. In these instances, the signal was driven rapidly downward during the onset of stress due to a short-circuit in the system. The peak values reported for these gages have been estimated by extrapolating the slopes prior to and following the short circuit.

The most prominent feature of Fig. C.28 is the approximate factor of 2 between the shot level stresses for the stemmed and unstemmed shots. Contrary to intuition, the stresses for the unstemmed shot are higher. In view of the known anomaly in the detonation of explosive for the stemmed shot, this is accepted as the source of the stress degradation seen in Fig. C.28.

In an effort to determine the nature of the anomalous detonations, a suite of

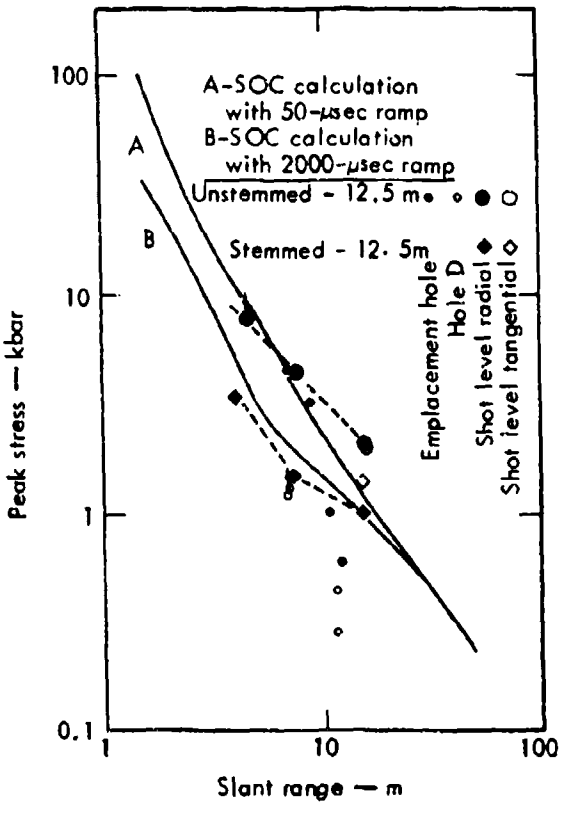

Fig. C.28. Peak stress as a function of slant range.

Table C.6. Peak stress measurements.[8]

Location	DOIIA-1 Unstemmed—12.5 m Station	Distance (m)	Component[a]	Stress[b] (kbar)	DOIIA-2 Stemmed—12.5 m Station	Distance (m)	Component[a]	Stress[b] (kbar)
Shot level	A40	4.51	R	7.8	A40	4.05	R	3.4
	A20	7.59	R	3.8	A20	7.31	R	1.5
	B40	15.15	R	2.1	B40	14.72	R	1.0
			T	2.1			T	1.4
	C40	30.39	R	—				
Emplacement hole	I40	~1.1	P	~80.	I40		P	—
	I18	7.01	R	4.5				
	I12	8.84	R	3.3				
	I07	10.36	R	1.0				
	I03	11.58	R	0.6				
Hole D	D18	6.86	V	1.2				
			HR	1.3				
	D03	11.36	V	0.44				
			HR	0.28				

[a]Notation: R = radial; T = tangential; P = pressure; V = vertical; HR = horizontal-radial.
[b]Estimated values due to irregular gage functioning.

SOC calculations was carried out using various explosive EOS formulations. These calculations are described in detail in Ref. 8. Only two of these calculations will be discussed here. The EOS formulation for composite explosives involves a two-phase detonation wave. The second phase energy is released gradually over a finite time interval herein referred to as the "ramp time."* As will be seen later, the observed ground motion between the two shots did not differ appreciably in spite of the disparity in the peak stress. This fact alone severely restricts the number of plausible explanations to those that would allow the shock energy to be spread over a broader front in the case of the stemmed event. More explicitly, the only explosive parameter satisfying this criterion is the ramp time. SOC calculations were made using ramp times of 50 and 2000 μsec. The resulting peak stress curves are plotted in Fig. C.28. The 2000 μsec ramp time calculation produced good agreement with the shot level gage results. These calculations are taken to be the best theoretical estimates for the unstemmed and stemmed 12.5-m (41-ft) events. Since no stress measurements were made on the 6-m (19.7-ft) stemmed event but detonation anomalies were known to exist, this 2000 μsec ramp time calculation will be assumed to best represent the 6-m (19.7-ft) event.

*The composite explosive EOS is discussed in detail in Chapter 4 and in Ref. 9.

Unstemmed Emplacement and Satellite Hole Stress Measurements

Four single crystal transducer systems were situated at Stations I03, I07, I12, and I18 in the open emplacement hole of the unstemmed shot in order to record radial (vertical) stress. In addition, pairs of transducers were emplaced at Stations D03 and D18 to record vertical and horizontal stress components (Fig. C.7).

The transducers in the open hole were placed in a jig that held them about 15.2 cm (6 in.) from the hole wall and equally spaced about the perimeter. Since pressures were expected to be several kilobars above the survival pressure for cables, the signal cables were protected with a lead covering over a length extending from the transducer location to a point slightly above the ground surface. Although the signals were received for several milliseconds, the stress gages appear to have failed. Because the gage at Station I18 shorted momentarily during rise, the reported peak value has been estimated by slope extrapolation. The peak values reported in Table C.6 and Fig. C.28 assume that failure occurred subsequent to maximum stress.

Both the horizontal and vertical stress gages at Station D18 in the satellite hole reported a relatively sharp spike at 3 msec. The narrow width of the spike suggests the signal source to be relatively small and it is believed to be due to the expanded gases in the emplacement hole. As noted earlier, there is reason to question the 10-msec arrival time reported by the vertical stress transducer at Station D03, 5 msec being a more reasonable value. Although of the proper magnitude, the peak value reported in Table C.6 is also questionable because the polarity of the recorded signal was negative. Study of the recording system and calibration procedures has not indicated how this could have occurred. Nevertheless, aside from its negative polarity, the wave shape and amplitude were reasonable.

Strain Measurement

The only strain measurement attempted in the DOIIA series was at the shot-level station C40 on the unstemmed event. In the experiment no strain history was actually measured because the VCO frequency went to band edge upon incidence of the shock front, indicating either component failure or overranging.

Accelerometer Data

Accelerometers were emplaced at three surface locations on all three shots to record vertical and horizontal surface accelerations, and at shot level on the two 12.5-m (41-ft) shots to record radial and tangential (vertical) accelerations. All accelerometers were piezoelectric devices constrained to function as charge generators connected to surface mounted shunt capacitors and VCO's.

The accuracies of the peak acceleration determinations are limited to about ±25%. This accuracy is controlled mainly by the filtering used in the playback system for the high-frequency components and by the signal-to-noise ratio for the low-frequency components. Neither of these problems should affect the accuracy of the peak velocity determinations. The baseline shifts experienced are, however, very critical—so much so

that accuracies are very difficult to assign to integrated velocities.

Shot-Level Accelerations

Of the five shot-level accelerometers on the 12.5-m (41-ft) events, three failed at shock arrival, one failed preshot, and the last failed from causes presently unknown. The peak values are given in Table C.7. As of this writing, analysis of the B40T and C40T signals on the 12.5-m (41-ft) stemmed event have not been completed. Final analysis will be contained in Ref. 8 when published.

Surface Accelerations

The peak vertical and horizontal accelerations recorded at the surface stations are listed in Table C.7 and plotted in Fig. C.29. Also shown in this figure are three curves derived from SOC calculations for the peak vertical acceleration. Calculations A (12.5-m unstemmed) and B (12.5-m stemmed) are the same calculations discussed previously in connection with peak stress. The curve labeled C is the same as B except for an adjustment to

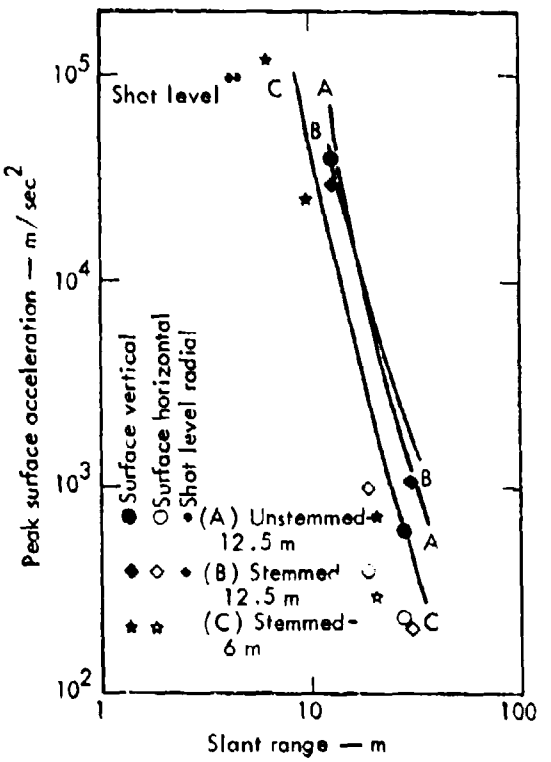

Fig. C.29. Peak surface acceleration as a function of slant range.

Table C.7. Recorded peak accelerations.[8]

Location	DOHA-1 Unstemmed—12.5 m Station[a]	Distance (m)	Acceleration[b] (g)	DOHA-2 Stemmed—12.5 m Station[a]	Distance (m)	Acceleration[b] (g)	DOHA-3 Stemmed—6 m Station	Distance (m)	Acceleration[b] (g)
Surface vertical	S05	12.59	4,000	S05	12.62	3,000	S05	6.22	12,000
	—	—	—	—	—	—	S20	9.69	2,500
	S80	27.34	63	S80	26.97	110	S65	20.66	75
Surface horizontal	S50	18.75	40	S50	18.41	100	—	—	—
	S80	27.34	24	S80	26.97	21	S65	20.66	30
Shot level	A40R	4.57	~10,000	A40R	4.35	~10,000			
	—	—	—	B10T	14.72	—			
	C40T	30.39	—	C40T	29.96	—			

[a]Notation: R - radial; T - tangential.

[b]Accuracy to ±25%.

a 6-m (19.7-ft) DOB. As the SOC calculations included no ground surface interface and assumed homogeneous material, several corrections had to be applied that resulted in the following expression for the vertical surface acceleration:

$$a_v(r) = \frac{2d}{r}\left(\frac{\tau}{\tau_c}\right)^2 a_c(r),$$

in which the subscript "c" denotes calculated quantities and "r" is slant range. The vertical component of the calculated radial acceleration is obtained by multiplication by the ratio "d/r" (depth of burial to slant range). The factor of 2 arises because of the presence of the free surface. The ratio of observed to calculated shock arrival times (τ/τ_c) follows from the Buckingham-Pi theorem[19] and represents a very significant correction at the larger distances. The arrival times were taken from Fig. C.27. The arrival time adjustment is an approximation to correct for the material layering that affected the peak surface measurements but could not be incorporated in the one-dimensional SOC calculations.

The accelerations calculated by SOC and adjusted as described above are typically a factor of 2 greater than observed. One possible explanation lies in the rapid acceleration rise times and in the fact that the accelerometers were emplaced about half a meter below the top surface of the concrete instrument pads. Under these conditions, the recorded acceleration could peak before the arrival of the rarefaction from the pad surface. The factor of 2 in the above equation would not then be justified because the observed peaks would actually represent free-field values. The records of the SO5 accelerometers on the two 12.5-m (41-ft) events both display a double peak structure that tends to support this hypothesis.

Particle Velocity Measurements

Surface and subsurface particle velocity information was obtained from three basic types of observation: integrated accelerometer records, velocity gage records, and high-speed photography correlated with postshot target surveys.

Integrated Accelerometer Records

Of the shot-level accelerometers on the two 12.5-m (41-ft) events, only those at the A40 stations functioned sufficiently long to merit integration, and then only to obtain minimum values for the peak velocities. These values appear in Table C.8 in which the peak values of all velocity measurements are summarized.

Integration of the surface accelerometer records was hindered by baseline shifts and poor signal-to-noise ratios that prevented any observation of a definite gas-acceleration phase. The surface velocity measurements are consequently limited to the early-time spallation phase. The peak horizontal and vertical surface velocities obtained from the integrations appear in Table C.8.

Velocity Gage Measurements

Particle velocity transducers were utilized at shot level on the 12.5-m (41-ft) events and at surface stations on all events (Figs. C.7 through C.9). The overall performance of the velocity transducer systems was poor. Of eleven

Table C.8. Recorded peak vertical and horizontal particle velocities.[8]

	DOIIA-1 Unstemmed—12.5 m				DOIIA-2 Stemmed—12.5 m				DOIIA-3 Stemmed—6 m			
Location	Station	Distance (m)	Gage	Velocity (m/sec)	Station	Distance (m)	Gage	Velocity (m/sec)	Station	Distance (m)	Gage	Velocity (m/sec)
Surface vertical	S00	12.5	HS[a]	~60	S00	12.5	HS[a]	42	S00	6.	HS[a]	180
	S05	12.58	AC	50	S05	12.62	AC	58	S05	6.22	AC	>30
	A	13.	HS	~60	—						HS	160
	S25	14.6	VE	40[b]	S25	15.	VE	—	S20	8.5	HS	81
			HE	25			HS	37		9.69	AC	60
	S50	18.75	VE	>14[b]	S50	18.41	VE	—	S40	14.97	VE	—
			HS	13			HS	18			HS	21
	B	20.	HS	11	B	20.	HS	15	—			
	S80	27.34	AC	6.0	S80	26.97	AC	6.2	S65	20.66	AC	7.0
Surface horizontal	A	13.	HS	~12	—				—			
	S25	14.6	HS	17	S25	15.	HS	15	S20	8.5	HS	30
	S50	18.75	AC	5.6	S50	18.41	AC	5.	S40	14.97	VE	—
			HS	11			HS	12			HS	20
	B	20	HS	9	B	20	HS	8	—			
	S80	27.34	AC	3.9	S80	26.97	AC	2.1	S65	20.66	AC	4.0
Shot level	A40	4.51	AC-R	>16[b]	A40	4.05	AC-R	>10[b]				
	B40	15.15	VE-R	—	B40	14.32	VE-R	—				
			VE-T	—			AC-T	—				
	C40	30.39	VE-R	—	C40	29.96	VE-R	—				
			AC-T	—			AC-T	—				

[a]HS = data from high-speed photography.

[b]Estimated values due to partial gage failure.

systems, only three produced any usable data. Four failed prior to detonation possibly because of water leakage. Two failed immediately upon shock incidence because of damage to the carrier oscillator system. Two continued to function but produced only spurious signals. Of the three usable signals, two survived only long enough to provide peak information before failure of the oscillator. These were at Stations S50 on DOIIA-1 and B40 on DOIIA-2. Analysis of the latter signal will be contained in Ref. 8 when published. The remaining gage (S25 on DOIIA-1) survived for over a hundred milliseconds and provided a good signal throughout except for the first 10 msec following shock arrival. The peak particle velocities determined for these gages appear in Table C.8.

High-Speed Photography

The velocity data obtained from the high-speed photography were presented in Table C.2 and discussed earlier in this chapter. The generalized data in Table C.2 have been separated into individual horizontal and vertical target velocities and are listed in Table C.8. The target spall velocities were found by two methods. The first involved fitting the observed vertical displacement to the ballistic equation to determine the initial velocity. The second involved the use of finite differences to deduce the early-time limit of the velocity. The results of these two techniques were found to be generally in agreement. The horizontal components were found from the known postshot target displacement and the initial vertical velocity component by assuming the validity of the ballistic equation. Effects of air friction were ignored.

The peak vertical surface velocities of Table C.8 have been plotted vs slant range in Fig. C.30. As was indicated earlier, there is very little difference between the surface velocities of the two 12.5-m (41-ft) events. Three theoretical curves have also been included in the figure. These were obtained from SOC calculations from the equation:

$$V_v(r) = \frac{2d}{r}\left(\frac{\tau}{\tau_c}\right)V_c(r),$$

in which the rotation is the same as that used in determining surface accelerations. Here, V_c is the radial peak velocity calculated by SOC. In the case of the 12.5-m (41-ft) events, the agreement is remarkable. The theoretical results for the 6-m (19.7-ft) event are about 30% low. This can be explained by the large uncertainty in the arrival times at the surface station, particularly S65 (see Fig. C.30).

The peak horizontal surface velocity components have been plotted in Fig. C.31. The three theoretical curves have been determined from:

$$V_H(r) = \left[1 - \left(\frac{d}{r}\right)^2\right]^{1/2}\left(\frac{\tau}{\tau_c}\right)V_c(r);$$

the theoretical curves appear to be bounded near SGZ by the photographic data, which is 50 to 100% high. At greater ranges, the curves are bounded by the gage velocities, which are low by 50 to 100%. No satisfactory explanation of this phenomenon has yet been found.

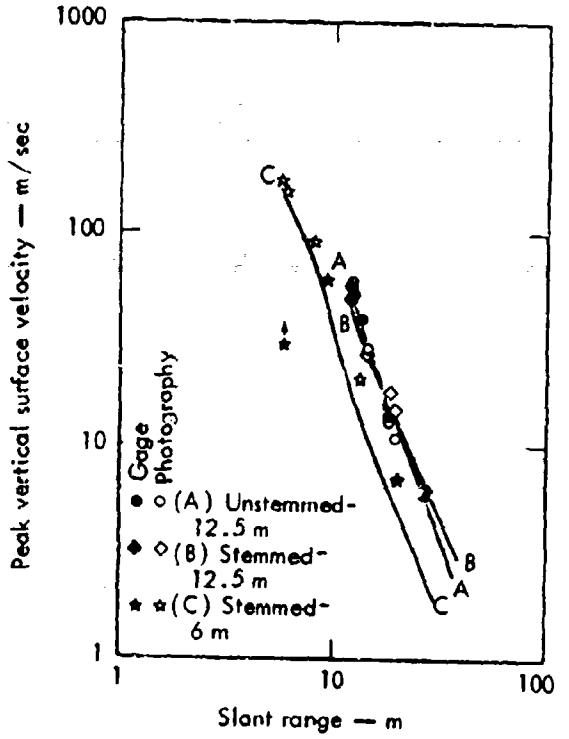

Fig. C.30. Peak vertical surface velocity as a function of slant range.

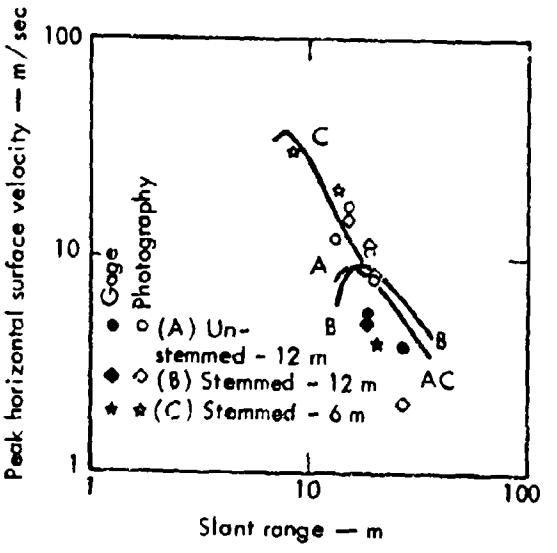

Fig. C.31. Peak horizontal surface velocity components as a function of slant range.

Airblast Measurements

Airblast gages were employed on each detonation. These gages were the Ballistics

Research Laboratory (BRL) self-recording-type gage and were operated by EERL. The overpressures experienced by the gage actuate a diaphragm, which in turn moves a stylis, which scribes a record on a negator-type spring. The spring is then removed from the gage and the record is interpreted using a digital microscope. These gages were actuated at minus 2 sec by a relay closure signal from the CP. Only one of the three gages employed on DOIIA-1 operated properly. A peak overpressure level of 7.0 mbar was recorded by this gage at a range of 1,220 m (4,000 ft). None of the three gages on the DOIIA-2 operated properly. There is evidence that these gages were under-ranged, although the two gages employed on the DOIIA-3 detonation appear to have reacted normally. Overpressure levels of 10.5 mbar at 305 m (1,000 ft) and 2.0 mbar at 1,220 m (4,000 ft) were recorded. Due to the heavy loss of data in this program, no comparisons have been attempted.

Ground Motion Measurements

Two seismic recording stations were employed on each of the DOIIA detonations. An additional seismic recording station was employed on the DOIIA-3 detonation to monitor a water well for possible seismic damage. These gages were Mark Products, L-4 canisters. Each canister contained three triaxially-mounted low-frequency geophones. Gage responses were recorded on Century Electronics Model 444 oscillographs. The gages were hard-wired to the oscillographs and the system was manually initiated just prior to zero time. Table C.9 shows the peak particle velocities and gage locations for each detonation. The largest component of velocity measured in each case was the vertical. The DOIIA-2 detonation produced the highest velocities as was expected. The combination of DOB and complete stemming resulted in a longer containment time as compared with the shallower DOIIA-3 and unstemmed DOIIA-1 detonations. This

Table C.9. Summary of measured peak particle velocities (intermediate range).

Detonation	Seismic	Range (m)	Range (ft)	Peak particle velocities (cm/sec) Vertical	Radial	Transverse
IIA-1	1	1,160	3,800	6.6	1.8	1.1
IIA-1	2	1,620	5,300	2.3	1.2	0.4
IIA-2	1	1,330	4,350	8.3	4.5	2.6
IIA-2	2	1,790	5,860	3.5	1.5	0.7
IIA-3	1	820	2,700	1.2	0.8	1.6
IIA-3	2	1,280	4,200	0.8	0.5	0.6
IIA-3	3	3,520	11,550	0.4	0.3	—[b]

[a] Vertical time history record shows that there was a conductivity problem between the geophone and recorder; this was most likely caused by a poor splice in a cable.

[b] There was no transverse geophone at this station.

longer containment time results in a better coupling of the explosive energy to the surrounding media. The effect of the differences in explosive detonation velocity is not known. This longer containment time is verified by the venting time for each detonation as obtained from the high-speed photography. The DOIIA-2 detonation vented at about 130 msec, whereas the DOIIA-1 detonation vented within the first msec, and the DOIIA-3 detonation vented at about 29 msec. The higher peak particle velocity obtained for the DOIIA-1 detonation, as compared with the DOIIA-3 detonation, must be attributed to the deeper DOB in the DOIIA-1 detonation. This indicates that DOB is more critical than the type of stemming in determining ground motion levels. This conclusion coincides with the Middle Course II results.[7] The velocities measured at the well on DOIIA-3 were considered insignificant and were actually lower than the levels produced by the vibrations generated by an electric pump used to operate the well.

Ejecta and Missile Measurements

Analysis of the continuous ejecta was conducted by means of the point-count technique as described in Ref. 17. This method was established to determine economically the block size distribution of crater fallback and ejecta using sampling techniques rather then the costly sieving and weighing of the same materials. Figure C.32 shows the ejecta particle size distribution curves for the three Phase IIA detonations. The curves represent averages of data taken along orthagonal lines crossing each SGZ. The three curves are of similar shape indicating the homogeneity of the media. These curves are sufficiently close together to prevent the determination of even subtle differences. The individual curves (not shown) for each surveyed line on each crater do indicate an appreciable increase in the amount of fines in the downwind direction. This was also visually observed on the ground following each detonation.

The maximum missile range for each detonation was determined by ground survey. A representative 15 deg sector was selected at each crater for determination of missile density and range data. A count of all missiles found outside the limits of the continuous ejecta was made in this sector. The distance each missile had traveled was determined by conventional surveying techniques. These density vs range data are important in determining safety stand-off distances. The maximum missile range in itself is not sufficient because the probability of

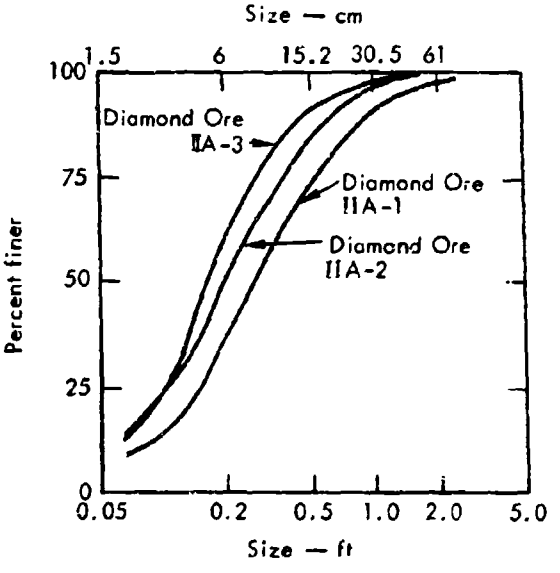

Fig. C.32. Particle size distribution curves for continuous ejecta.

an object being struck by a missile at the maximum range is very, very small. These data were obtained for a separate EERL troop safety effects study. The missile density and range data obtained for each detonation are plotted in Fig. C.33. The significantly higher densities at longer ranges for the DOIIA-3 detonation are attributed to the higher mound velocity produced by the shallower DOB. The slightly steeper curve produced by the DOIIA-1 detonation as compared to the DOIIA-2 curve can be attributed to the effects of the open access hole. The horizontal pressures exerted against the access hole walls by the explosive gases escaping up the access hole produce larger horizontal velocity components in the material ejected by the detonation.

SUMMARY

The most significant results of the Diamond Ore Phase IIA detonations were the discovery of problems in the reproducibility of the detonation characteristics of the explosive (Chapter 4). These problems and the subsequent attempts at stabilizing the detonation history are described in Chapter 5. Because of the significant differences in the manner in which the three explosive charges detonated, all comparisons between the experimental results must be considered suspect. A general comparison of the craters produced shows the 6-m (19.7-ft) stemmed detonation excavated the largest volume of material due primarily to its significantly larger apparent depth. The unstemmed detonation produced a more

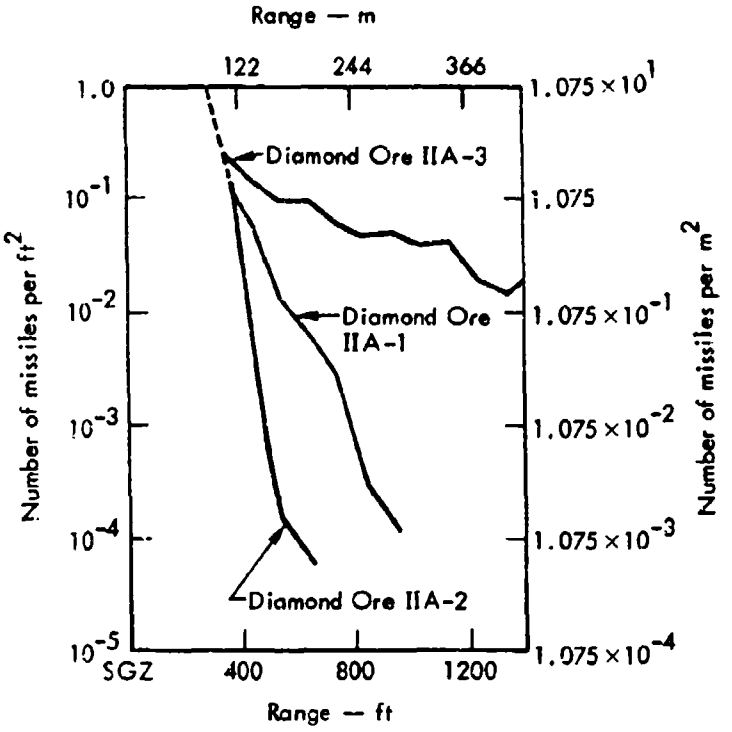

Fig. C.33. Missile density as a function of range.

rounded or bowl-shaped crater. This effect is attributed to the horizontal pressures exerted on the medium by the gases escaping up the open access hole during crater formation. The effects of the shallower DOB for the 6-m (19.7-ft) detonations were indicated by a higher mound velocity, significantly larger maximum missile range, and larger missile densities out to that maximum range, and a larger radius of continuous ejecta. The ground motion data indicated that changes in DOB were more critical to peak particle velocities than was the type of stemming. High-speed photography of the unstemmed detonation indicated an interruption of the venting by an apparent hole closure at about 90 msec. This phenomenon was also observed on the Middle Course II M-16 detonation. This 1-ton detonation had a 10-cm (4-in.)-diameter open access hole that apparently closed during venting.[7] Additional research into the detonation characteristics of composite explosives, both simple and complex, is being contemplated by the Chemistry Department at LLL.

Appendix D
Fallout Disposition Data, Detonation IT-6, Phase IIB, Project Diamond Ore

This appendix contains the mass and iridium deposition data generated in support of the fallout simulation program conducted in conjunction with the Diamond Ore Phase IIB IT-6 detonation at Fort Peck, Montana, in October 1972. The generation and use of these data are discussed in Chapter 6 and explained in Ref. 4.

1T-6 MASS DEPOSITION

TRAY POSITION		DISTANCE (YARDS)	TOTAL WEIGHT (GM/M**2)	<125 (GM/M**2)	125-175 (GM/M**2)	175-350 (GM/M**2)	350-991 (GM/M**2)	991-2794 (GM/M**2)	>2794 (GM/M**2)
1A	7	30.0	42448.20	237.25	161.46	563.47	2316.50	6217.96	32951.36
2A	7	35.0	7031.66	48.07	48.07	212.04	514.73	927.56	5281.20
3A	7	40.0	5670.92	29.99	35.68	143.86	250.97	550.39	4653.63
4A	7	45.0	16801.74	149.47	121.97	493.85	1884.53	4215.08	9936.83
B	7	50.0	4589.14	90.49	42.95	151.85	478.55	1509.26	2316.04
1B	7	55.0	10084.81	92.89	72.37	306.75	1390.08	2606.26	5616.47
C	7	75.0	154.43	3.41	2.73	13.57	18.65	7.95	116.13
D	7	110.0	72.36	2.45	1.36	8.61	19.67	24.89	15.39
E	7	170.0	0.76	0.	0.	0.	0.	0.	0.
G	7	250.0	0.34	0.	0.	0.	0.	0.	0.
I	7	370.0	0.02	0.	0.	0.	0.	0.	0.
L	7	500.0	0.02	0.	0.	0.	0.	0.	0.
F	19	210.0	46.27	2.57	1.56	6.85	15.10	7.98	12.21
H	19	313.0	0.40	0.	0.	0.	0.	0.	0.
A	30	25.0	41837.57	198.03	146.37	514.88	2484.84	6533.25	31960.21
1A	30	30.0	32678.12	244.86	202.54	804.11	3455.24	6206.12	21765.26
2A	30	35.0	16191.11	75.05	55.25	185.56	790.05	2698.38	12386.82
3A	30	40.0	6523.25	41.03	29.84	99.88	403.66	1157.94	4790.90
4A	30	45.0	4711.27	51.21	25.61	75.31	251.53	915.75	3391.87
B	30	50.0	2932.10	12.66	10.42	33.75	104.47	383.63	2387.17
1B	30	55.0	1770.02	6.10	5.16	17.84	59.15	219.46	1462.30
C	30	75.0	419.99	10.53	7.38	25.16	87.73	145.80	143.40
D	30	113.0	184.40	3.91	3.14	7.81	37.00	62.08	69.27
E	30	173.0	2.42	0.29	0.48	0.26	0.13	0.27	0.
G	30	253.0	0.97	0.	0.	0.	0.	0.	0.
I	30	373.0	1.17	0.	0.	0.	0.	0.	0.
L	30	500.0	0.30	0.	0.	0.	0.	0.	0.
H	41	313.0	0.70	0.	0.	0.	0.	0.	0.
K	41	483.0	0.45	0.	0.	0.	0.	0.	0.
N	41	733.0	0.17	0.	0.	0.	0.	0.	0.
1A	52	30.0	62913.72	422.39	291.84	1036.79	4101.37	11673.44	45388.19
2A	52	35.0	64134.98	423.57	348.97	1128.72	3903.60	9234.34	49095.79
3A	52	40.0	28403.71	136.54	95.71	329.24	1477.74	4287.74	22076.75
4A	52	45.0	16633.63	97.41	71.10	243.18	1171.09	3249.47	13801.37
B	52	50.0	2838.95	12.43	11.78	38.39	127.96	347.67	1492.81
1B	52	55.0	3880.05	11.73	10.31	38.84	145.05	538.26	2344.66
C	52	75.0	457.95	3.39	2.88	7.31	25.19	75.82	343.36
D	52	110.0	2.10	0.17	0.48	0.78	0.12	0.15	0.48
E	52	170.0	1.10	0.	0.	0.	0.	0.	0.
G	52	250.0	1.12	0.	0.	0.	0.	0.	0.
I	52	370.0	0.46	0.	0.	0.	0.	0.	0.
M	52	580.0	0.05	0.	0.	0.	0.	0.	0.
O	52	880.0	0.22	0.	0.	0.	0.	0.	0.
P	52	100.0	0.04	0.	0.	0.	0.	0.	0.
H	64	310.0	0.52	0.	0.	0.	0.	0.	0.

IT-6 MASS DEPOSITION

TRAY POSITION		DISTANCE (YARDS)	TOTAL WEIGHT (GM/M**2)	<125 (GM/M**2)	125-175 (GM/M**2)	175-350 (GM/M**2)	350-991 (GM/M**2)	991-2794 (GM/M**2)	>2794 (GM/M**2)
K	64	480.0	0.40	0.	0.	0.	0.	0.	0
N	64	730.0	0.09	0.	0.	0.	0.	0.	0.
P	64	1100.0	0.08	0.	0.	0.	0.	0.	0.
Q,	64	1300.0	0.03	0.	0.	0.	0.	0.	0.
A	75	25.0	78790.10	1027.82	754.69	2828.31	10005.99	12279.96	51894.23
1A	75	30.0	37563.16	193.0	163.11	638.83	4655..0	4827.92	26835.20
2A	75	35.0	41837.57	144.24	93.95	375.71	1881.89	5930.79	33411.82
3A	75	40.0	8196.43	23.16	15.92	57.45	284.11	1117.29	6697.51
4A	75	45.0	3978.51	16.44	15.11	47.99	214.17	632.28	3052.53
B	75	50.0	2676.55	13.70	13.70	47.15	200.05	469.08	1932.07
1B	75	55.0	2517.84	10.28	7.60	27.54	147.96	424.66	1899.81
C	75	75 0	365.81	3.41	2.73	4.90	11.82	30.30	312.95
E	75	178.0	1.18	0.	0.	0.	0.	0.	0.
G	75	250.0	0.97	0.	0.	0.	0.	0.	0.
I	75	370.0	0.22	0.	0.	0.	0.	0.	0.
M	75	580.0	0.17	0.	0.	0.	0.	0.	0.
O	75	880.0	0.02	0.	0.	0.	0.	0.	0.
Q	75	1300.0	0.25	0.	0.	0.	0.	0.	0.
R	75	1600.0	0.17	0.	0.	0.	0.	0.	0.
H	86	310.0	0.30	0.	0.	0.	0.	0.	0.
K	86	480.0	0.15	0.	0.	0.	0.	0.	0.
N	86	730.0	0.1	0.	0.	0.	0.	0.	0.
P	86	1100.0	0.07	0.	0.	0.	0.	0.	0.
Q	86	1300.0	0.02	0.	0.	0.	0.	0.	0.
R	86	1600.0	0.17	0.	0.	0.	0.	0.	0.
S	86	1900.0	0.27	0.	0.	0.	0.	0.	0.
1A	97	30.0	46111.98	212.55	164.55	582.79	2872.79	7243.67	35035.64
2A	97	35.0	43058.83	155.46	111.04	351.64	1251.09	1769.29	39430.32
3A	97	40.0	24739.93	66.43	54.62	194.86	831.11	2291.09	21301.82
4A	97	45.0	21076.15	245.34	105.15	356.33	1197.51	4036.48	15135.74
B	97	50.0	2630.82	15.49	13.70	48.55	257.32	658.30	1645.47
1B	97	55.0	5447.25	19.97	13.54	41.30	198.01	797.81	4376.62
C	97	75.0	330.17	4.73	3.72	7.63	22.79	41.89	249.43
D	97	110.0	1.67	0.44	0.59	0.37	0.10	0.17	0.
E	97	170.0	1.08	0.	0.	0.	0.	0.	0.
G	97	250.0	0.76	0.	0.	0.	0.	0.	0.
I	97	370.0	0.22	0.	0.	0.	0.	0.	0.
K	97	480.0	0.32	0.	0.	0.	0.	0.	0.
M	97	580.0	0.08	0.	0.	0.	0.	0.	0.
N	97	730.0	0.07	0.	0.	0.	0.	0.	0.
O	97	880.0	0.15	0.	0.	0.	0.	0.	0.
P	97	1100.0	0.19	0.	0.	0.	0.	0.	0.
Q	97	1300.0	0.01	0.	0.	0.	0.	0.	0.
R	97	1600.0	0.09	0.	0.	0.	0.	0.	0.
S	97	1900.0	0.05	0.	0.	0.	0.	0.	0.

1T-6 MASS DEPOSITION

TRAY POSITION	DISTANCE (YARDS)	TOTAL WEIGHT (GM/M**2)	<125 (GM/M**2)	125-175 (GM/M**2)	175-350 (GM/M**2)	350-991 (GM/M**2)	991-2794 (GM/M**2)	>2794 (GM/M**2)
T 97	2000.0	0.08	0.	0.	0.	0.	0.	0.
H 109	310.0	0.41	0.	0.	0.	0.	0.	0.
K 109	480.0	0.04	0.	0.	0.	0.	0.	0.
N 109	730.0	0.03	0.	0.	0.	0.	0.	0.
P 109	1100.0	0.06	0.	0.	0.	0.	0.	0.
Q 109	1300.0	0.14	0.	0.	0.	0.	0.	0.
Q 109	1300.0	0.09	0.	0.	0.	0.	0.	0.
R 109	1600.0	0.30	0.	0.	0.	0.	0.	0.
S 109	1900.0	0.10	0.	0.	0.	0.	0.	0.
T 109	2000.0	0.20	0.	0.	0.	0.	0.	0.
A 120	25.0	34165.69	187.06	100.51	329.46	1887.39	6449.52	25211.75
1A 120	30.0	28403.71	225.06	163.68	605.02	3066.01	6544.14	17799.81
2A 120	35.0	16191.11	67.59	42.69	152.97	955.58	3003.43	12068.85
3A 120	40.0	5810.40	30.18	26.34	95.48	391.79	1145.73	4120.89
4A 120	45.0	1102.90	5.80	5.90	19.07	60.32	153.49	858.42
B 120	50.0	2635.12	20.14	10.79	40.29	238.12	989.88	1335.91
1B 120	55.0	446.54	2.48	3.27	10.88	32.19	82.95	314.76
C 120	75.0	153.33	1.92	2.22	3.45	4.44	19.94	121.36
D 120	110.0	15.41	2.90	1.58	3.17	3.86	3.00	1.88
D 120	110.0	0.19	0.	0.	0.	0.	0.	0.
E 120	170.0	1.62	0.	0.	0.	0.	0.	0.
G 120	250.0	0.87	0.	0.	0.	0.	0.	0.
I 120	370.0	0.41	0.	0.	0.	0.	0.	0.
K 120	480.0	0.33	0.	0.	0.	0.	0.	0.
M 120	580.0	0.09	0.	0.	0.	0.	0.	0.
N 120	730.0	0.01	0.	0.	0.	0.	0.	0.
P 120	1100.0	0.17	0.	0.	0.	0.	0.	0.
Q 120	1300.0	0.07	0.	0.	0.	0.	0.	0.
R 120	1600.0	0.06	0.	0.	0.	0.	0.	0.
T 120	2000.0	0.23	0.	0.	0.	0.	0.	0.
T 120	2000.0	0.02	0.	0.	0.	0.	0.	0.
H 131	310.0	1.16	0.	0.	0.	0.	0.	0.
K 131	480.0	0.37	0.	0.	0.	0.	0.	0.
M 131	580.0	0.26	0.	0.	0.	0.	0.	0.
N	730.0	0.03	0.	0.	0.	0.	0.	0.
P 131	880.0	0.16	0.	0.	0.	0.	0.	0.
131	1100.0	0.02	0.	0.	0.	0.	0.	0.
131	1300.0	0.68	0.	0.	0.	0.	0.	0.
R 131	1600.0	0.10	0.	0.	0.	0.	0.	0.
S 131	1900.0	0.10	0.	0.	0.	0.	0.	0.
T 131	2000.0	0.03	0.	0.	0.	0.	0.	0.
1A 142	30.0	21686.78	173.66	102.62	565.72	1999.75	4557.33	14287.70
2A 142	35.0	8863.55	80.30	62.86	392.18	1194.79	1390.67	5742.75
3A 142	40.0	16801.74	80.19	65.61	277.84	970.95	2682.87	12725.08
4A 142	45.0	19244.26	114.94	71.50	251.61	1343.11	4928.04	12535.06

1T-6 MASS DEPOSITION

TRAY POSITION	DISTANCE (YARDS)	TOTAL WEIGHT (GM/M**2)	<125 (GM/M**2)	125-175 (GM/M**2)	175-358 (GM/M**2)	358-991 (GM/M**2)	991-2794 (GM/M**2)	>2794 (GM/M**2)
B 142	50.0	1336.93	4.72	3.07	15.09	36.55	117.99	1159.51
1B 142	55.0	4013.48	17.14	12.03	42.73	199.08	822.91	2919.59
C 142	75.0	31.04	2.16	1.37	1.57	1.68	4.42	19.85
D 142	110.0	12.64	0.79	0.44	0.51	0.98	1.98	7.94
E 142	170.0	0.43	0.	0.	0.	0.	0.	0.
G 142	250.0	0.33	0.	0.	0.	0.	0.	0.
I 142	370.0	0.41	0.	0.	0.	0.	0.	0.
K 142	480.0	0.23	0.	0.	0.	0.	0.	0.
M 142	580.0	0.47	0.	0.	0.	0.	0.	0.
N 142	730.0	3.22	0.	0.	0.	0.	0.	0.
O 142	880.0	0.02	0.	0.	0.	0.	0.	0.
P 142	1100.0	0.02	0.	0.	0.	0.	0.	0.
Q 142	1300.0	0.03	0.	0.	0.	0.	0.	0.
R 142	1600.0	0.09	0.	0.	0.	0.	0.	0.
S 142	1900.0	0.02	0.	0.	0.	0.	0.	0.
T 142	2000.0	0.06	0.	0.	0.	0.	0.	0.
H 154	310.0	0.21	0.	0.	0.	0.	0.	0.
K 154	480.0	0.02	0.	0.	0.	0.	0.	0.
N 154	730.0	6.14	0.	0.	0.	0.	0.	0.
P 154	1100.0	0.22	0.	0.	0.	0.	0.	0.
O 154	1300.0	0.12	0.	0.	0.	0.	0.	0.
R 154	1600.0	0.23	0.	0.	0.	0.	0.	0.
S 154	1900.0	0.03	0.	0.	0.	0.	0.	0.
A 165	25.0	76958.21	425.73	253.14	947.36	3582.31	10535.97	61213.71
A 165	25.0	76958.21	518.54	380.91	1531.63	4889.08	10746.96	58984.08
2A 165	35.0	36341.90	182.05	103.33	365.43	1172.69	3910.06	30588.34
3A 165	40.0	10084.81	91.47	113.63	418.14	569.62	1400.43	7391.32
4A 165	45.0	4454.64	24.46	33.92	104.37	204.83	675.47	3411.59
1B 165	55.0	936.81	2.97	1.98	9.01	27.94	33.91	803.00
C 165	75.0	441.51	2.49	1.68	3.94	19.54	67.71	346.15
D 165	110.0	1.13	0.	0.	0.	0.	0.	0.
E 165	170.0	0.25	0.	0.	0.	0.	0.	0.
I 165	370.0	0.24	0.	0.	0.	0.	0.	0.
M 165	580.0	0.18	0.	0.	0.	0.	0.	0.
O 165	880.0	1.78	0.	0.	0.	0.	0.	0.
P 165	1100.0	0.46	0.	0.	0.	0.	0.	0.
Q 165	1300.0	0.21	0.	0.	0.	0.	0.	0.
Q 165	1300.0	0.17	0.	0.	0.	0.	0.	0.
R 165	1600.0	0.20	0.	0.	0.	0.	0.	0.
R 165	1600.0	0.12	0.	0.	0.	0.	0.	0.
H 176	310.0	0.17	0.	0.	0.	0.	0.	0.
K 176	480.0	0.24	0.	0.	0.	0.	0.	0.
N 176	730.0	0.22	0.	0.	0.	0.	0.	0.
P 176	1100.0	0.12	0.	0.	0.	0.	0.	0.
O 176	1300.0	0.19	0.	0.	0.	0.	0.	0.

1T-6 MASS DEPOSITION

TRAY POSITION	DISTANCE (YARDS)	TOTAL WEIGHT (GM/M**2)	<125 (GM/M**2)	125-175 (GM/M**2)	175-350 (GM/M**2)	350-991 (GM/M**2)	991-2794 (GM/M**2)	>2794 (GM/M**2)
Q 176	1300.0	0.09	0.	0.	0.	0.	0.	0.
2A 187	35.0	42448.20	201.01	155.13	559.33	1990.44	5348.63	34193.66
3A 187	40.0	29624.97	229.04	205.35	874.03	2990.57	6686.88	18639.01
4A 187	45.0	10695.44	90.32	96.34	358.25	785.75	1396.89	7967.89
B 187	50.0	14969.85	238.26	177.68	573.43	1627.42	3121.56	9231.48
1B 187	55.0	4539.14	66.13	84.24	251.47	457.86	588.27	3041.17
C 187	75.0	782.58	8.01	8.01	10.54	21.79	72.75	661.46
D 187	110.0	57.14	1.72	0.55	1.20	3.97	12.52	37.38
D 187	110.0	40.67	8.05	4.83	9.56	13.15	3.70	1.38
E 187	170.0	0.25	0.	0.	0.	0.	0.	0.
G 187	250.0	0.44	0.	0.	0.	0.	0.	0.
I 187	370.0	0.22	0.	0.	0.	0.	0.	0.
M 187	580.0	0.19	0.	0.	0.	0.	0.	0.
P 187	1100.0	0.11	0.	0.	0.	0.	0.	0.
R 187	1600.0	0.02	0.	0.	0.	0.	0.	0.
H 199	310.0	0.27	0.	0.	0.	0.	0.	0.
K 199	480.0	0.03	0.	0.	0.	0.	0.	0.
N 199	730.0	0.09	0.	0.	0.	0.	0.	0.
2A 210	35.0	36341.90	396.82	335.02	1278.29	4153.64	5718.17	24459.96
3A 210	40.0	20465.52	235.75	224.65	811.24	2185.50	2974.56	14033.82
4A 210	45.0	10084.81	75.74	72.38	284.45	573.95	1100.21	7978.08
B 210	50.0	12527.33	109.42	102.13	375.16	1201.57	2037.35	8701.71
1B 210	55.0	4610.66	48.69	36.66	135.41	405.13	611.93	3372.85
C 210	75.0	10541.57	208.40	81.64	296.49	1412.63	4055.28	4487.12
D 210	110.0	1.86	0.	0.	0.	0.	0.	0.
E 210	170.0	1.12	0	0.	0.	0.	0.	0.
G 210	250.0	0.30	0.	0.	0.	0.	0.	0.
I 210	370.0	0.19	0.	0.	0.	0.	0.	0.
L 210	500.0	0.02	0.	0.	0.	0.	0.	0.
F 221	210.0	0.27	0.	0.	0.	0.	0.	0.
H 221	310.0	0.02	0.	0.	0.	0.	0.	0.
J 221	440.0	0.02	0.	0.	0.	0.	0.	0.
1A 232	30.0	31454.86	194.01	164.91	597.55	1911.00	4163.47	24425.92
2A 232	35.0	8252.92	72.26	59.98	335.37	922.24	904.87	5988.10
3A 232	40.0	8863.55	65.36	59.63	350.59	821.85	1222.20	6363.82
4A 232	45.0	19244.26	104.60	64.26	279.44	954.39	2339.47	15451.60
B 232	50.0	7031.66	29.32	23.32	94.61	586.37	1440.44	4857.00
1B 232	55.0	3133.85	37.40	34.26	112.56	315.46	380.27	2247.70
C 232	75.0	170.82	1.60	0.87	2.58	11.20	25.65	117.99
D 232	110.0	27.38	0.78	0.33	0.04	3.79	11.87	9.78
E 232	170.0	0.19	0.	0.	0.	0.	0.	0.
I 232	370.0	0.08	0.	0.	0.	0.	0.	0.
L 232	500.0	0.04	0.	0.	0.	0.	0.	0.
F 244	210.0	0.08	0.	0.	0.	0.	0.	0.
H 244	310.0	0.02	0.	0.	0.	0.	0.	0.

IT-6 MASS DEPOSITION

TRAY POSITION	DISTANCE (YARDS)	TOTAL WEIGHT (GM/M**2)	<125 (GM/M**2)	125-175 (GM/M**2)	175-350 (GM/M**2)	350-991 (GM/M**2)	991-2794 (GM/M**2)	>2794 (GM/M**2)
J 244	440.0	0.12	0.	0.	0.	0.	0.	0.
1A 255	30.0	46111.38	298.99	222.74	976.95	3419.32	5869.51	35326.47
2A 255	35.0	40615.31	423.94	334.48	1454.61	4783.38	7249.72	26369.68
3A 255	40.0	17412.37	113.45	75.34	294.25	1094.59	2664.24	13170.51
4A 255	45.0	32067.49	221.84	165.09	682.73	2041.30	4539.79	24316.74
B 255	50.0	15580.48	93.62	75.73	268.92	818.72	1833.64	12489.88
1B 255	55.0	8252.92	50.80	39.13	126.32	499.12	1221.36	6316.19
C 255	75.0	413.05	2.25	1.28	3.79	13.09	26.74	366.07
D 255	110.0	0.65	0.	0.	0.	0.	0.	0.
E 255	170.0	1.14	0.	0.	0.	0.	0.	0.
G 255	250.0	0.12	0.	0.	0.	0.	0.	0.
I 255	370.0	0.61	0.	0.	0.	0.	0.	0.
L 255	500.0	0.13	0.	0.	0.	0.	0.	0.
E 266	170.0	3.13	0.19	0.07	0.26	0.75	1.99	2.88
H 266	310.0	0.05	0.	0.	0.	0.	0.	0.
2A 277	35.0	25961.19	127.28	73.69	235.80	1000.83	3140.48	21383.11
2A 277	35.0	25961.19	101.39	62.26	217.01	989.00	3032.81	21558.73
3A 277	40.0	14969.85	69.19	43.06	165.24	813.98	2563.21	11314.28
4A 277	45.0	15580.48	171.35	73.44	232.54	1093.37	4124.61	9885.18
B 277	50.0	15580.48	159.75	54.91	154.76	703.69	2328.40	11586.77
1B 277	55.0	24739.93	292.83	127.64	412.96	1591.77	4782.80	17531.94
C 277	75.0	1317.89	8.72	5.22	16.23	58.22	156.10	1072.48
D 277	110.0	23.62	0.98	0.61	0.80	1.58	7.12	12.54
E 277	170.0	0.08	0.	0.	0.	0.	0.	0.
G 277	250.0	0.11	0.	0.	0.	0.	0.	0.
I 277	370.0	0.47	0.	0.	0.	0.	0.	0.
L 277	500.0	0.13	0.	0.	0.	0.	0.	0.
F 289	210.0	0.05	0.	0.	0.	0.	0.	0.
H 289	310.0	0.04	0.	0.	0.	0.	0.	0.
J 289	440.0	0.02	0.	0.	0.	0.	0.	0.
A 300	25.0	51436.88	267.40	133.70	403.78	1419.91	5088.69	57117.39
A 300	25.0	64433.88	371.14	234.22	998.12	4230.29	10528.89	48068.23
1A 300	30.0	60767.10	209.49	152.36	525.63	1771.14	5088.68	53019.81
2A 300	35.0	92519.86	366.56	253.77	981.25	4037.60	9395.23	77485.24
3A 300	40.0	29014.34	154.20	106.39	381.31	1551.54	4229.09	22591.81
4A 300	45.0	8252.92	44.69	36.13	143.56	442.57	1049.62	6535.35
B 300	50.0	8252.92	22.36	17.47	68.48	368.97	1234.79	6540.84
1B 300	55.0	3979.51	7.45	4.10	13.03	58.91	236.00	3659.13
C 300	75.0	221.09	2.88	1.35	3.54	16.07	51.94	145.31
D 300	110.0	1.56	0.	0.	0.	0.	0.	0.
G 300	250.0	0.07	0.	0.	0.	0.	0.	0.
L 300	500.0	0.70	0.	0.	0.	0.	0.	0.
L 300	500.0	0.20	0.	0.	0.	0.	0.	0.
F 311	210.0	0.18	0.	0.	0.	0.	0.	0.
H 311	310.0	0.39	0.	0.	0.	0.	0.	0.

1T-6 MASS DEPOSITION

TRAY POSITION	DISTANCE (YARDS)	TOTAL WEIGHT (GM/M**2)	<125 (GM/M**2)	125-175 (GM/M**2)	175-350 (GM/M**2)	350-991 (GM/M**2)	991-2794 (GM/M**2)	>2794 (GM/M**2)
J 311	440.0	0.49	0.	0.	0.	0.	0.	0.
A 322	25.0	0.	0.	0.	0.	0.	0.	0.
2A 322	35.0	38173.79	227.41	174.23	671.23	2983.85	6369.33	27747.75
3A 322	40.0	30235.60	140.11	97.53	417.59	1791.25	4454.39	23324.72
4A 322	45.0	11306.07	253.91	123.43	380.87	1079.12	2567.32	6901.43
B 322	50.0	23513.67	221.87	133.67	526.95	2514.88	6295.68	13820.92
1B 322	55.0	7031.66	32.91	23.42	95.57	495.57	1491.78	4892.42
C 322	75.0	285.09	0.99	0.58	1.96	8.47	25.63	247.46
D 322	110.0	26.90	0.59	0.35	0.95	3.78	5.05	16.73
E 322	170.0	0.14	0.	0.	0.	0.	0.	0.
G 322	250.0	0.03	0.	0.	0.	0.	0.	0.
I 322	370.0	0.25	0.	0.	0.	0.	0.	0.
L 322	500.0	0.05	0.	0.	0.	0.	0.	0.
F 334	210.0	0.08	0.	0.	0.	0.	0.	0.
H 334	310.0	0.18	0.	0.	0.	0.	0.	0.
J 334	440.0	0.06	0.	0.	0.	0.	0.	0.
A 345	25.0	49165.13	276.05	242.25	1312.65	3323.87	4559.05	39351.26
A 345	25.0	49165.13	268.87	214.00	838.39	3091.70	6312.83	37941.34
1A 345	33.0	35129.64	260.29	193.80	744.78	3231.82	6655.54	24034.41
2A 345	35.0	28483.71	189.21	156.13	693.32	2345.92	3981.31	21037.83
3A 345	40.0	5810.40	23.34	15.07	50.57	226.11	822.28	4673.02
4A 345	45.0	9474.18	55.42	45.18	237.05	632.97	1335.51	7167.05
B 345	50.0	10084.81	32.41	23.25	115.55	305.79	715.86	8831.94
1B 345	55.0	5810.40	31.33	20.34	89.04	380.91	963.00	4325.78
C 345	75.0	2114.42	40.03	19.28	74.63	251.39	522.92	1205.98
D 345	110.0	7.26	0.50	0.32	0.84	1.86	1.42	3.12
E 345	170.0	0.10	0.	0.	0.	0.	0.	0.
G 345	250.0	0.07	0.	0.	0.	0.	0.	0.
I 345	370.0	0.04	0.	0.	0.	0.	0.	0.
L 345	500.0	0.05	0.	0.	0.	0.	0.	0.
F 356	210.0	0.13	0.	0.	0.	0.	0.	0.
H 356	310.0	0.03	0.	0.	0.	0.	0.	0.
J 356	440.0	0.06	0.	0.	0.	0.	0.	0.

IT-6 TOTAL IRIDIUM DEPOSITION

TRAY POSITION	DISTANCE (YARDS)	TOTAL IRIDIUM (GM/M**2)	<125 (GM/M**2)	125-175 (GM/M**2)	175-350 (GM/M**2)	350-991 (GM/M**2)	991-2794 (GM/M**2)
1A 7	30.	1.21E-03	2.44E-04	1.53E-04	2.38E-04	2.46E-05	5.42E-04
2A 7	35.	1.46E-03	2.67E-04	2.51E-04	4.45E-04	3.21E-04	1.94E-04
3A 7	40.	1.02E-03	1.50E-04	1.67E-04	3.35E-04	2.24E-04	1.45E-04
4A 7	45.	2.02E-03	2.94E-04	1.86E-04	5.21E-04	4.65E-04	5.59E-04
B 7	50.	6.74E-04	2.38E-04	7.34E-05	1.04E-04	9.61E-05	1.63E-04
1B 7	55.	8.77E-04	1.65E-04	5.44E-05	1.76E-04	1.90E-04	3.53E-04
C 7	75.	1.05E-04	2.93E-05	1.40E-05	4.66E-05	1.30E-05	1.93E-06
D 7	110.	5.67E-05	9.45E-06	3.20E-06	2.08E-05	1.79E-05	7.25E-06
E 7	170.	3.47E-06	0.	0.	0.	0.	0.
G 7	250.	1.89E-06	0.	0.	0.	0.	0.
I 7	370.	2.63E-07	0.	0.	0.	0.	0.
L 7	500.	0.	0.	0.	0.	0.	0.
F 19	210.	1.69E-04	3.80E-05	1.37E-05	2.94E-05	3.88E-05	4.52E-05
H 19	310.	4.83E-06	0.	0.	0.	0.	0.
A 30	25.	1.43E-03	3.28E-04	1.30E-04	2.59E-04	2.01E-04	4.73E-04
1A 30	30.	1.20E-03	2.32E-04	1.32E-04	2.54E-04	3.45E-04	1.52E-04
2A 30	35.	5.92E-04	1.50E-04	8.55E-05	1.91E-04	9.58E-05	7.08E-05
3A 30	40.	3.90E-04	8.93E-05	5.12E-05	9.15E-05	6.40E-05	3.44E-05
4A 30	45.	3.79E-04	1.41E-04	6.51E-05	1.07E-04	6.27E-05	7.02E-05
B 30	50.	1.39E-04	3.27E-05	2.41E-05	5.01E-05	1.72E-05	1.50E-05
1B 30	55.	8.02E-05	1.43E-05	1.65E-05	3.18E-05	1.03E-05	7.32E-06
C 30	75.	1.14E-04	2.73E-05	1.82E-05	4.13E-05	1.55E-05	1.14E-05
D 30	110.	5.43E-05	1.31E-05	1.15E-05	1.53E-05	7.13E-06	7.20E-06
E 30	170.	2.20E-05	4.83E-06	4.98E-06	1.18E-05	8.18E-07	4.02E-07
G 30	250.	1.19E-05	0.	0.	0.	0.	0.
I 30	370.	1.25E-06	0.	0.	0.	0.	0.
L 30	500.	4.94E-06	0.	0.	0.	0.	0.
K 41	480.	4.29E-06	0.	0.	0.	0.	0.
N 41	730.	1.47E-06	0.	0.	0.	0.	0.
1A 52	30.	4.11E-03	7.21E-04	4.04E-04	7.02E-04	7.79E-04	1.50E-03
2A 52	35.	2.65E-03	5.31E-04	4.56E-04	5.85E-04	5.35E-04	5.43E-04
3A 52	40.	6.78E-04	1.52E-04	1.04E-04	1.13E-04	5.96E-05	2.50E-04
4A 52	45.	1.37E-04	6.48E-05	2.76E-05	4.48E-05	0.	0.
B 52	50.	1.48E-04	2.82E-05	3.65E-05	5.74E-05	1.70E-05	2.05E-05
1B 52	55.	1.06E-04	1.58E-05	2.32E-05	2.30E-05	1.05E-05	4.32E-05
C 52	75.	3.99E-05	8.65E-06	1.20E-05	1.19E-05	2.68E-06	4.66E-06
D 52	110.	1.76E-05	3.05E-06	5.96E-06	7.75E-06	4.94E-07	3.04E-07
E 52	170.	1.84E-05	0.	0.	0.	0.	0.
G 52	250.	2.22E-05	0.	0.	0.	0.	0.
I 52	370.	3.11E-06	0.	0.	0.	0.	0.
M 52	520.	4.48E-07	0.	0.	0.	0.	0.
O 52	680.	8.75E-07	0.	0.	0.	0.	0.
P 52	1100.	2.63E-07	0.	0.	0.	0.	0.
H 64	310.	8.13E-06	0.	0.	0.	0.	0.
K 64	480.	3.74E-07	0.	0.	0.	0.	0.

IT-5 TOTAL IRIDIUM DEPOSITION

TRAY POSITION		DISTANCE (METERS)	TOTAL IRIDIUM (GM/M**2)	<125 (GM/M**2)	125-175 (GM/M**2)	175-350 (GM/M**2)	350-991 (GM/M**2)	991-2794 (GM/M**2)
N	64	730.	2.21E-08	0.	0.	0.	0.	0.
P	64	1100.	1.3?E-07	0.	0.	0.	0.	0.
O	64	1300.	0.	0.	0.	0.	0.	0.
[illegible]	75	25.	?.66E-02	2.83E-03	1.14E-03	3.17E-03	7.00E-03	?.42E-03
1A	75	30.	[illegible]	?.33E-04	2.24E-04	4.46E-04	?.52E-03	?.37E-04
2A	75	?5.	?.60E-03	2.??E-04	1.?7E-04	2.43E-04	6.36E-04	?.33E-0?
3A	75	40.	?.25E-04	[illegible]	[illegible]	3.??E-05	4.38E-05	?.67E-04
4A	75	45.	[illegible]	?.21E-05	?.37E-05	1.07E-06	1.25E-05	?.29E-05
6	75	?5.	[illegible]	[illegible]	[illegible]	2.??E-05	1.06E-03	?.32E-05
1?	75	[illegible]	[illegible]	1.03E-05	[illegible]	1.07E-05	0.	?.67E-05
[illegible]	75	[illegible]	4.45E-05	[illegible]	1.76E-05	1.14E-05	6.92E-07	?.38E-05
E	75	172.	[illegible]	0.	0.	0.	0.	0.
[illegible]	75	[illegible]	1.61E-0?	0.	0.	0.	0.	0.
I	75	?70.	3.52E-0?	0.	0.	0.	0.	0.
M	75	5??.	2.27E-07	0.	0.	0.	0.	0.
O	75	?00.	0.	0.	0.	0.	0.	0.
Q	75	[illegible]	1.9?E-0?	0.	0.	0.	0.	0.
R	75	[illegible]	7.14E-0?	0.	0.	0.	0.	0.
H	86	[illegible]	4.??E-0?	0.	0.	0.	0.	0.
K	86	?82.	[illegible]	0.	0.	0.	0.	0.
N	86	[illegible]	1.92E-0?	0.	0.	0.	0.	0.
P	86	1100.	[illegible]	0.	0.	0.	0.	0.
O	86	1?00.	1.14E-0?	0.	0.	0.	0.	0.
R	86	[illegible]	?.40E-0?	0.	0.	0.	0.	0.
S	86	[illegible]	?.1?E-0?	0.	0.	0.	0.	0.
1A	97	?0.	[illegible]	?.21E-04	?.94E-04	4.21E-04	7.95E-04	1.31E-03
2A	97	[illegible]	[illegible]	[illegible]	1.43E-04	2.?4E-04	2.94E-04	?.69E-04
3A	97	[illegible]	1.97E-0?	[illegible]	[illegible]	[illegible]	1.99E-04	?.43E-04
4A	97	45.	1.69E-03	4.??E-04	1.79E-04	[illegible]	3.00E-04	?.30E-04
6	97	[illegible]	4.3?E-0?	[illegible]	1.13E-05	1.??E-05	0.	4.13E-0?
13	97	[illegible]	[illegible]	?.11E-0?	2.?5E-05	[illegible]	1.57E-05	?.87E-05
C	97	75.	6.03E-05	2.??E-0?	2.2?E-05	1.34E-05	3.16E-05	0.
D	97	1?3.	?.15E-0?	?.9?E-05	3.33E-05	4.5?E-06	8.09E-07	?.75E-07
E	97	172.	1.6?E-0?	0.	0.	0.	0.	0.
G	97	[illegible]	[illegible]	0.	0.	0.	0.	0.
I	97	[illegible]	3.7?E-0?	0.	0.	0.	0.	0.
K	97	45?.	5.43E-0?	0.	0.	0.	0.	0.
M	97	5??.	[illegible]	0.	0.	0.	0.	0.
N	97	?70.	9.6?E-0?	0.	0.	0.	0.	0.
O	97	?00.	4.9?E-0?	0.	0.	0.	0.	0.
P	97	1100.	1.91E-05	0.	0.	0.	0.	0.
Q	97	[illegible]	1.07E-08	0.	0.	0.	0.	0.
R	97	[illegible]	2.2?E-0?	0.	0.	0.	0.	0.
S	97	1??0.	5.7?E-0?	0.	0.	0.	0.	0.
[illegible]	97	2??0.	2.9?E-0?	0.	0.	0.	0.	0.

IT-E TOTAL IRIDIUM DEPOSITION

TRAY POSITION	DISTANCE (YARDS)	TOTAL IRIDIUM (GM/M**2)	<125 (GM/M**2)	125-175 (GM/M**2)	175-350 (GM/M**2)	350-991 (GM/M**2)	991-2794 (GM/M**2)
H 109	310.	7.53E-06	0.	0.	3.	0.	0.
K 109	480.	5.17E-07	0.	0.	0.	0.	0.
N 109	730.	2.77E-07	0.	0.	0.	0.	0.
P 109	1120.	0.	0.	0.	0.	0.	0.
Q 109	1300.	3.28E-08	0.	0.	0.	0.	0.
R 109	1500.	5.36E-07	0.	0.	0.	0.	0.
T 109	1900.	9.54E-08	0.	0.	0.	0.	0.
S 109	1900.	5.60E-07	0.	0.	0.	0.	0.
T 109	2000.	2.63E-07	0.	0.	0.	0.	0.
A 120	25.	1.34E-03	2.61E-04	1.11E-04	2.11E-04	3.53E-04	3.92E-04
1A120	30.	3.37E-03	5.94E-04	2.58E-04	5.41E-04	1.13E-03	7.84E-04
2A120	35.	9.17E-04	1.74E-04	5.40E-05	1.81E-04	2.33E-04	3.45E-04
3A120	40.	4.55E-04	1.08E-04	7.48E-05	1.21E-04	8.42E-05	7.79E-05
4A120	45.	7.18E-05	1.56E-05	1.59E-05	1.03E-05	7.91E-06	9.57E-06
B 120	50.	1.54E-04	4.68E-05	2.03E-05	1.85E-05	2.01E-05	4.29E-05
1B120	55.	4.93E-04	6.43E-05	1.16E-05	2.35E-05	5.66E-05	5.13E-06
C 120	75.	5.23E-05	1.51E-05	1.94E-05	1.57E-05	1.13E-05	8.18E-07
D 120	110.	3.20E-05	9.98E-06	1.29E-05	3.78E-06	1.46E-06	7.28E-07
D 120	110.	1.07E-07	0.	0.	0.	0.	0.
E 120	170.	2.67E-05	0.	0.	0.	0.	0.
G 120	250.	1.33E-05	0.	0.	0.	0.	0.
I 120	370.	6.17E-06	0.	0.	0.	0.	0.
K 120	480.	3.39E-06	0.	0.	0.	0.	0.
M 120	580.	9.32E-07	0.	0.	0.	0.	0.
N 120	730.	0.	0.	0.	0.	0.	0.
P 120	1100.	3.08E-07	0.	0.	0.	0.	0.
Q 120	1300.	1.55E-07	0.	0.	0.	0.	0.
R 120	1520.	7.25E-08	0.	0.	0.	0.	0.
T 120	2000.	4.14E-07	0.	0.	0.	0.	0.
T 120	2000.	0.	0.	0.	0.	0.	0.
H 131	310.	1.74E-05	0.	0.	0.	0.	0.
K 131	480.	4.58E-06	0.	0.	0.	0.	0.
M 131	580.	3.01E-06	0.	0.	0.	0.	0.
N 131	730.	0.	0.	0.	0.	0.	0.
O 131	880.	3.89E-07	0.	0.	0.	0.	0.
P 131	1100.	0.	0.	0.	0.	0.	0.
Q 131	1300.	3.30E-07	0.	0.	0.	0.	0.
R 131	1500.	2.24E-07	0.	0.	0.	0.	0.
S 131	1900.	1.93E-07	0.	0.	0.	0.	0.
T 131	2000.	3.03E-07	0.	0.	0.	0.	0.
1A142	30.	8.37E-03	1.32E-03	5.62E-04	1.83E-03	3.34E-03	1.32E-03
2A142	35.	5.98E-03	7.23E-04	3.93E-04	1.52E-03	2.63E-03	7.15E-04
3A142	40.	2.79E-03	4.36E-04	2.78E-04	6.99E-04	9.33E-04	4.47E-04
4A142	45.	4.52E-04	1.02E-04	4.64E-05	1.30E-04	1.66E-04	0.
B 142	50.	1.37E-04	2.08E-05	1.57E-05	3.86E-05	2.69E-05	2.75E-05

1T-6 TOTAL IRIDIUM DEPOSITION

TRAY POSITION	DISTANCE (YARDS)	TOTAL IRIDIUM (GM/M**2)	<125 (GM/M**2)	125-175 (GM/M**2)	175-350 (GM/M**2)	350-991 (GM/M**2)	991-2794 (GM/M**2)
1B142	55.	1.42E-04	3.07E-05	1.57E-05	3.35E-05	9.38E-06	7.22E-06
C 142	75.	5.14E-05	2.51E-05	1.09E-05	8.25E-06	2.57E-06	5.81E-07
D 142	110.	1.53E-05	5.79E-06	4.33E-06	2.29E-06	1.05E-06	1.92E-07
E 142	170.	5.50E-06	0.	0.	0.	0.	0.
G 142	250.	4.36E-06	0.	0.	0.	0.	0.
I 142	370.	5.66E-06	0.	0.	0.	0.	0.
K 142	490.	2.82E-06	0.	0.	0.	0.	0.
M 142	590.	3.30E-06	0.	0.	0.	0.	0.
N 142	730.	9.05E-07	0.	0.	0.	0.	0.
O 142	880.	0.	0.	0.	0.	0.	0.
P 142	1100.	0.	0.	0.	0.	0.	0.
R 142	1600.	1.23E-07	0.	0.	0.	0.	0.
S 142	1900.	0.	0.	0.	0.	0.	0.
T 142	2800.	4.01E-07	0.	0.	0.	0.	0.
H 154	310.	1.38E-05	0.	0.	0.	0.	0.
K 154	480.	0.	0.	0.	0.	0.	0.
N 154	730.	9.40E-07	0.	0.	0.	0.	0.
P 154	1100.	0.	0.	0.	0.	0.	0.
Q 154	1300.	1.09E-07	0.	0.	0.	0.	0.
R 154	1600.	2.03E-07	0.	0.	0.	0.	0.
S 154	1900.	0.	0.	0.	0.	0.	0.
A 165	25.	1.41E-03	3.41E-03	1.53E-03	3.02E-03	3.20E-03	1.30E-03
A 165	25.	1.19E-03	1.54E-03	8.28E-04	1.38E-03	2.33E-03	4.45E-03
2A165	35.	2.48E-03	4.94E-04	3.48E-04	9.13E-04	7.63E-04	7.56E-05
3A165	42.	4.03E-03	7.51E-04	2.16E-04	1.84E-03	6.01E-04	1.92E-04
4A165	45.	1.09E-03	1.97E-04	8.52E-04	4.12E-04	9.99E-05	1.20E-04
1B165	55.	5.15E-05	2.54E-06	7.64E-06	5.77E-05	6.79E-06	3.07E-05
C 165	75.	2.13E-05	1.15E-05	5.31E-06	2.36E-05	1.22E-05	4.09E-07
D 165	110.	1.47E-05	0.	0.	0.	0.	0.
E 165	170.	2.57E-06	0.	0.	0.	0.	0.
I 165	370.	7.76E-07	0.	0.	0.	0.	0.
M 165	590.	1.91E-06	0.	0.	0.	0.	0.
O 165	880.	1.39E-06	0.	0.	0.	0.	0.
P 165	1100.	7.17E-07	0.	0.	0.	0.	0.
Q 165	1300.	7.17E-07	0.	0.	0.	0.	0.
Q 165	1300.	1.29E-06	0.	0.	0.	0.	0.
R 165	1600.	8.84E-08	0.	0.	0.	0.	0.
H 176	310.	7.96E-07	0.	0.	0.	0.	0.
K 176	480.	2.39E-07	0.	0.	0.	0.	0.
N 176	730.	5.12E-07	0.	0.	0.	0.	0.
P 176	1100.	1.10E-07	0.	0.	0.	0.	0.
Q 176	1300.	2.58E-07	0.	0.	0.	0.	0.
Q 176	1300.	0.	0.	0.	0.	0.	0.
R 175	1600.	2.44E-07	0.	0.	0.	0.	0.
2A187	35.	5.95E-03	1.09E-03	7.02E-04	1.27E-03	1.73E-03	1.26E-03

IT-5 TOTAL IRIDIUM DEPOSITION

TRAY POSITION	DISTANCE (YARDS)	TOTAL IRIDIUM (GM/MM2)	<125 (GM/MM2)	125-175 (GM/MM2)	175-350 (GM/MM2)	350-991 (GM/MM2)	991-2794 (GM/MM2)
3A187	40.	7.72E-03	1.17E-03	9.49E-04	2.31E-03	2.24E-03	1.06E-03
4A187	45.	3.50E-03	6.74E-04	2.16E-04	1.31E-03	5.36E-04	2.73E-04
B 187	50.	4.85E-03	1.15E-03	9.32E-04	1.29E-03	5.03E-04	2.77E-04
1B187	55.	3.21E-03	4.09E-04	5.95E-04	7.97E-04	2.82E-04	1.37E-04
C 187	75.	2.19E-04	1.08E-04	5.32E-05	5.20E-05	1.19E-05	2.42E-06
D 187	110.	3.79E-05	1.69E-05	5.77E-07	5.60E-07	6.52E-07	5.62E-07
D 197	110.	1.41E-05	6.87E-06	1.77E-06	5.30E-07	1.01E-05	1.99E-06
E 187	170.	7.16E-07	0.	0.	0.	0.	0.
G 187	250.	9.66E-07	0.	0.	0.	0.	0.
I 187	370.	1.02E-06	0.	0.	0.	0.	0.
M 187	550.	2.50E-08	0.	0.	0.	0.	0.
P 187	1100.	0.	0.	0.	0.	0.	0.
R 187	1600.	1.76E-07	0.	0.	0.	0.	0.
H 199	310.	5.44E-07	0.	0.	0.	0.	0.
K 199	480.	0.	0.	0.	0.	0.	0.
N 199	730.	2.78E-07	0.	0.	0.	0.	0.
2A210	35.	8.37E-03	1.45E-03	9.57E-04	1.93E-03	2.46E-03	1.77E-03
3A210	40.	5.82E-03	1.33E-03	1.02E-03	2.01E-03	1.26E-03	1.64E-04
4A210	45.	3.86E-03	5.40E-04	4.80E-04	9.30E-04	5.39E-04	5.75E-04
B 210	50.	1.85E-03	3.78E-04	3.94E-04	5.26E-04	3.58E-04	2.83E-04
1B210	55.	4.98E-04	1.05E-04	5.82E-05	1.30E-04	9.22E-05	5.24E-05
C 210	75.	1.24E-04	4.12E-05	1 04E-04	2.04E-04	6.55E-05	4.52E-04
D 210	110.	1.19E-05	0.	0.	0.	0.	0.
E 210	170.	6.87E-06	0.	0.	0.	0.	0.
G 210	250.	1.45E-06	0.	0.	0.	0.	0.
I 210	370.	1.39E-07	0.	0.	0.	0.	0.
L 210	500.	0.	0.	0.	0.	0.	0.
F 221	210.	5.82E-07	0.	0.	0.	0.	0.
H 221	310.	0.	0.	0.	0.	0.	0.
J 221	440.	0.	0.	0.	0.	0.	0.
1A232	30.	3.98E-03	3.92E-04	2.79E-04	4.52E-04	6.13E-04	1.34E-03
2A232	35.	5.57E-03	5.47E-04	3.12E-04	1.40E-04	1.61E-03	2.95E-03
3A232	40.	2.52E-03	3.69E-04	2.39E-04	8.60E-04	7.76E-04	3.29E-04
4A232	45.	1.69E-03	3.53E-04	1.53E-04	4.43E-04	4.80E-04	2.63E-04
B 232	50.	3.71E-04	7.69E-05	4.73E-05	5.98E-05	8.91E-05	9.87E-05
1B232	55.	3.44E-04	7.13E-05	5.17E-05	9.69E-05	7.36E-05	7.02E-05
C 232	75.	5.55E-06	2.66E-05	1.02E-06	5.85E-07	4.36E-07	9.45E-07
D 232	110.	3.19E-06	1.12E-06	3.79E-07	2.72E-07	4.25E-08	1.39E-06
E 232	170.	6.96E-07	0.	0.	0.	0.	0.
I 232	373.	2.85E-07	0.	0.	0.	0.	0.
L 232	500.	0.	0.	0.	0.	0.	0.
F 244	210.	0.	0.	0.	0.	0.	0.
H 244	310.	0.	0.	0.	0.	0.	0.
J 244	440.	2.27E-07	0.	0.	0.	0.	0.
1A255	30.	7.52E-03	1.30E-03	6.53E-04	1.73E-03	2.41E-03	1.42E-03

1T-6 TOTAL IRIDIUM DEPOSITION

TRAY POSITION	DISTANCE (YARDS)	TOTAL IRIDIUM (GM/M**2)	<125 (GM/M**2)	125-175 (GM/M**2)	175-350 (GM/M**2)	350-991 (GM/M**2)	991-2794 (GM/M**2)
2A255	35.	8.14E-03	1.36E-03	7.21E-04	1.90E-03	3.38E-03	1.08E-03
3A255	40.	2.08E-03	3.32E-04	1.72E-04	3.75E-04	5.72E-04	6.25E-04
4A255	45.	3.74E-03	5.55E-04	3.45E-04	9.63E-04	7.93E-04	1.05E-03
B 255	50.	1.74E-03	2.14E-04	1.48E-04	3.14E-04	2.98E-04	7.65E-04
1B255	55.	4.27E-04	7.97E-05	3.80E-05	5.87E-05	1.07E-04	1.44E-04
C 255	75.	2.47E-05	9.25E-06	3.72E-06	4.34E-06	4.59E-06	2.77E-06
D 255	110.	3.78E-06	0.	0.	0.	0.	0.
E 255	170.	1.81E-07	0.	0.	0.	0.	0.
G 255	250.	2.60E-07	0.	0.	0.	0.	0.
I 255	370.	0.	0.	0.	0.	0.	0.
L 255	500.	3.85E-07	0.	0.	0.	0.	0.
E 266	170.	1.40E-06	3.48E-07	3.41E-07	3.03E-07	2.58E-07	1.50E-07
H 266	310.	0.	0.	0.	0.	0.	0.
2A277	35.	1.65E-03	3.33E-04	1.52E-04	2.80E-04	5.44E-04	2.27E-04
2A277	35.	2.65E-03	5.28E-04	2.29E-04	3.41E-04	5.67E-04	5.66E-04
3A277	40.	2.28E-03	3.11E-04	1.22E-04	2.58E-04	4.09E-04	1.10E-03
3A277	40.	2.47E-03	3.35E-04	1.40E-04	2.89E-04	4.90E-04	1.22E-03
4A277	45.	1.60E-03	4.07E-04	1.39E-04	1.77E-04	2.97E-04	5.76E-04
B 277	50.	4.39E-04	1.34E-04	7.23E-05	4.63E-05	7.34E-05	1.86E-04
1B277	55.	4.87E-03	1.25E-03	5.29E-04	5.17E-04	7.16E-04	1.25E-03
C 277	75.	1.41E-04	5.74E-05	1.32E-05	2.31E-05	1.88E-05	4.39E-05
D 277	110.	1.54E-05	8.31E-06	3.86E-06	1.72E-06	5.89E-07	9.21E-07
E 277	170.	3.83E-07	0.	0.	0.	0.	0.
G 277	250.	5.37E-08	0.	0.	0.	0.	0.
I 277	370.	0.	0.	0.	0.	0.	0.
L 277	500.	3.42E-07	0.	0.	0.	0.	0.
F 289	210.	0.	0.	0.	0.	0.	0.
H 289	310.	2.20E-07	0.	0.	0.	0.	0.
J 289	440.	0.	0.	0.	0.	0.	0.
A 300	35.	3.98E-03	1.86E-03	7.91E-04	1.91E-03	2.58E-03	1.84E-03
A 300	35.	4.85E-03	1.05E-03	4.08E-04	4.58E-04	7.30E-04	2.13E-03
1A300	50.	4.09E-03	7.79E-04	3.57E-04	6.56E-04	8.46E-04	1.45E-03
2A300	55.	6.29E-03	7.76E-04	3.34E-04	9.36E-04	1.63E-03	2.57E-03
3A300	40.	1.41E-03	2.37E-04	1.35E-04	2.89E-04	1.93E-04	5.87E-04
4A300	45.	7.16E-04	1.25E-04	5.35E-05	1.08E-04	2.17E-04	1.22E-04
B 300	50.	2.36E-04	4.49E-05	1.80E-05	3.69E-05	8.25E-05	5.35E-05
1B300	55.	6.74E-05	1.51E-05	5.50E-06	9.63E-06	7.30E-06	2.68E-05
C 300	75.	1.34E-05	7.91E-06	2.56E-06	1.67E-06	1.31E-06	0.
D 300	110.	7.53E-06	0.	0.	0.	0.	0.
G 300	250.	2.29E-07	0.	0.	0.	0.	0.
L 300	500.	2.39E-07	0.	0.	0.	0.	0.
L 300	500.	0.	0.	0.	0.	0.	0.
F 311	210.	2.39E-07	0.	0.	0.	0.	0.
H 311	310.	1.19E-06	0.	0.	0.	0.	0.
J 311	440.	3.93E-07	0.	0.	0.	0.	0.

IT-6 TOTAL IRIDIUM DEPOSITION

TRAY POSITION	DISTANCE (YARDS)	TOTAL IRIDIUM (GM/M**2)	<125 (GM/M**2)	125-175 (GM/M**2)	175-350 (GM/M**2)	350-991 (GM/M**2)	991-2794 (GM/M**2)
A 322	25.	2.22E-15	1.14E-15	5.38E-16	2.85E-16	1.11E-15	8.22E-17
2A322	35.	2.77E-03	5.66E-04	1.59E-04	3.93E-04	5.81E-04	1.33E-03
3A322	40.	4.58E-03	2.43E-04	2.12E-04	5.71E-04	1.02E-03	1.04E-03
4A322	45.	2.24E-03	3.24E-04	1.93E-04	2.91E-04	2.70E-04	1.05E-04
B 322	50.	2.14E-03	4.08E-04	2.39E-04	1.93E-04	4.15E-04	1.92E-04
1B322	55.	1.39E-04	5.61E-05	2.46E-05	3.10E-05	2.35E-05	0.
C 322	75.	4.75E-06	1.97E-06	1.07E-07	4.91E-07	8.19E-07	1.79E-07
D 322	110.	2.66E-16	9.77E-07	7.24E-07	1.97E-07	5.56E-07	1.04E-07
E 322	170.	4.14E-07	0.	0.	0.	0.	0.
G 322	250.	8.05E-08	0.	0.	0.	0.	0.
I 322	370.	4.93E-07	0.	0.	0.	0.	0.
L 322	500.	0.	0.	0.	0.	0.	0.
F 334	210.	5.19E-07	0.	0.	0.	0.	0.
H 334	310.	3.80E-07	0.	0.	0.	0.	0.
J 334	440.	0.	0.	0.	0.	0.	0.
A 345	25.	5.95E-03	1.13E-03	6.24E-04	1.29E-03	1.42E-03	1.39E-03
A 345	25.	6.29E-03	1.32E-03	8.17E-04	1.48E-03	2.62E-03	1.07E-03
1A345	30.	1.80E-03	4.19E-04	1.98E-04	3.70E-04	5.24E-04	1.81E-04
2A345	35.	4.44E-03	6.11E-04	3.22E-04	9.84E-04	1.53E-03	1.57E-04
3A345	40.	7.30E-04	1.06E-04	3.33E-05	3.34E-05	1.95E-04	4.98E-04
4A345	45.	1.12E-03	1.58E-04	9.74E-05	3.14E-04	2.85E-03	1.75E-04
B 345	50.	5.49E-04	8.89E-05	3.08E-05	1.49E-04	1.46E-03	1.29E-04
1B345	55.	2.66E-04	5.57E-05	1.56E-5	7.07E-05	5.40E-05	5.81E-05
C 345	75.	3.15E-04	1.36E-05	2.60E-05	7.57E-05	9.09E-05	1.95E-05
D 345	110.	1.20E-06	4.61E-07	2.42E-07	1.45E-07	1.84E-07	1.12E-07
E 345	170.	2.91E 07	0.	0.	0.	0.	0.
G 345	250.	2.59E-07	0.	0.	0.	0.	0.
I 345	370.	4.39E-07	0.	0.	0.	0.	0.
L 345	500.	4.15E-07	0.	0.	0.	0.	0.
F 356	210.	4.40E-07	0.	0.	0.	0.	0.
H 356	310.	0.	0.	0.	0.	0.	0.
J 356	440.	3.57E-07	0.	0.	0.	0.	0.

References

1. Headquarters, Department of the Army, "Employment of Atomic Demolition Munitions (ADM)," FM 5-26, August 1971.
2. T. F. Butkovich, The Gas Equation of State for Natural Materials, Lawrence Livermore Laboratory, Rept. UCRL-14729, January 1967.
3. W. C. Day and R. A. Paul, Trace Elements in Common Rock Types and Their Relative Importance in Neutron-Induced Radioactivity Calculations, U. S. Army Engineer Waterways Experiment Station Explosive Excavation Research Laboratory, Livermore, Calif., Rept. NCG TM 67-7, January 1967.
4. E. J. Leahy, D. Oltmans, C. M. Snell, T. J. Donlan, and W. B. Lane, Fallout Simulation: Nuclear Cratering Device (Project Diamond Ore), U. S. Army Engineer Waterways Experiment Station Explosive Excavation Research Laboratory, Livermore, Calif., Rept. TR-E-73- (to be published).
5. B. K. Crowley, D. E. Burton, and J. B. Bryan, Bearpaw Shale: Material Properties Derived from Experiment and One-Dimensional Studies, Lawrence Livermore Laboratory, Rept. UCID-15915, September 1971.
6. R. F. Bourque, User's Manual for Crater Data: A Computer Code for Analyzing Experimental Cratering Tests, U. S. Army Engineer Waterways Experiment Station Explosive Excavation Research Laboratory, Livermore, Calif., Rept. NCG/TM 70-15, October 1970.
7. K. E. Sprague, Middle Course II Cratering Series, U. S. Army Engineer Waterways Experiment Station Explosive Excavation Research Laboratory, Livermore, Calif., Rept. TR-E-73-3, July 1973.
8. C. J. Sisemore, J. B. Bryan, and D. E. Burton, Instrumentation and Data for Diamond Ore, Phase IIA, Experimental Measurements, Lawrence Livermore Laboratory (in preparation).
9. M. Finger, et al., Explosive Investigations in Support of Project Diamond Ore, Lawrence Livermore Laboratory, in preparation.
10. M. Finger, H. C. Hornig, E. L. Lee, and J. W. Kury, Metal Acceleration by Composite Explosives, Proc. Symp. Detonation, 5th, 1969, Office of Naval Research, Washington, D. C. Rept. ACR-184 (1970).
11. E. L. Lee, H. C. Hornig, and J. M. Kury, Adiabatic Expansion of High Explosive Detonation Products, Lawrence Livermore Laboratory, Rept. UCRL-50422, May 1968.
12. C. Grant, Dow Chemical Company, Minneapolis, Minn., private communication, May 1971, July 1972.
13. J. L. Trocino, Thickening and Gelling of Nitromethane, Joseph L. Trocino and Associates, Sherman Oaks, Calif., Bulletin JLTN-72-102, May 1972.
14. J. L. Trocino, Techniques for Sensitizing and Detonating Nitromethane-Based Explosive Systems, Joseph L. Trocino and Associates, Sherman Oaks, Calif., Bulletin JLTN-2 (Preliminary), April 1972.

15. D. E. Burton, The NCG Fallout Scaling Model: A Graphic-Numerical Method of Predicting Fallout Patterns for Nuclear Cratering Detonations, U. S. Army Engineer Waterways Experiment Station Explosives Excavation Research Laboratory, Livermore, Calif., Rept. NCG/TR-19, January 1970.
16. C. M. Snell, D. E. Burton, and J. M. O'Connor, Fallout Prediction for Subsurface ADM's, U. S. Army Engineer Waterways Experiment Station Explosive Excavation Research Laboratory, Livermore, Calif., Rept. EERO/TR-22, September 1971.
17. B. D. Anderson, II, A Simple Technique to Determine the Size Distribution of Crater Fallback and Ejecta, U. S. Army Engineer Waterways Experiment Station Explosive Excavation Research Laboratory, Livermore, Calif., Rept. NCG/TR 18, March 1970.
18. LTC M. K. Kurtz, Jr., Project Pre-Gondola I, Technical Director's Summary Report, U. S. Army Engineer Waterways Experiment Station Explosives Excavation Research Laboratory, Livermore, Calif., Rept. PNE-1102, May 1968.
19. W. E. Baker and P. S. Westine, A Short Course on Modeling Weapon Effects, Southwest Research Institute, San Antonio, Tex., October 1972.